1-1-1970

Lateral thrust exerted by frozen granular soils due to temperature change.

Jan T. Laba
University of Windsor

Follow this and additional works at: https://scholar.uwindsor.ca/etd

LATERAL THRUST EXERTED BY FROZEN GRANULAR
SOILS DUE TO TEMPERATURE CHANGE

A THESIS

Submitted to the Faculty of Graduate Studies Through the
Department of Civil Engineering in Partial Fulfillment
of the Requirements for the Degree of
Doctor of Philosophy of Applied Science
at the University of Windsor

by

JAN T. LABA

Windsor, Ontario, Canada
March, 1970

UMI Number:DC52652

UMI®

NBX 5335

APPROVED BY:

Cameron MacInnis

H. Trau

J. B. Kennedy

A. C. Smith

ABSTRACT

The object of the investigation presented in this dissertation was, to measure the expansive force of sand-ice specimens exerted on retaining boundaries, under conditions approaching those in a fully restrained frozen sand layer.

Two different sands made into 130 specimens, composed of either sand and a variety of ice contents were included in the programme. The strain in the frozen soil was measured by means of bonded resistance strain gauges embedded in the sand-ice system.

The pressure (σ) exerted by the frozen sand was found to be a function of five variables; the initial temperature (T_0) of the sample, the rate of increase of the sample's temperature (θ), the time (t) of temperature increase, initial porosity of the soil (n) and degree of ice saturation (S_i).

Experimental results when plotted in the form of "pressure-time" curves, showed the same tendency for every curve to attain its maximum after a certain time and then decrease to zero. The values of maximum pressure (σ max) and the required time (t_m) to reach this pressure were measured for each experiment and graphs were drawn showing the influence of the parameters (T_0, θ, S_i, n) on "σ max" and "t_m".

Summarizing the experimentally obtained results the following three general equations were derived;

(a)   for "pressure-time curves,"

(b)   for values of maximum pressure developed by a sand-ice layer,

(c)   for period of time required by the sand-ice layer to reach its maximum pressure.

Applying viscoelastic model analogy to the frozen sand-ice layer, it was possible to study changes occurring in the elastic and plastic strain, during the time when the frozen soil layer was subjected to a uniform temperature increase and therefore to a varying lateral stress.

ACKNOWLEDGMENTS

TABLE OF CONTENTS

LIST OF FIGURES

LIST OF FIGURES (cont'd)

LIST OF FIGURES (cont'd)

LIST OF FIGURES (cont'd)

xiii

LIST OF FIGURES (cont'd)

LIST OF TABLES

LIST OF TABLES (cont'd)

NOMENCLATURE

A	coefficient
a, b	constant
C	specific heat, term in Eqs. (19) and (21)
C_v	volumetric heat
E	modulus of elasticity
E_o'	initial modulus of elasticity, expressed as a ratio of equal biaxial stresses to the uniaxial strain
$E_{(t)}'$	modulus of elasticity, expressed as a ratio of equal biaxial stresses to the uniaxial strain
e	base of natural system of logarithms
K	thermal conductivity, term in Eqs. (20) and (22)
k_1, k_2, k_3	coefficients
i	ice content
L	latent heat of fusion, exponent in Eqs. (20) and (22)
m	exponent in Eqs. (19) and (21)
n	initial soil porosity
p	exponent in Eqs. (20) and (21)
s	slope
S_i	degree of ice saturation
T	temperature
T_a	air temperature
T_i	ice temperature
T_o	initial soil temperature
ΔT	increase in temperature
t	time

(t)	a subscript, indicating a time-dependent function
w	water content
α	average coefficient of thermal expansion of material
γ_d	dry unit weight of soil
ϵ	strain
ϵ_{el}	elastic strain
ϵ_{pl}	plastic (creep) strain
ϵ_T	strain caused by temperature increase
ϵ_{Tv}	vertical strain caused by temperature increase
$\epsilon_{\sigma v}$	vertical strain (deformation) caused by lateral compressive stress
η	coefficient of viscosity (proportionality)
$\eta'_{(t)}$	coefficient of viscosity, expressed as a ratio of equal biaxial stresses to the unixial velocity gradient of the plastic flow
θ	rate of increase of temperature
μ_1	Poisson's ratio in the elastic range
μ_2	Poisson's ratio in the plastic range
σ	radial stress, pressure exerted by expanding sand-ice system, thermal stress
σ_x, σ_y	biaxial stresses, principal stresses

CHAPTER I

INTRODUCTION

In North America in areas having a moderate climate, during the winter, the top foot or more of soil is frozen. Frozen soil containing ice, when subjected to a temperature rise, will exert pressure against confining boundaries. At the present time, very little is known about the magnitude of this pressure.

When designing hydraulic structures the horizontal ice pressure is recognized as an important "force of nature" and consequently is included in the stability computations. On the other hand, when designing soil retaining structures, the lateral thrust developed by a frozen soil layer due to a temperature increase, is completely disregarded.

Lateral thrust in soils will develop when all the following conditions exist:

(a) The frozen soil layer is restrained from expanding by retaining structures.

(b) Consecutive cycles of cooling and warming occur in the frozen soil layer during winter or spring.

(c) Ice-wedges form in the soil layer itself or along the contact area between the soil mass and retaining structure.

In frozen soil subjected to cooling from the earth's surface downwards, the formation of "frost cracks" is a

common occurence. They are produced by a non-uniform
change of temperature in the soil layer, causing uneven
shrinkage of individual soil layers and the appearance
of stresses which attain their maximum values near the
surface of the soil. Under sufficiently intense cooling,
the stresses can exceed the ultimate strength of the soil
and cause the appearance of fissures extending to a
certain depth into the frozen soil. In frost susceptible
soils, there is another factor which contributes to the
creation of frost cracks, i.e. the formation of local
ice lenses due to irregular migration of moisture. During
the winter, as well as in the spring, water seeps into
these vertical cracks, where after freezing, it forms
ice-wedges, thus causing a tight fit between the frozen
soil layer and retaining structures and creating the
required conditions for a soil expansive thrust to develop.

The object of the investigation presented in this
research programme, was to measure the lateral expansive
force exerted by a 4-inch thick frozen sand layer on
retaining boundaries under conditions approaching those
that exist in a fully restrained layer. Granular material
was chosen for this experimental work, because being frost
non-susceptible, it is considered by many engineers to be
a select material and is used in areas subjected to frost
action.

The work presented in this dissertation can be

divided into two parts:

The first part (Chapters III and IV) deals with the magnitudes of lateral pressure developed by a sand-ice system when subjected to a temperature increase. The frozen sand specimens were investigated under conditions of full radial restraint to determine the maximum pressures that the frozen sand layer can exert on rigid retaining structures when prevented from expansion. This knowledge in turn, can be applied to a frozen sand stratum in nature if the penetration of the temperature wave from the surface into the soil-ice system is known.

In the second part (Chapter V), a theoretical viscoelastic model showing the time-dependent behaviour of a frozen soil layer subjected to a temperature increase is introduced. By submitting the theoretical model to loading conditions equal to actual pressures exerted by a sand-ice system that were measured experimentally, it was possible to determine both the viscous (plastic) flow and elastic strain in a frozen soil layer.

CHAPTER II

REVIEW OF LITERATURE

To the knowledge of this writer, little work directly related to the measurement of expansive pressures exerted by a soil-ice system due to temperature changes has been carried out. However, a number of researchers have studied the magnitude of ice pressures on structures, since these studies were indirectly an aid to the research work undertaken, they are included in the following review of the literature.

Ice pressure against structures

An analysis of the elastic and plastic properties of ice demonstrates some of the difficulties of estimating theoretically ice thrust due to thermal expansion. The analysis is complicated by the influence of such factors as temperature, crystallographic structure, state of stress and duration of load application. Local conditions, particularly the reservoir shore line defined by the water level, also have an influence on thrust which is difficult to determine. For these reasons, there is no accurate method of determining the static pressure caused by the thermal expansion of ice sheets.

One of the pioneers in this field was Royen (1922), who undertook the study of pressure caused by thermal expansion of ice sheets. Working at a time when the rheological properties of this material were practically

unknown, he carried out laboratory investigations on ice
samples taken from salt water, which incidentally does
not have the same mechanical properties as fresh water
ice. Royen's results showed that the relative deformation
ϵ of sea ice samples at the ice temperature $T = - 3^{\circ}C$ and
applied stress $\sigma = 7.9$ kg/cm^2 followed closely the law

$$\epsilon = k_1 t^q \qquad (1)$$

where the coefficient k_1 and the exponent q are
functions of T and σ. For the above mentioned con-
ditions, Royen obtained for q the value $1/3$.

When studying the relationship between the creep
strain ϵ and stress σ at a given time, Royen experienced
difficulties in obtaining ice specimens of completely
identical composition; therefore, to overcome this problem
he used paraffin for his experiments. He found linear
law which he in turn applied to ice

$$\epsilon = k_3 \sigma \qquad (2)$$

where k_3 is a coefficient. Since paraffin does not
represent the ice structure, it is quite evident that the
empirical formula (2) in no way represents the actual
stress deformation behaviour of ice.

In contrast, Gold (1965) while studying columnar-
grained ice subjected to compression perpendicularly to
the long axis for a given ice temperature (- 9.5 ± 0.5°C),
expressed the relationship between the creep strain and

the stress at a given time in the form:

$$(\epsilon)_t = A(t) \, \sigma^{n(t)} \qquad (3)$$

where $(\epsilon)_t$ is the creep strain at time t, σ is the constant compressive stress and $A(t)$ and $n(t)$ are constant for given time t.

On the basis of experimental data using sea ice samples, Royen described the relationship between the plastic deformation of ice in compression and temperature by the empirical formula:

$$\epsilon = \frac{k_2}{1 + T} \qquad (4)$$

where T is the absolute value of the ice temperature, k_2 is a varying coefficient.

Taking into account the three empirical formulae pertaining to the duration of the load (1), the stress intensity (2) and the ice temperature (4), Royen derived his well-known formula commonly used to calculate the deformation of ice in compression (ϵ) and the thermal stress in the ice (σ):

$$\epsilon = K \, \frac{\sigma \, t^{\frac{1}{3}}}{1 + T} \qquad (5)$$

where $K = f(k_1, k_2, k_3) = 6$ to 9×10^{-4}, t is the time over which the load is applied and T is the ice temperature in degrees absolute.

The above empirical formula is subject to wide criticism for the following reasons: First, by using

paraffin instead of ice, Royen obtained a linear relationship (untrue for ice) between the relative compressive strain and the stress value. Second, he ignored completely the elastic deformations and also made no distinction between the different creep stages, namely primary, secondary and tertiary. Third, the dependence of creep strain on time was obtained from experiments carried out with sea ice specimens only.

To complete his work, Royen derived a formula for thermal stress in ice. He maintained that the average temperature of an ice sheet varies linearly with time $\left(\frac{dT}{dt} = \frac{T}{t} \right)$, where t represents the period of time required to raise the initial average ice temperature T to $0°C$.

For a completely restrained ice sheet, the resulting stresses are determined by the relationship

$$\frac{d\varepsilon}{dt} = \alpha \frac{dT}{dt} = \alpha \frac{T}{t} \tag{6}$$

where α is the linear coefficient of thermal expansion of ice.

Differentiating Eq. (5) with respect to time and equating this to the relationship expressed in (6), Royen found the following equation for σ max.

$$\sigma \max = \alpha f(K) (T + 1)^{5/3} \left(\frac{T}{t} \right)^{1/3} \quad kg/cm^2 \tag{7}$$

For $K = 60 \times 10^{-5}$; $f(K) = 1630$, where K is Royen's

coefficient which is dependent upon δ , T and t.

Royen arbitrarily assumed the initial minimum average temperature of an ice sheet 0.75 to 1.0 meter thick as being - 12°C. He also proposed the following values for t: 100, 170 and 360 hours. Placing these values into Eq. (7), Royen obtained stresses ranging from 22.5 to 34.5 metric tons per square meter, or from 32 to 54 pounds per square inch. These results have long been used in Europe, especially in the Nordic countries, even though it is highly unlikely that the average temperature of an ice sheet will increase linearly during a period of 100, 170 or 360 hours.

Work done in the U.S.S.R. shows further attempts to expand Royen's theory by introducing actual field measurements of temperature distribution in ice covers. After observations made on a Siberian river, Kouzoub (cited by Korzhavin, 1962) concludes that the relationship between the average temperature T_i of an ice cover and the average air temperature T_a during a period of 24 hours can be expressed by

$$T_i = 0.35 \, T_a \; {}^\circ C \tag{8}$$

Also, Estifeev (cited by Korzhavin) developed an empirical relationship similar to Eq. (8) for the maximum rate of change of the average temperature of ice as

$$\dot{T}_i = 0.35 \, \frac{\Delta T_a}{t_1} \tag{9}$$

where ΔT_a is the maximum change of air temperature for a given period of time t_1 within the preceding 24 hours. Using Eq. (8) and the measured values for coefficient of thermal expansion of ice ($\alpha = f(T)$), the value of $\alpha f(K)$ from Royen's equation can be written in terms of the air temperature during the preceding 24 hours. Estifeev suggested that

$$\alpha f(K) = 0.78 \ T_a^{-0.88} \tag{10}$$

where T_a is in degrees absolute.

Combining Eqs. (8), (9) and (10), Royen's formula as modified by Estifeev (cited by Korzhavin), can be written:

$$\sigma \max = 0.78 \ \frac{(0.35 \ T_a + 1)^{5/3}}{(T_a)^{0.88}} \left(0.35 \ \frac{\Delta T_a}{t_1}\right)^{1/3} \quad kg/cm^2 \tag{11}$$

It can be noted that in both empirical formulae (8) and (9), the thickness of the ice sheet was not taken into account.

The U.S.S.R. norms CN-76-56 (1959) (cited by Drouin, 1966), based on Royen's theory combined with field observation, give the range of ice pressure from 7 to 85.5 psi, depending on the restraint of the ice sheet, the top figure being for complete restraint.

Of all the experiments carried out by different scientists since 1922, only those of Brown and Clarke (1932) and Monfore (1951,1952) can be compared directly. Monfore's laboratory tests designed especially to secure

data on pressure exerted by expanding ice, were essentially

the same as those performed by Brown and Clarke, some

nineteen years before. Small ice cylinders 4 in. in diameter

and 4 in. long (Monfore) or 3 in. cubes (Brown and Clarke)

were subjected to temperature increases and the pressure

required to prevent vertical expansion was measured. All

ice specimens were oriented in such a way that the pressure

would act normal to the optical axes of crystals and there-

fore in the same direction relative to crystal structure

as a thrust that can develop in the field.

The results of one of Monfore's typical experiments

are shown in Figure 1. Monfore always obtained the same

shape for every "pressure-time" curve, i.e. slightly convex,

attaining its maximum after a certain time and the decreas-

ing. Monfore did not prolong his experiments longer than

the required time to record the maximum pressure for each

pressure-time curve.

Considering only the maximum pressure for an initial

ice temperature and for the different rates of temperature

increase, Monfore (1952) summarized his results in six

curves shown in Fig. 2a. He also recorded the period of

time necessary to obtain the maximum pressure for the

various initial temperatures (Fig. 2b).

Variations of an average of 25% were found by Monfore

in the maximum pressures reached by different ice samples

tested under the same laboratory conditions. As a possible

explanation for such large variations in otherwise
apparantly identical samples, he pointed out that the
crystal structure could form either a strong or weak sample.

Assur (1959) presented a mathematical expression
for the maximum ice pressure obtained from the Monfore
experiments in the following form:

$$\mathcal{G}\,\text{max} = - a\, T_o\, (1 + b\, T_o)\, \left(\frac{dT}{dt} + T_1\right) \text{ ton/m}^2 \qquad (12)$$

where, T_o initial temperature ($^\circ C$), $\frac{dT}{dt}$ linear rate of
warming, constant $a = 0.33694$, $b = 0.010137$ and $T_1 = 21.1$.

A comparison between the results of two identical
ice pressure tests carried out by Brown & Clarke (1932)
and Monfore (1951), made by Drouin (1966) is shown in
Fig. 3. For each test carried out by Monfore, the "pressure-
time" curve attained a maximum after a certain time and
then decreased. Brown and Clarke did'nt obtain similar
behaviour in their three experiments, even after an
11-hour period of temperature increase.

The great difference between Brown & Clark's and
Monfore's results could possibly be caused by the rather
rudimentary equipment available to the former investiga-
tors at that time. A Swedish researcher Lofquist (1952)
working on biaxially restrained ice samples also obtained
ice pressure values significantly higher than those found
by Brown and Clarke. Furthermore, an interesting aspect
of Monfore's laboratory work was the close agreement

obtained between ice expansive forces measured in the field and forces calculated by using temperatures measured in the field and expansive stresses measured in the laboratory. The reported values calculated and measured respectively were: 6 and 6, 11 and 14, 13 and 12 kips per lin. ft.

Ground temperatures

Close examination of ground temperatures indicates that at some depth below the top soil layer which follows air temperature changes, the ground temperature remains relatively constant throughout the year. Figure 4 shows an idealized variation of ground temperatures with depth for winter, spring, summer and fall.

The temperature at any point in the ground depends on the heat transfer between three heat sources: the air, the soil in the zone of temperature changes and the soil which remains at a relatively constant temperature. The lower soil zone is a mass that is only very slightly smaller than the planet Earth itself. Being a very large heat reservoir it can release or absorb substantial quantities of heat with virtually no change in temperature, the air on the other hand, can undergo substantial temperature changes during a 24 hr period and even larger changes throughout the year. Between the two so radically different zones is a zone of soil which serves as the buffer with its top layer tending to follow the air

temperature while the bottom layer remains at a nearly constant temperature. This is the active zone of temperature change which freezes in the winter and thaws in the spring. The ground temperature depends mainly on the heat transfer between soil and air, but also some heat comes from the zone of constant temperature and this should not be overlooked.

Figure 5 shows the depth of the $32^{\circ}F$ soil temperatures beneath a highway shoulder in New Jersey reported by Turner and Jumikis (1956). This data shows that approximately 60% of the warming occured from the top (air) and 40% occured from the bottom. A review of similar data indicates that warming from the bottom ranges from 25 to 50% of the total. While an exact percentage cannot be readily determined, it remains an important fact that some warming of the soil occurs due to heat transfer from the soil beneath the active zone.

During the winter of 1953-54, subsurface temperature measurements were performed on six New Jersey soils by Lobdell, Turner and Jumikis (1957). The studies revealed that:

(1) Granular, non plastic soils are better conductors of heat (and cold) than fine-grained soils and react to temperature changes more quickly.

(2) A concrete slab is a better conductor of heat than soil of the same thickness. Therefore, freezing

and complete thaw cycles occur more often below
a concrete slab or pavement than in the adjacent
shoulder.

(3) A combination of a concrete slab over granular
soil is one that reacts most quickly to cold and
warm spells. A shoulder of fine-grained soils shows
little reaction to cold and warm spells (except at
the surface) and reflects the over-all intensity
of cold of the winter.

(4) The freezing line generally penetrates to a greater
depth in granular soils than in fine-grained soils.

(5) There is a lag between the minimum air temperature
of winter and the maximum penetration of the 32
degree line. In the cases studied the lag was one
day, except for some of the shoulders of fine-
grained soils where the lag was several days.

(6) Maximum heaving does not necessarily occur at the
time of the maximum depth of the 32 degree line.

(7) Most thawing in soil occurs from the top downward
during thaw periods; however, some thawing takes
place from the bottom.

Based on the field observations, the conclusions
reached by the above mentioned three authors can be
understood and judged better if the thermal properties
of soils are brought into the picture.

Thermal properties of soil

Thermal conductivity, volumetric heat and latent heat are three thermal properties of soil which are of interest. They are primarily dependent on the dry unit weight and water (or ice) content of the soil.

Thermal conductivity (K) is the quantity of heat which flows normally across a surface of unit area per unit time and per unit of temperature gradient normal to surface. Being a measure of the ease with which heat can get through material, K may be expressed in Btu/hr/ft/$^\circ$F. Thermal conductivity varies with soil type; some representative values are tabulated in Table I, published by Aldrich (1956) and Jumikis (1966).

Volumetric heat (C_v) expresses the change of thermal energy in a unit volume of soil per unit change of temperature. Volumetric heat is derived from the specific heat which expresses the change in the thermal energy per unit weight per unit temperature change. Typical values of specific heat (C) in Btu/lb/$^\circ$F are: C (water) = 1.0, C (ice) = 0.5, C (dry soil, soil mineral matter) = 0.2. Using these values of specific heat, the volumetric heat C_v in Btu/cu ft/$^\circ$F can be expressed as follows:

For unfrozen soil: $\qquad C_v = \gamma_d \left(0.2 + \dfrac{w}{100} \right) \qquad\qquad (13)$

For frozen soil: $\qquad C_v = \gamma_d \left(0.2 + \dfrac{0.5\,w}{100} \right) \qquad\qquad (14)$

where: γ_d is dry weight of soil and w is water content
of the soil expressed, in per cent of dry weight.

Latent heat of fusion (L) is the thermal energy in
Btu's, that have to be taken out of the water in order to
change the water to ice without changing the temperature.
Latent heat depends only on the amount of water in a unit
volume of soil. Since one pound of water gives off
143.4 Btu's as it freezes, it can be expressed:

$$L = 1.434 \; w \; \gamma_d \tag{15}$$

On the basis of presented data and the foregoing
concepts, it can be seen that the rate at which heat can
be extracted from, or introduced into the soil, will vary
with the soil type, water content, density and whether the
soil is frozen or unfrozen. The amount of heat which must be
extracted to cause the soil to freeze, is also dependent
on the soil type, water content and density. It may appear
easy to conclude that a certain type of soil may be the
best from the standpoint of permitting the least depth of
freezing; however, when consideration is given to moisture
content and soil density, the situation is less clear.
In view of this, a statement that "granular, non plastic
soils are better conductors of heat (and cold) than fine-
grained soils", can be open to discussion and criticism.
Thermal conductivity of granular soil is less than that
of fine-grained soil (silt), but on the other hand, less

depth of freezing could be expected in the fine-grained
soil due to its larger quantity of water, which upon
freezing liberates more heat and delays the process of
frost penetration.

Air Temperature

The temperature at any point in the ground depends
primarily on the amount of heat that has been transferred
to or from the air above it, also on the thermal properties
of the soil. The colder the air temperature, with all
other factors constant, the greater is the heat extraction
and the greater is the depth of the freezing front. A
measure of how cold the air temperature has been is needed
in order to evaluate or even compare the effects of air
temperature. The amount of heat extraction and therefore,
the depth of the frost penetration depends upon the number
of days of freezing temperatures and also how cold it
became. The Freezing Index provides one of the means of
comparing potential freezing problems.

On the other hand, daily changes in winter air
temperature will impress the corresponding changes in
ground temperature, causing the frozen top soil layer to
expand or contract. Brown in 1966 presented results from
his study on the "Relation between mean annual air and
ground temperatures in the permafrost region of Canada".
Unfortunately, only one city, Ottawa, located outside
the permafrost area in a moderate climate zone, was included

in his research.

Brown reported that "air and ground temperature records show that the latter are warmer by a wide range, varying from 1°F at Key River, Alta., to 12°F at Taurcanis, N.W.T". He also observed that, the mean annual ground temperatures in permafrost decrease with depth from the ground surface to a depth of 50 to 100 ft and then steadily increase under the influence of the geothermal gradient.

Referring to the city of Ottawa, the observed difference between mean annual air temperature and ground temperature was $6 - 8^{\circ}$F, depending on the depth below ground surface.

Brown's work clearly indicates, that mean annual ground temperatures are several degrees warmer than the corresponding mean annual air temperatures. The difference between ground and air temperatures varies from place to place, being also influenced by climatic factors other than air temperature i.e. snow cover, vegetation, surface and subsurface drainage etc.

Except for direct measurements, at the present time there is no reliable method available to evaluate soil temperatures. However, presently existing approximate formulas for calculating the depth of frost penetration, can be of some use. Using Stefan's Equation (1890), presented with some modifications by Aldrich (1956) and

Yong & Warkentin (1966), the depth of frost penetration
can be calculated as a function of the ground surface
(air) temperature or the freezing index. With the known
depth of frost penetration, the ground surface temperature
and the ground temperature profile (linear temperature
change can be assumed for Stefan's Model), the temperature
at any depth of a frozen soil layer can be calculated.

However, this procedure can only be used when the
investigated soil layer was exposed for rather a long
period of time to the action of relatively constant and
below freezing air temperature. Only then, could Stefan's
or a modified Berggren Model (Aldrich, 1956) be used to
obtain an approximation of the ground temperature profile.
If a spell of cold weather is followed by a warming period,
then the ground temperature profile will change. This
will take place because the coldest part of the soil
layer, the ground surface, will first be subjected to a
progressing temperature increase. Therefore, in the
frozen soil layer, the existing (initial) soil temperature
profile will take a new and quite different shape than
that which is assumed by frost depth penetration theories.

CHAPTER III.

THE SOIL, APPARATUS AND TEST PROCEDURE

The soil

Two different sands were used in the experimental investigation. Sand No. 1 was a crushed uniform sand from Ottawa, Illinois (uniformity coefficient 1.5), while sand No. 2 was a natural well-graded sand from Paris, Ontario (uniformity coefficient 3.82). The grain size distributions are shown in Fig. 6. The soil specimens tested were composed of either sand and a variety of ice contents.

Apparatus

The apparatus (see Fig. 7) used in this research work, followed the idea originated by Willmot (1956), who had conducted studies on pure ice. It consisted of a steel cylinder with a cylindrical rubber diaphragm positioned inside and sealed to both ends of the steel cylinder. The small void between the 1/8 inch thick diaphragm and cylinder was filled with oil and connected to a hydraulic pressure pump, so that the oil pressure could be applied through the diaphragm to the specimen and thereby provide any desired amount of restraint. The oil pressure was measured by means of an external pressure test gauge connected to the pressure line. Strain in the frozen sand was measured by means of BLH Type A-9 bonded resistance strain gauges embedded in the sand and connected to the SR-4 Type N strain

indicator via the switching and balancing unit.

To increase the bond between the frozen soil and
strain gauges, the latter were coated on both sides with
Eastman 910 Adhesive Cement and then covered with particles
of sand, (see Fig. 8). To compensate for the effect of
temperature changes on the strain measurements a "dummy"
gauge was used; it was loosely attached to a flat concrete
bar and buried in a box containing dry sand of the same
type as the specimen being investigated. For each experiment
the thickness of the sand cover over the "dummy" gauge was
adjusted so that the strain gauge was always exposed to
the same temperature environment as the "active" gauge,
but isolated from mechanical strain.

The steel cylinder of the apparatus was insulated
all around except for the top surface of the sample so that
the heat flow into the sand-ice system followed the pattern
existing in nature.

Preparation of samples

The sand-ice specimens were prepared as follows:
A known weight of dry sand and the required amount of
water were thoroughly mixed together to provide the desired
ice content or degree of ice saturation when frozen. The
prepared soil was placed in the hollow core of the apparatus
and gently compacted to form a $9\frac{5}{8}$ inch diameter and 4 inch
high sample of a certain void ratio. Two 6 inch long strain

gauges (previously described) were placed crossways,
horizontally halfway down the sample's depth, symmetrically
about the specimen's centroidal axis. In a large number
of samples, two vertical gauges BIH Type A-9-4 were also
installed to measure the vertical displacement of the frozen
sand, (see Fig. 9). When used, the vertical gauges were
connected to a separate strain indicator and the effect of
the temperature changes was compensated for by a separate
"dummy" gauge of the same type as the vertical "active"
gauges.

The temperature of the sample was measured by means
of four copper constantan thermocouples placed in the
specimen at three different levels and connected to the
potentiometer through a multi-polar rotary switch. One
thermocouple was located $\frac{1}{4}$ inch below the top surface,
two were placed at a 2 inch depth (one at the centre and
the other 1 inch from the side of sample) the fourth was
embedded $\frac{1}{4}$ inch from the bottom. In addition to the above,
a fifth thermocouple recorded the air temperature above
the sand-ice specimen and a sixth measured the sand
temperature around the "dummy" gauge.

On completion of sample preparation, the apparatus
was placed in the freezing chamber (see Fig. 10) where
the specimen was frozen. Before being tested, the frozen
sample was left in a selected constant temperature (referred

to as "initial temperature") for not less than 24 hours
to insure uniform temperature distribution throughout the
sample.

The freezing chamber, a 5.25 ft x 7 ft x 7 ft high
walk-in type freezer was used for this research work. The
temperature inside the chamber was controlled by a hospital
type thermostat, which reacted to air temperature changes
of $\pm \frac{1}{2}°F$. The large type freezer provided many advantages
over the small standard type, the foremost being that it was
less prone to rapid uncontrolled changes in temperature,
also it permitted, even during the progress of the experiment,
inspection of the sample and apparatus inside the freezer.

Test procedure

The test method consisted of zeroing the strain
bridge with the frozen soil at a constant initial temperature
and then raising the soil temperature at a desired rate
while simultaneously applying and measuring the resisting
pressure required to prevent the soil-ice system from
expanding. The rate of the sample's temperature increase
was controlled by the forced flow of air of the desired
temperature, above the frozen specimen's top surface. The
source of heat was provided by a remote controlled heating
element augmented by heat reflecting plates and air fan,
placed inside the freezing chamber. More than one hundred
and thirty specimens were included in the program, with

starting temperatures of 0, 10, 20, 25 and 30°F. They were
then subjected to a constant rate of temperature increase
of either 3, 6 or 9°F.

During the progress of the experiment, the heat flow
in the soil progressed from the top surface towards the
bottom; therefore, the representative temperature of the
specimen for plotting and comparing purposes was assumed to
be the average temperature existing at the mid-hight of the
soil sample. Temperatures although observed continously
were recorded every five minutes, at the same time that the
applied pressure on the sample was adjusted.

After completion of each test, the specimen was un-
loaded and allowed to recover at 31.5°F for a period of
36 hours before being used again. No more than three tests
were performed on each sample; this was sufficient to complete
a set of experiments comprised of three different constant
rates of temperature increase, starting from the same
initial temperature.

The selected experimental range for starting temper-
atures and rates of temperature rise represent typical
values for soils in the most populated parts of Canada, as
well as for large areas of the U.S.A. The "Monthly Record"
published by the Meteorological Division of the Department
of Transport, Canada and the air temperature records
presented by Lobdell, Turner & Jumikis (1957) for New Jersey

and McRostic & Schriever (1967) for the City of Ottawa
indicate, that in the above mentioned climatic regions,
the frozen ground temperature rarely reaches $0^\circ F$ and the
daily average maximum rate of air temperature rise seldom
will exceed $10^\circ F/hr$.

Verification of the reliability of the strain gauges

Since the validity of the work undertaken depended
on the reliability of the bond developed between the
frozen sand-ice system and the embedded strain gauges, it
was necessary to check the efficiency of the bond.

Maihak Transmitters MDS 53, together with Maihak
Receiver MDS 3 (see Fig. 11) were chosen for this purpose.
The reason for selecting the above was, that this strain
measuring method did not require existence of the bond
between the soil and the transmitter, but only a direct
soil pressure on the measuring device. Transmitters MDS 53
were actually developed for measuring strain in concrete
and operate on the principle of attaining the coincidence
in frequency of vibration between stretch measuring wire
(transmitter) and standard wire (receiver).

The preparation of the sand samples for the "bond
test" followed the previously described procedure, except
that in this case one strain gauge BLH Type A-9 and one
Maihak Transmitter MDS 53 were located parallel to each
other, halfway down in the sample and as close as possible

to its centre. After freezing and before being tested, each sample remained in the freezer at a constant selected sub-freezing temperature for not less than 24 hours, to attain a uniform temperature in the whole frozen soil mass.

The testing procedure was conducted as follows: The frozen sample, while remaining at a selected constant temperature, was subjected to a progressively increased radial stress of a selected magnitude. Compressive stress was applied to the soil specimen by oil through a rubber diaphragm and it was allowed to remain constant for 3 minutes. Before the next increase in load took place, the the lateral pressure and corresponding strains indicated by both measuring systems were recorded.

Results obtained from the tests conducted on a number of frozen sand samples, showed good agreement between stress-strain curves obtained by the two methods. Figures 12 and 13 show typical results obtained for two specimens of sand No. 1, having the same initial porosity n = 46.6%, both tested at a different constant soil temperature (T) and each having a different ice saturation (S_i). The above mentioned figures show clearly the satisfactory behaviour of the sand coated strain gauges; even when subjected to relatively large strain there was no trace of weakening in the bond between the strain gauge and the sand-ice mass. All bond-tests were conducted at a constant

frozen soil temperature to eliminate the effect on the strain measurements caused by differences in thermal expansion (or contraction) between the sand-ice system and the Maihak transmitter.

CHAPTER IV

DISCUSSION OF TEST RESULTS

A discussion of the experimental results obtained in this research programme is presented in the sequence in which it was developed.

Lateral pressure exerted by sand-ice system

The main purpose of this research work was to study the lateral thrust exerted by a soil-ice system on rigid retaining boundaries, when subjected to temperature increases.

The pressure ($\mathfrak{S}$) exerted by the frozen sand specimens was investigated as a function of five variables: the initial sample temperature (T_0), the rate of increase of sample temperature (θ), the time (t) of temperature increase, the initial porosity of the soil (n) and the degree of ice saturation (S_i) or ice content (i).

The first set of experiments consisted of sixty tests performed on twenty sand-ice specimens of sand No. 1, all with a constant initial soil porosity of 46.6%. The selected ice contents of 10, 15, 25 and 30% corresponded to ice saturations of 33.3, 50, 83.3 and 100%. It has been indicated by Tsytovich (1960), that in granular soils, the unfrozen water content is negligible; therefore the ice content in each frozen specimen was assumed to be equal to its water content before freezing took place. The degree of ice saturation however, was based on a 9%

volume expansion of the pore water upon freezing.

Figures 14 to 25 show the relationship obtained between the average pressure exert d by frozen sand samples and time, for different values of T_o, θ and S_i. The results from all experiments show the same tendency, i.e. all "pressure-time" curves tend to attain their maximum after a certain time and then decrease to zero when the sample's average temperature reaches the vicinity of 30 to 32°F. Maximum pressures thus developed by frozen sand specimens vary from 0.5 to 91 psi, depending on the conditions under which the experiments were conducted. The shape of each curve reflects the different stages of creep to which each sample has been subjected, until the time when destruction of the crystalline structure takes place. Figures 26, 27 and 28 show more clearly the configuration of the "pressure-time" curves, obtained by connecting experimentally recorded values of pressure (previously shown in Figs. 18, 19 and 21) with straight lines.

For each "pressure-time" curve, the relationship between pressure and time can be approximated by the following equation:

$$6 = A\ t\ \exp\ (-t/t_m) \tag{16}$$

Where: A = coefficient $\left[psi/min\right]$, t = time $\left[min\right]$

t_m = time required to reach maximum pressure $\left[min\right]$

From Eq. (16) it follows that:

$$\sigma_{max} = 0.3679 \ A \ t_m \qquad (17)$$

As the values of maximum pressure (σ_{max}) and the required time (t_m) to reach this pressure were measured for each experiment, it was possible to calculate the corresponding values of the coefficient "A" using Eq. (18).

$$A = \sigma_{max}/0.3679 \ t_m \qquad (18)$$

The broken lines shown in Figs. 14 to 25 represent the theoretical "pressure-time" curves obtained from Eq. (16). The measured values of "σ_{max}" and "t_m", also the calculated values of "A" are tabulated in Tables II to V, as a function of the following parameters: S_i, θ, T_o and n.

All sixty theoretical "pressure-time" curves show good agreement with the experimentally obtained results, during the time when the expansive pressure increases from $\sigma = 0$ to $\sigma = \sigma_{max}$. However, during the period of time when the pressure decreases from $\sigma = \sigma_{max}$ to $\sigma = 0$, some differences between the measured values of pressure and the calculated values (theoretical) from Eq. (16) can be observed. These differences are more pronounced for the specimens having a higher degree of ice saturation. It can also be noticed that at the time when thawing of the sand-ice system takes place, the theoretical curves (contrary to observed behaviour) still indicate the existance of some expansive thrust. Nevertheless, Eq. (16)

is of major importance because of its simple form and also, because it approximates very closely the most important part (for practising engineers) of the "pressure-time" curves, showing the pressure increase from zero to σ max.

For each theoretical "pressure-time" curve, coefficient A is a constant, controlling the magnitude of the expansive pressure reached and it has dimensions representing the rate of pressure change. Figures 29 to 32, show the influence of the initial temperature of the frozen specimen (T_0) on the magnitude of the coefficient A, for different values of Θ and S_i. The above mentioned graphs were constructed by plotting the values of A, derived from Eq. (18) using the experimentally measured values of σ max and t_m.

It can be seen that for conditions indicated in Figs. 29 to 32 and for a sand-ice system subjected to a constant rate of temperature increase (Θ), coefficient A decreases with an increase of the sample's initial temperature (T_0). The same behaviour can be observed for the four different ice saturations, 33.3, 50, 83.3 and 100%. However, when the initial sand temperature is kept constant, the magnitude of coefficient A increases with an increase of S_i and also with an increase of Θ.

Maximum pressure and time required to reach this pressure

As the values of maximum pressure (σ max) and the

required time (t_m) to reach this pressure were recorded

for each experiment, it was possible to plot the influence

of the previously described parameters T_o, θ, S_i on

$\mathfrak{S}$ max and t_m. The results obtained are summarized in

Figs. 33 to 39 and lead to the following observations:

(a)   The maximum pressure increases with an increase in

the rate of temperature rise and also with an

increase of ice saturation, but decreases with an

increase in the initial temperature of the sample.

(b)   The time required to reach maximum pressure

decreases with an increase in the rate of temperature

rise and also with an increase of the sample's

initial temperature, but increases with an increase

in ice saturation.

It can also be observed that for conditions indicated

in Figs. 37, 38 and 39, the maximum pressure appears to

be directly proportional to the ice content or degree of

ice saturation of the frozen sand.

The values of maximum pressure developed by the

confined "sand No. 1 - ice system" for a constant initial

porosity n = 46.6%, can be expressed by the following

empirical equation, derived by searching systematically

for unknown functions by means of an electronic computor:

$$\mathfrak{S} \text{ max} = 0.475 \ S_i \ (1 - T_o/30) \ \theta^m + C \qquad (19)$$

Where: $\mathfrak{S}$ max = maximum pressure $\left[\text{psi} \right]$

m = 0.225 + 0.00075 S_i

$$C = 0 \quad \text{for} \quad T_o \leqslant 25^\circ F$$

$$C = \frac{(T_o - 25) \theta S_i}{2500} \quad \text{for} \quad 25^\circ F \leqslant T_o \leqslant 30^\circ F$$

S_i = degree of ice saturation $[\%]$

θ = rate of sample's temperature increase $[^\circ F/hr]$

T_o = initial sample temperature $[^\circ F]$

The period of time (t_m) required for the frozen sand layer (sand No. 1 and n = 46.6%) to reach its maximum pressure can be obtained with fairly good accuracy from the following equation which was derived in the same manner as Eq. (19);

$$t_m = K \; e^{L\theta} \; (S_i)^{0.85} \; (\theta)^p \qquad [\text{min}] \qquad (20)$$

Where: For $T_o \leqslant 20^\circ F$

$K = 4.95 - 0.11 \; T_o$

$L = - (0.076 - 0.015 \; T_o/20)$

$p = - (0.06 + 6.5 \; T_o/1500)$

For $20^\circ F \leqslant T_o \leqslant 30^\circ F$

$K = 6.9 \; (1 - T_o/31.8)$

$L = - (0.183 - 0.0061 \; T_o)$

$p = - (0.113 + T_o/750)$

Both Eqs. (19) and (20) summarize only the results shown in Figs. 33 to 39; therefore, they do not include the effect which variation of the soil porosity could have on $\mathcal{6}$ max or time t_m.

Tables VI to IX show the values of $\mathcal{6}$ max and t_m

measured experimentally and (for comparison) the same values calculated from Eqs. (19) and (20). Figures 40 to 46 also show the same relationship plotted graphically, where the solid lines represent experimentally obtained curves and the broken lines the curves obtained from the above mentioned equations. It can be observed that except for the specimens with a low degree of ice saturation S_i = 33.3% (see Fig. 40), for which the calculated values of maximum pressure are lower than the measured values, the agreement between the measured and calculated values for both $\mathfrak{S}$ max and t_m is satisfactory.

Effect of initial soil porosity on maximum pressure

All results discussed so far, were obtained by investigating frozen samples of sand No. 1 at a constant porosity of 46.6%. To study the influence of soil porosity on the maximum pressure developed, more than fifty additional experiments were conducted on sand-ice specimens having a wide range of porosities, with a constant degree of ice saturation. Specimens of sand No. 2 were added to this experimental investigation to enlarge its scope and range of porosity.

The values of maximum pressure ($\mathfrak{S}$ max) and the required time (t_m) to reach this pressure were measured for each experiment, as a function of the following parameters: T_o, Θ, n and S_i. The experimental results obtained are summarized in Tables X to XIII and also

partially in Figs. 47 and 48.

Figure 47 shows the relationship between maximum pressure and initial soil porosity. This relationship was obtained at a constant ice saturation of 50% for two different values of initial temperature (10°F and 25°F), as well as for three different rates of temperature increase of 3, 6 and 9°F/hr. It can be seen that frozen samples of sand No. 2, were investigated at two different porosities, 36% and 40.8%, while samples composed of sand No. 1 were investigated at three different porosities 40.8%, 43.5% and 46.6%. The straight line relationship between maximum pressure and porosity is visible and each straight line when extended to zero would pass through the origin.

Figure 48 shows the same relationship, maximum pressure versus porosity, but for an ice saturation of 100%. The broken lines shown in Figs. 47 and 48 are not actually the lines of best fit, but are theoretical lines indicating the values of maximum pressure calculated from the following general formula:

$$6 \max = \frac{n}{46.6} \left[0.475 \, S_i \, (1 - T_0/30) \, \theta^m + C \right] \quad (21)$$

Where: n = initial sand porosity $\left[\% \right]$

It can be observed, that the general Equation (21) was obtained by mutiplying Eq. (19) by the term $\frac{n}{46.6}$, indicating the effect of the porosity change on the

maximum pressure developed. Therefore, Eq. (19) is a
special case of Eq. (21), derived for the initial soil
porosity n = 46.6% and the "porosity term" $\frac{n}{46.6}$ = 1.

Figure 49, shows the summary of the relationship;
maximum pressure versus porosity for 100% saturated sand-
ice specimens, obtained from Eq. (21) for a variety of
initial soil temperatures and rates of temperature increase.
The solid portions of the straight lines define the porosity
range in which sands can be found in nature. When projected
to n = 100%, the lines point to the maximum pressure
exerted by pure ice. It is of interest to mention that,
the magnitude of ice pressure thus indicated came close to
the results reported by Monfore (see Fig. 2) who inves-
tigated pure ice samples subjected to uniaxial restraint
only. The solid lines shown in Fig. 49 are of some
additional interest, being derived for a fully saturated
sand-ice system and under conditions of full radial
restraint, they therefore indicate the largest values of
lateral pressure that a 4-inch thick frozen sand layer
can exert on a rigid retaining structure.

Further studies into the values of maximum pressure
exerted by specimens of sand No. 1 and sand No. 2 while
investigated at the same initial porosity n = 40.8%,
(shown in Figs. 47 and 48) leads to the following: Both
sands when tested under the same conditions of porosity,
saturation, initial temperature and rate of temperature

change, develop almost the same values of maximum pressure.
This in turn, leads to the conclusion that the pressure
developed by a sand-ice system is practically independent
of the sand's gradation and particle shape. Taking into
consideration that the average coefficient of thermal
expansion of sand particles is almost three times smaller
than that of ice, it is not suprising that the expansive
behaviour of the sand-ice system is governed by its ice
component.

When investigating the influence of the initial
soil porosity on the magnitude of the expansive pressure
developed, frozen soil specimens were subjected to a
constant temperature increase of 3, 6 or $9^{\circ}F$/hr for a
period not longer that the required time to reach maximum
pressure only. This procedure shortened the time required
to complete each experiment and at the same time permitted
measurements of sought values of 6 max and t_m. It was
mentioned before, that experimental results thus obtained,
are summarized in Tables X to XIII. Typical pressure-
time curves obtained for specimens of sand No. 1 and sand
No. 2, having the same initial porosity of 40.8% are
shown in Figs. 50 to 61. Each pressure-time curve shown
was constructed by connecting experimentally recorded
values of pressure with straight lines.

Effect of soil porosity on the time required to reach maximum pressure

It was mentioned previously, that for conditions indicated in Figs. 37, 38 and 39, (constant parameters n, Θ and T_o) the maximum pressure developed by a sand-ice system was directly proportional to the ice content or degree of ice saturation of the frozen sand. A straight line relationship was also obtained when maximum pressure was plotted against soil porosity, as shown in Figs. 47 and 48; in the latter case however, the parameters S_i, Θ and T_o were kept constant.

Similarly, it can be expected that the relationship between the period of time required to reach maximum pressure (t_m) and initial soil porosity (n), when plotted for constant values of S_i, Θ and T_o, will form a curve resembling in shape the curves that show the relationship "t_m" vs. degree of ice saturation. The above mentioned curves (t_m vs. S_i) are shown in Figs. 37 to 39 and it can be noticed that they do not differ greatly from straight lines. This is more evident when only a short length of each curve is considered. Therefore, for practical purposes, the relationship between t_m and n, for given constant values of S_i, Θ and T_o, can be assumed to be a straight line. As the porosity range in which all sands in nature are found is rather small ($n = 29\%$ to $n = 50\%$), the resulting error from the above approximation is negligible.

Figure 62 shows the relationship between the period of time required to reach maximum pressure and initial soil porosity. Using specimens of both sand No. 1 and sand No. 2, this relationship was obtained at a constant ice saturation of 50% for two different values of initial temperature (10°F and 25°F) and for three different rates of temperature increase of 3, 6 and 9°F/hr. The solid lines represent the lines of best fit that can be drawn for the experimentally obtained points. The broken lines on the other hand, indicate the period of time required for a 4-inch thick frozen soil layer to reach its maximum pressure, calculated from the following general equation:

$$t_m = \frac{n + 60}{106.6} \left[K \, e^{L\theta} \, (S_i)^{0.85} \, (\theta)^p \right] \tag{22}$$

Where: Values of coefficients K, L and p are the same as used in Eq. (20)

n = initial soil porosity $[\%]$

Equation (22) was obtained by multiplying the previously derived Eq. (20) by the simplified "porosity term" $\frac{n + 60}{106.6}$. It can be noticed, that for n = 46.6%, the porosity term will be unity.

Figure 63 shows the same relationship, t_m vs. n, but for a constant ice saturation of 100%. The broken lines as before indicate theoretical values of t_m calculated from Eq. (22) and the solid lines are the

lines of best fit for the experimentally obtained points.
When studying Figs. 62 and 63, it can be observed, that
with one exception only (in the case where $S_i = 100\%$,
$T_o = 10^\circ F$ and $\Theta = 3^\circ F/hr$), the vertical distances between
corresponding solid and broken lines do not exceed 5 minutes.
This indicated that the precision with which the empirical
Eq. (22) can predict the values of t_m is satisfactory,
especially when taking into consideration that all the
pressure-time curves were constructed by plotting the
soil expansive pressure at time intervals of 5 minutes.
It should also be mentioned, that the pressure-time
curves obtained for sand specimens subjected to the low
temperature increase i.e. $3^\circ F/hr$, did not show very well
the exact time when the maximum pressure occured.

Judging from the results plotted in Figs. 62 and 63,
obtained for both sand No. 1 and sand No. 2 and for the
limited porosity range of 36% to 46%, the assumed
straight line relationship between t_m vs. n, does not
introduce any serious deviation from actual behaviour.
However, unlike Eq. (21), Eq. (22) cannot be extended to
predict the behaviour of pure ice.

It can also be noticed that the type of sand used
(crushed uniform or natural well-graded) appears to have
no visible influence on the obtained values of t_m.
Therefore, as before in the case of 6 max, we may conclude
that the sand's particle shape, size and gradation have

no significant influence on the magnitude of the required time to reach maximum pressure.

Reproducibility of the apparatus and technique used

When carrying out the experimental work, it was observed that identical sand-ice specimens when tested under the same conditions did not develop the same magnitude of maximum pressure. Closer investigation into the causes for this behaviour points to the following contributing factors:

(a)   The reproducibility of the apparatus and experimental technique used.

(b)   Mechanical properties of the frozen sand samples, especially the behaviour of their ice matrix.

Check tests were run on several samples to determine the reproducibility of the apparatus and technique. Table XIV shows tabulated values of maximum pressure obtained from a number of frozen sand specimens subjected to duplicate tests. Each sample when used for the first time in a duplicate test, was subjected to a selected constant temperature increase for a period not longer than the required time to record the value of δ max. Before being used again, the sample was allowed to recover at a constant temperature of $31^{\circ}F$ for a period of 36 hours, then prepared for testing and tested under exactly the same conditions as before.

To draw a reasonable comparison for each set of experiments, the following items were recorded: the measured values of σ max, the range (R) indicating the difference between the highest and lowest observations, standard variation (v) and coefficient of variation (V) expressing the dispersion of results on a percentage basis.

In Table XIV, it can be seen that for frozen sand specimens tested at low initial soil temperatures i.e. $T_o = 0^{\circ}F$ or $10^{\circ}F$, the recorded ranges (R) between corresponding values of σ max were 3 and 4 psi respectively. For the above mentioned specimens, the calculated coefficients of variation (which are also the measure of the degree of experimental accuracy achieved) are not in excess of 4%. This is considered to be a satisfactory level of precision.

On the other hand, the frozen sand samples tested at high initial temperatures ($T_o = 20^{\circ}F$ and $25^{\circ}F$), show rather small ranges between corresponding values of maximum pressure; 2 psi and 1 psi respectively. However, their larger coefficients of variation (V = 11.1 % and 9.1%) indicate the lower accuracy in the recording of the experimental results.

This reduction in accuracy, can be attributed to following factors:

(a)   Increase in the plastic behaviour of the ice matrix in the frozen samples caused by an increase in the initial temperature.

(b)   Difficulties in applying the exact amount of
counteracting pressure required to prevent the
soil-ice system from expanding, when these were
smaller than 1 lb.

Larger variations were found in the values of
maximum pressure reached by the reproduced, equivalent
sand-ice samples tested under the same conditions. Table
XV shows the results thus obtained and also that, on the
average, the coefficients of variation listed in this
table are approximately twice as large as the corresponding
coefficients recorded in Table XIV for duplicate tests.

In every experiment conducted, a frozen sand specimen
was subjected to a selected constant temperature increase,
causing the frozen sand-ice layer to expand. The rep-
resentative temperature for each tested specimen was
assumed to be the average temperature existing at the
plane located halfway down the depth of the soil sample
and measured by two thermocouples located at this plane,
one at the centre and the other 1 inch from the side of
the sample. In the majority of frozen samples used, there
was no visible difference between the temperatures indicated
by both thermocouples. However, in a few cases differences
in temperature approximately $\frac{1}{4}°F$ between the two locations
were recorded.

Since the pressure exerted by the frozen sand layer

was investigated as a function of a constant rate of the sample's temperature increase, no larger difference than $\frac{1}{2}°F$ was permitted to occur at any time between the required temperature and the actual average temperature of the sample.

From the above discussion of the results obtained and the experimental procedure adapted, it can be concluded that the apparatus and the technique used, cannot alone be responsible for the variations in values of δ max recorded in Table XV. Mechanical properties and crystalline structure of the sand's matrix are also important contributing factors.

At the present time, little is known about the interactions between sand grains and ice for saturated or partially saturated frozen sand under stress. It was mentioned in Chapter III, that the frozen samples used in this research were prepared by mixing thoroughly distilled water with dry sand No. 1 or sand No. 2. It seems reasonable to expect that after freezing the specimen, a massive and polycrystalline structure of ice matrix will be formed with sand particles dispersed uniformly. The formation of the polycrystalline ice structure, (irregular ice crystals orientation), contributes to and is responsible for the variations in the maximum pressure reached by reproduced, equivalent sand-ice samples tested under the same conditions. It is very unlikely and practically impossible, even for identically prepared

frozen sand samples, to develop identical polycrystalline ice matrices.

Ice changes shape under an applied load, both elastically and plastically, the latter being manifested as movement along planes of imperfection, called slip planes. Slip in the ice crystals occurs most easily on the basel plane, located perpendicular to the axis of the hexagonal symmetry i.e. the C axis of the crystal, (Krausz, 1966 and Gold, 1967). The rate at which the dislocations move along the slip plane in the ice matrix, that is, the rate at which the ice crystals change their shape, depends upon the temperature and the shear stress acting on the slip planes.

The load applied to frozen soil can also cause a concentration of stresses at the contacts between mineral particles and ice crystals. Increase in pressure can lead to a decrease in the melting temperature of ice, followed by ice melting in places of increased pressure and then movement of the water to places where the pressure is lower. There, after attaining a state of equilibrium with temperature and pressure, water would freeze again; some of it may even be pressed out onto the free surface.

The above discussion points to the fact that once the sample is subjected to a pressure-time test, permanent changes, no matter how small, will take place in the specimen's ice matrix.

The sand-ice specimens with the initial temperature $T_o = 30°F$, were not included in Tables XIV and XV, as they represent a separate group where the ice matrix begins to lose its bonding properties. It was observed frequently, that when 6 max was recorded, the top of the investigated specimen after reaching a temperature of $32°F$ began to thaw. The most characteristic property of a sand-ice system at a temperature close to $32°F$ is the ease of flow under even an extremely small load, resulting from the plastic properties of ice and often the presence of some amount of water. Under these conditions, the values of maximum pressure exerted by the investigated sand-ice samples were small (0.5 to 1.5 psi) and difficult to measure. Therefore, a large mistake i.e. 50% in the recorded magnitude of 6 max could easily be made, having practically little importance due to the small magnitude of the lateral pressure developed in the first place.

Recorded dispersion of the values of 6 max listed in Table XV and obtained by studying seven different sets of reproduced equivalent sand samples, show the smallest coefficient of variation as 4.8% and the largest as 18.2%. Larger values of V were obtained where at least one of the following conditions existed: high initial temperature of the sample, low ice saturation or low rate of temperature increase in the frozen soil. The values of R, v and V listed in Table XV are not excessive,

taking into consideration all previously discussed mechanical properties and the behaviour of the ice matrix.

Only on the basis of information gathered in Tables XIV and XV can one assess the accuracy with which Eq. (21) will predict the values of 6 max. Inspection of Figs. 40 to 46 and Tables VI to IX clearly indicate that the difference between experimentally obtained values of 6 max and values calculated from Eq. (21), percentagewise are smaller than the corresponding coefficients of variation, thus showing satisfactory accuracy for Eq. (21).

Vertical displacement of specimens

In sixty samples of sand No. 1, vertical gauges (BLH Type A-9-4) were installed to measure the vertical strain in frozen specimens. Two gauges, each having a 4-in. long carrier and a 2.5-in. long grid, were placed in the soil specimens, one close to the centre and the other 1-in. from the side of the sample. These gauges were installed only in samples having an initial porosity of 46.6%, as this was obtained with practically no compacting effort. Vertical compaction, when properly conducted, did not disturb the horizontal gauges, but did tend to displace or bend the vertical gauges. For this reason, the vertical strain gauges were omitted in all sand samples where compactive effort was required (n $<46.6\%$).

Placing the vertical gauges in the specimens after compaction was considered, but rejected. Such a procedure would have required cutting two vertical shafts, 1.5-in.

in diameter and 4-in. deep, in the compacted sample and therefore creating, after installation of the gauges, two soil pockets having a different porosity and often a different saturation than the rest of the specimen. This could affect the accuracy of the experiments conducted for the basic purpose of determining the magnitude of the lateral thrust developed by a sand-ice system, when subjected to a temperature increase.

The largest accumulative average (from two gauges) vertical strain of 550 micro-inches per inch was recorded for the sand-ice specimens tested under the following conditions: S_i = 100%, T_o = 0°F and θ = 9°F/hr. This strain produced a vertical displacement of 0.0022-in. in a 4-in. thick soil sample. On the other hand, the smallest accumalative average vertical strain of 15 micro-inches per inch was observed in the frozen specimen where S_i = 50%, T_o = 30°F and θ = 3°F/hr.

The relationship between the vertical displacement (strain) and time (t) obtained for five different initial temperatures T_o = 30, 25, 20, 10 and 0°F, while keeping n, θ and S_i constant, is shown in Figs. 64 to 68. The influence of ice saturation (S_i) on the vertical strain-time relationship (when n, θ and T_o are kept constant) can be observed by studying Figs. 68 to 70.

The vertical displacement developed by a radially confined sand-ice system subjected to a constant rate

of temperature increase is the sum of the following
components:

(a)   Vertical deformation caused by vertical thermal
       expansion of the frozen specimen.

(b)   Vertical deformation caused by horizontal radial
       stress (Poisson ratio effect).

When a frozen soil layer subjected to a uniform
temperature increase is free to expand in a vertical
direction, the vertical thermal strain (ϵ_{T_v}) can be
expressed as:

$$\epsilon_{T_v} = \alpha \, \Delta T = \alpha \, \theta \, t \qquad\qquad (23)$$

where: α = average coefficient of thermal expansion of
        sand-ice $\left[1/^\circ F \right]$ $\left[^\circ F \right]$

   ΔT = increase in temperature $\left[^\circ F \right]$

      θ = rate of sample's temperature increase $\left[^\circ F/min \right]$

      t = time $\left[min \right]$

Since both α and θ are constant values for every
individual soil specimen, therefore the vertical strain ϵ_{T_v}
increases linearly with time from zero (at $t = 0$ min),
to a maximum value which occurs just before the thawing
of the frozen specimen begins.

On the other hand, the vertical deformation (ϵ_{σ_v})
caused by lateral compressive stress acting on a frozen
specimen is proportional to the magnitude of that stress.
For every investigated sample, the corresponding "pressure-
time" curve shows its loading history. Comparison between

two "vertical strain-time" curves developed by a frozen
specimen ($T_0 = 0°F$, n = 46.6%, $\theta = 6°F/hr$, $S_i = 100\%$)
shown in Fig. 70 and their corresponding "pressure-time"
curve shown in Fig. 28, leads to the following observation:
The part of either of the vertical displacement-time
curves which are located above the straight broken line
(shown in Fig. 70), resemble in shape the "pressure-time"
curve. It can also be noticed that the slope of the
vertical displacement-time curves changes with time during
the first 220 minutes and after that remains relatively
constant for the next 70 minutes, until the thawing of
the specimen from the top surface down begins.

Similar behaviour is shown by two curves representing
the side and centre of the sample, in Fig. 69. Here again,
the slope of both curves remains practically constant from
t = 170 min. to 290 min., at the time when the lateral
pressure decreases rapidly to zero.

The exact values of ϵ_{T_v} and ϵ_{6_v} could not be
calculated, because at the present time the Poisson ratios
and the coefficients of thermal expansion for a sand-ice
system (visco-elastic material) are not available. However,
with some degree of approximation, it can be assumed that
the broken straight lines shown in Figs. 29 and 30,
represent the average vertical strain caused by thermal
expansion only. The slope of each broken line when divided
by θ gives the average coefficient of thermal expansion.

For specimens described in Figs. 69 and 70, the corres-
ponding average coefficients of thermal expansion thus
obtained, are : α = 15 x 10⁻⁶ and α = 17 x 10⁻⁶ per °F
repectively. These values are considerably smaller than
the average value of α = 30 x 10⁻⁶ per °F obtained by
Willmot (1956) for pure natural ice.

In a number of cases, especially where the lateral
applied pressure was small, the slope of the straight
line representing the vertical displacement caused by
thermal expansion was difficult to determine (for example
see Fig. 68). Under these circumstances, the obtained
values of α would be subject to a large error.

On the basis of the experimental work conducted on
sand No. 1 with constant porosity of n = 46.6%, the
following observations were made:

(a)   The magnitude of α increases with an increase in
        ice saturation.

(b)   The coefficient of thermal expansion of pure ice
        is larger than the coefficients developed by a
        sand-ice system.

Only fourteen typical vertical strain-time curves
are included to support the above mentioned findings. It
was found unecessary to progress with further study on
ϵ_{Tv}, ϵ_{6v} and α , since they were not directly connected
with the evaluation of the magnitude of the lateral
pressure developed by a confined sand-ice system, subjected
to a temperature increase.

CHAPTER V

VISCOELASTIC MODEL ANALOGY

In the preceding chapters, the magnitude of the lateral thrust exerted by a frozen sand layer on rigid confining boundaries due to uniform temperature increase, was discussed. This was accomplished without knowledge of the viscoelastic (rheological) behaviour of a sand-ice system, but knowing only the following physical soil properties: n, S_i, T_o and Θ .

Recorded pressure-time curves (Figs. 14 to 25) show clearly the time-dependent behaviour of the developed pressures. Creep (the change in dimension with time at a given load), and relaxation (the loss of stress with time at a given deformation), are two manifestations of the time effect.

The sand-ice system resembles closely a viscoelastic material and its behaviour under applied pressure can be compared with the behaviour of the viscoelastic model. The simple but accurate idealization of a viscoelastic body is given by the Maxwell model, which combines elastic and viscous (plastic) response and shows the appropriate physical picture of the time dependent material. The above mentioned model consists of a spring and a dashpot in series, its main characteristic being, that the strain (ϵ) at all times is the sum of the elastic component (ϵ_{el}) and the viscous component (ϵ_{pl}):

$$\epsilon = \epsilon_{el} + \epsilon_{pl} \qquad (24)$$

Lets assume that the Maxwell model is placed horizontally between two rigid walls located a distance L apart (see Fig. 71) and that the model is subjected to a uniform temperature increase. As the rigid walls cannot be moved apart (L is constant), the linear expansion caused by temperature increase will not take place, but instead, pressure on the confining boundaries will develop. The counteractive pressure provided by retaining walls will in turn apply a compressive force on the spring and the dashpot. Under these circumstances, the resultant horizontal linear strain must be zero as:

$$\epsilon_T - \left(\epsilon_{el} + \epsilon_{pl} \right) = 0 \qquad (25)$$

Where: ϵ_T = strain caused by temperature increase

ϵ_{el} = strain in elastic component (spring)

ϵ_{pl} = strain in viscous element (dashpot)

The analogy between the behaviour of the theoretical viscoelastic model and the investigated sand-ice specimens is obvious, assuming that the elastic behaviour of the frozen soil is represented by the action of the spring and the plastic flow (creep) in the ice matrix by the motion of the dashpot.

Each investigated sand-ice specimen was circular in shape (dia. = $9\frac{5}{8}$ in.) and during the testing was subjected

to a radial stress σ uniformly distributed around its circumference. Since both the sample itself and the external loading were symmetrical about the sample's centre, the sample remained perfectly circular in form for the duration of the experiment. Assuming the frozen sand to be a homogeneous and isotopic material, then both the radial and circumferential strains must be uniform and equal throughout the soil sample. It follows that each element such as N or P shown in Fig. 72, will be subjected to biaxial stresses equal in magnitude and that:

$$\sigma_x = \sigma_y = \sigma \tag{26}$$

Where: σ_x, σ_y = principal stresses

σ = radial stress

According to the law of elasticity, the value of elastic stress can be expressed:

$$\epsilon_{el} = \frac{\sigma}{E} \tag{27}$$

Where: E = modulus of elasticity

The plastic deformation may be determined from Newton's law of viscosity:

$$\frac{d\epsilon_{pl}}{dt} = \frac{\dot{\sigma}}{\eta} \qquad \therefore or, \quad \epsilon_{pl} = \int_0^t \frac{\sigma}{\eta} \, dt \tag{28}$$

Where: η = coefficient of viscosity (proportionality).

The strain caused by a uniform temperature increase:

$$\epsilon_T = \alpha \theta t \tag{29}$$

Where: α = average coefficient of thermal expansion of
the material

Θ = rate of sample's temperature increase

t = time

Referring to the stress conditions of element N shown
in Fig. 72 and combining Eqs. (25), (27), (28) and (29),
it follows that:

$$\alpha \Theta t = \left(1 - \mu_1\right) \frac{\sigma_{(t)}}{E_{(t)}} + \left(1 - \mu_2\right) \int_0^t \frac{\sigma_{(t)}}{\eta_{(t)}} \, dt \qquad (30)$$

Where: μ_1 = Poisson's ratio in the elastic range

μ_2 = Poisson's ratio in the plastic range

(t) = a subscript, indicating a time-dependent
function

$\therefore$ the present time, values of μ_1 and μ_2 are not available
for frozen sand and very little is known about Poisson's
ratio in the plastic range. Experiments conducted on steel
plates and columns by M. Feigen (1953) indicated that;
in the inelastic range, Poisson's ratio is no longer a
constant when the axial load is increasing.

Equation (30) can also be written in a different
form, without including directly Poisson's ratios μ_1 and
μ_2 :

$$\alpha \Theta t = \frac{\sigma_{(t)}}{E'_{(t)}} + \int_0^t \frac{\sigma_{(t)}}{\eta'_{(t)}} \, dt \qquad (31)$$

Where: $E'_{(t)}$ = modulus of elasticity, expressed as a
ratio of equal biaxial stresses to the
uniaxial strain.

$\eta'_{(t)}$ = coefficient of viscosity, expressed as a
ratio of equal biaxial stresses to the
uniaxial velocity gradient of the plastic
flow.

In Eq. (31), only values of $E'_{(t)}$ and $\eta'_{(t)}$ are
unknown, as the values of $\sigma_{(t)}$ were obtained experimentally
and are shown in Figs. 14 to 25 in the form of "pressure-
time" curves. The relationship between pressure and time
was expressed in Chapter IV by the following equation:

$$\sigma_{(t)} = A\, t\, e^{-t/t_m} \tag{16}$$

Combining Eqs. (16) and (31) and differentiating with
respect to t, the following differential equation is
obtained:

$$\alpha\,\theta = \frac{d}{dt}\left(\frac{A\,t\,e^{-t/t_m}}{E'_{(t)}}\right) + \frac{A\,t\,e^{-t/t_m}}{\eta'_{(t)}} \quad , \text{ or}$$

$$\frac{\alpha\,\theta\,e^{t/t_m}\,E'_{(t)}}{A} = 1 - t/t_m - \frac{\dot{E}'_{(t)}}{E'_{(t)}}\,t + \frac{E'_{(t)}}{\eta'_{(t)}}\,t \tag{32}$$

The modulus of elasticity of a sand-ice specimen
before being subjected to a temperature increase can be
obtained from Eq. (32), by introducing the following
boundary conditions; At t = 0, $\sigma = 0$ and $E'_{(t)} = E'_o$, so

$$\frac{\alpha \Theta E_o'}{A} = 1$$

$$E_o' = \frac{A}{\alpha \Theta} \tag{33}$$

where: E_o' = initial modulus of elasticity of a frozen sand.

Substituting for A into Eq. (32), $A = \alpha \Theta E_o$, it gives

$$\frac{E_{(t)}'}{E_o'} e^{t/t_m} = 1 - t/t_m - \frac{\dot{E}_{(t)}'}{E_{(t)}'} t + \frac{E_{(t)}'}{\eta_{(t)}'} t \tag{34}$$

Temperature effect on E_o'

Equation (33) shows that E_o' is directly proportional to the coefficient A and inversely propertional to α and Θ. It was indicated in Chapter IV (see Figs. 29 to 32), that A was a function of T_o, S_i, Θ and n; and therefore, it can be expected that the modulus of elasticity (E_o') of a sand-ice system will also be influenced by the above mentioned parameters, with the possible exception of Θ. Using values of A obtained from fifteen experiments (sand No. 1, n = 46.6%, S_i = 50%, Θ = 3, 6 and 9°F/hr) and $\alpha = 15 \times 10^{-6}$ per $^\circ$F, coefficients of elasticity (E_o') were calculated and recorded in Table XVI.

Figure 73 shows graphically the relationship between E_o' and the initial soil temperature (T_o) for three different rates of temperature increase (Θ). It

can be observed that the modulus of elasticity decreases with an increase in the frozen sand's initial temperature. On the other hand, it appears that the rate of temperature increase (Θ) has very little if any influence on E_0'. The dispersion in values of E_0' obtained for three different rates of Θ, at the same initial soil temperature (T_0), could be caused by the experimental errors discussed in Chapter IV.

The relationship between E_0' and T_0 shown in Fig. 73, can be represented by the following equation,

$$E_0' = 11.3 \times 10^5 - 1030 \ T_0^2 \qquad \left[\text{psi}\right] \qquad (35)$$

or less accurately, by a straight line equation,

$$E_0' = (11.3 - 0.2 \ T_0) \times 10^5 \qquad \left[\text{psi}\right] \qquad (36)$$

Recent literature dealing with the properties of pure ice, supports the observations made on sand-ice specimens. Experimental work conducted by Gold (1958), Veinberg (cited by Tsytovich, 1959) and Voitkovskii (1960), established that the elastic modulus of ice decreases with an increase in ice temperature.

Modulus of elasticity $E_{(t)}'$ and coefficient of viscosity $\eta_{(t)}'$

An analysis of the viscoelastic behaviour of the sand-ice system was carried out using the specimen of sand No. 1, having $n = 46.6\%$, $S_i = 50\%$, $T_0 = 0°F$ and

subjected to a temperature rise of $\Theta = 0.1^\circ F/min$. The selected sample has been called specimen "Z" and its pressure-time curves (both experimental and theoretical) are shown in Fig. 19. The theoretical (idealized) pressure-time curve was cumputed from Eq. (16), using the experimentally obtained values of $A = 1.631$ and $t_m = 60$ min., which gives

$$\bar{G}_{(t)} = 1.631 \ t \ e^{-t/60} \quad \left[\text{psi}\right] \qquad (37)$$

Figure 74 shows once again, the theoretical pressure-time curve calculated from Eq. (37), which will be used as a loading record of the selected specimen. Figure 75 shows the slope of the pressure-time curve at any time during the duration of the experiment.

Before being subjected to a constant rate of temperature increase of $\Theta = 0.1^\circ F/min.$, the selected soil specimen "Z" was at the initial temperature of $T_0 = 0^\circ F$ and therefore had an initial modulus of elasticity $E_0' = 11.3 \times 10^5$ psi (see Fig. 73). During the progress of the experiment the frozen specimen while uniformly increasing in temperature, was at the same time subjected to a constantly changing stress $\bar{G}_{(t)}$. Since both the stress and the soil temperature increase (ΔT) are time dependent, it can therefore be expected that the modulus of elasticity $(E_{(t)}')$ of the specimen "Z" will decrease with time from its maximum value $E_{(t)}' = E_0'$ at $t = 0$ min.,

in the same way as the broken curve shown in Fig. 73.
Equation (35), which indicates the effect of the temper-
ature increase on the initial elastic modulus of the sand-
ice system, can be used as a fair approximation of the
relationship $E'_{(t)}$ vs. time, when the independent variable
T_o is replaced by $\Delta T = \theta t$. This is because Eq. (35)
was derived for the sand-ice system subjected to similar
stresses and temperature changes as the specimen now being
discussed. Therefore, the elastic modulus of the specimen
"Z" at any time after subjecting it to a temperature
increase, can be expressed:

$$E'_{(t)} = E'_o - a \Delta T^2 = E'_o - b \, t^2 \qquad \left[\, psi \,\right] \qquad (38a)$$

Where: $E_o = 11.3 \times 10^5$ $\left[\, psi \,\right]$

$\Delta T = (\theta t)$ = increase of soil temperature $\left[\, ^o F \,\right]$

   $a = 1030$ t = time $\left[\, min \,\right]$

   $b = (a\theta^2) = 10.3$

Equation (38a) can be open to criticism, as it
involves some degree of approximation; therefore, two
additional, less accurate equations for $E'_{(t)}$ were
included in the analyses. This will help to evaluate the
effect which the changes in function $E'_{(t)}$ will induce on
$\eta'_{(t)}$ and also on the magnitude of the plastic strain
(ϵ_{pl}).

Assuming that the elastic modulus decreases uniformly
with time (see Fig. 73), then

$$E'_{(t)} = E'_0 - s_1 \Delta T = E'_0 - st \quad [psi] \qquad (39a)$$

Where: $E'_0 = 11.3 \times 10^5 \quad [psi]$

$\Delta T = (\theta t) =$ increase in soil temperature $\quad [^\circ F]$

$s_1 = 20,000$

$s = (\theta s_1) = 2000$

Assuming that modulus of elasticity is a constant, then

$$E'_{(t)} = E'_0 = 11.3 \times 10^5 \quad [psi] \qquad (40a)$$

The curves showing the three equations for $E'_{(t)}$ are drawn in Fig. 76 (see also Table XVII). The circular points plotted in the same figure indicate the effect of temperature increase in the soil's initial modulus of elasticity, when $\theta = 6^\circ F/hr$. The same points are shown in Fig. 73, and were obtained from Eq. (33). Substituting in turn, Eqs. (38a), (39a) and (40a) for $E'_{(t)}$ into differential Eq. (34), the following corresponding functions for coefficient of viscosity ($\eta'_{(t)}$) are obtained in lb-min/in^2:

$$\eta'_{(t)} = \frac{(E'_0 - bt^2) t}{\dfrac{(E'_0 - bt^2) e^{t/t_m}}{E'_0} - \dfrac{2bt^2}{E'_0 - bt^2} + t/t_m - 1} \qquad (38b)$$

$$\eta'_{(t)} = \frac{(E'_0 - st) t}{\dfrac{(E'_0 - st) e^{t/t_m}}{E'_0} - \dfrac{st}{E'_0 - st} + t/t_m - 1} \qquad (39b)$$

$$\eta'_{(t)} = \frac{E'_0 t}{e^{t/t_m} + t/t_m - 1} \qquad (40b)$$

Where: $E_0' = 11.3 \times 10^5$ [psi]

Constants: $b = 10.3$, $s = 2000$, $t_m = 60$ min.

The tabulated values for $\eta'_{(t)}$ (from three equations) are compiled in Table XVIII and the corresponding curves are drawn in Fig. 77.

It can be observed, that the curves showing the three different functions of $\eta'_{(t)}$ are practically identical, except during the first 60 min., when the curve representing Eq. (39b) indicates larger values for the coefficient of viscosity than the remaining two. On the other hand, there is no significant difference at any time between the corresponding values of $\eta'_{(t)}$ from either Eq. (38b) or Eq. (40b), even though each equation was derived from a different function of $E_{(t)}'$. The reason for this is that the increase in the difference between the two functions of $E_{(t)}'$ represented by Eq. (38a) and (40a) (see Fig. 76), changes rather slowly during the first hour, after commencement of the experiment. After this time, the influence of $E_{(t)}'$ on $\eta'_{(t)}$ appears to be negligible.

This leads to the conclusion, that for all practical purposes, the coefficient of viscosity ($\eta'_{(t)}$) of the specimen "Z", during the time when the confined frozen sand sample is subjected to a constant rate of temperature increase from $0^\circ F$ to $30^\circ F$, can be expressed satisfactorily by Eq. (40b), the simplest of the three equations introduced.

Elastic strain ϵ_{el} and plastic deformation (creep) ϵ_{pl}

Knowing the functions defining the modulus of elasticity and the coefficient of viscosity for the investigated specimen "Z", its horizontal elastic strain and plastic-viscous deformation can be determined at any time when the specimen is subjected to a temperature increase and hence to varying lateral stress. Following the viscoelastic model analogy, the sum of the elastic and plastic strain, at all times in the frozen specimen is equal to the strain caused by the uniform rate of warming.

The elastic strain resulting from elastic deformations of the sand-ice system can be calculated for the problem at hand from the following equation:

$$\epsilon_{el} = \frac{\sigma_{(t)}}{E'_{(t)}} \tag{41}$$

Substituting for $E'_{(t)}$, the best available function

$$E'_{(t)} = E'_o - bt^2 = 11.3 \times 10^5 - 10.3\ t^2 \ , \ \text{then}$$

$$\epsilon_{el} = \frac{At\ e^{-t/t_m}}{E'_o - bt^2} = \frac{t\ e^{-t/60}}{6.928 \times 10^5 - 6.315\ t^2} \quad \left[\text{in/in}\right] \tag{42}$$

or, if assuming that $E'_{(t)}$ is a constant

$$E'_{(t)} = E'_o = 11.3 \times 10^5, \ \text{then}$$

$$\epsilon_{el} = \frac{At\ e^{-t/t_m}}{E'_o} = \frac{t\ e^{-t/60}}{6.928 \times 10^5} \quad \left[\text{in/in}\right] \tag{43}$$

Tables XIX and XX present the tabulated values for ϵ_{el}, obtained from Eq. (42) and Eq. (43) respectively, for the time period of 0 to 300 min.

Equation (39a), representing the function $E'_{(t)}$,

used previously for comparison purposes, will not be taken

into consideration at this time. The constant rate of

decrease in the values of the elastic modulus given by

Eq. (39a), i.e., s = 2000 psi/min., appears to be excessive

and unsupported by the experimental findings for the first

few minutes after the test commences. At that time, the

negligible change in the sand-ice temperature and the

absence of large plastic deformations (Goughnour and

Andersland, 1968) in the ice matrix, cannot warrant the

immediate drastic changes in the values of $E'_{(t)}$,

indicated by the large slope of "s".

The plastic-viscous irreversible deformation in

specimen "Z", resulting from the ice flow and possibly

from displacement of sand particles, can be obtained from

equation,

$$\epsilon_{pl} = \int_0^t \frac{\sigma_{(t)}}{\eta'_{(t)}} \, dt = A \int_0^t \frac{t \, e^{-t/60}}{\eta'_{(t)}} \, dt \qquad (44)$$

or from the more simple equation

$$\epsilon_{pl} = \alpha \theta t - \epsilon_{el} = 1.5 \times 10^{-6} t - \epsilon_{el} \quad \left[in/in \right] \qquad (45)$$

Tables XIX and XX present the tabulated values for ϵ_{pl},

obtained from Eq. (45) where for comparison purposes the

function ϵ_{el} is represented in turn by Eq. (42) and Eq. 43)

respectively. The average coefficient of thermal expansion

$\alpha = 15 \times 10^{-6}$ per °F used in Eq. (45) was determined

previously (see Chapter IV) from the study of the vertical displacement of specimen "Z".

Fig. 78 shows the relationship between plastic and elastic strain during the period of 300 min., when the temperature in the investigated specimen "Z" increased from $0°F$ to $30°F$. It can be seen that during the first 41 min. after exposing the radially confined sand-ice layer to a temperature change, the plastic component of the horizontal strain increases rapidly, but still is smaller than the elastic component. Approximately at $t = 41.5$ min., both strain components are equal and after that time, the plastic component representing the accumulative creep (from $t = 0$ min.) of the sand-ice specimen is predominant.

Since ϵ_{el} is directly proportional to the applied stress σ, therefore, the function of ϵ_{el} resembles in shape the pressure-time curve of specimen "Z". Regardless of which of the two equations introduced for ϵ_{el} were used, the maximum elastic strain occurred at time $t = t_m = 60$ min., when the specimen was subjected to the largest radial stress (σ max $= 36$ psi).

It can be noticed that all time-dependent functions, namely the elastic modulus, coefficient of viscosity, plastic strain and elastic strain were not extended beyond the time $t = 300$ min. or $T = 30°F$. At this time, the theoretical pressure-time curve of specimen "Z" still

indicates the existence of some radial pressure, while the measured ressure dropped to zero. The reason for this behaviour was, that when the progressively increasing average sample temperature (measured at mid-height of the sample) reached $30^{\circ}F$, the top part of the 4-in. thick soil layer was experiencing some thawing of the ice matrix. During the ice melting process, the lateral thrust exerted by a soil-water-ice layer remains zero; therefore, the elastic and plastic strains experienced by the sand-ice system ceased to exist.

Figure 78 also shows the comparison between two " ϵ_{el} - time" curves, obtained from Eqs. (42) and (43) respectively. It can be observed that, the difference in the magnitude of ϵ_{el} given by the two curves increases progressively with time and reaches its maximum at t = 300 min. However, at that time, not only the difference discussed, but also the va ies of ϵ_{el} itself obtained from either equation are negligible, when compared with the magnitude of the creep sustained by the frozen soil specimen. If a comparison is made at t = 300 min. (see Tables XIX and XX), then from Eqs. (42) and (45), the following values for the elastic and plastic strain are obtained: ϵ_{el} = 16 micro in/in. and ϵ_{pl} = 434 micro in/in. On the other hand, the corresponding values obtained from Eqs. (43) and (45) are: ϵ_{el} = 3 micro in/in. and ϵ_{pl} = 447 micro in/in.

The resulting difference between the two functions of ϵ_{el} has only a small influence on the large magnitude of ϵ_{pl} and therefore, for all practical purposes, the modulus of elasticity $E'_{(t)}$ for specimen "Z" can be assumed to be the constant value $E'_{(t)} = E'_0$, without distorting seriously the corresponding values of $\eta'_{(t)}$ and also ϵ_{pl}.

CHAPTER VI

CONCLUSIONS AND RECOMMENDATIONS

Based on experimental results obtained and the analysis presented in the previous chapters, the following conclusions can be drawn:

1.   The pressure (σ) exerted by the frozen sand was found to be a function of five variables; the initial temperature (T_0) of the sample, the rate of increase of the sample's temperature (Θ), the time (t) of temperature increase, initial porosity of the soil (n) and degree of ice saturation (S_i).

2.   The temperature of the sand-ice system at the time when it begins to be subjected to temperature increase, is of great importance. At the high initial temperature of $30^\circ F$, a frozen sand layer will exert lateral pressure approximately fifty times smaller than when it is at $0^\circ F$. In view of this, it can be expected that (exposed to the same soil conditions of Θ, S_i and n), a heated basement wall will be subjected to a smaller lateral thrust than an unheated one. The heat flow into a frozen soil layer, increases the initial soil's temperature on the wall-soil contact area and therefore creates a protective barrier around its perimeter.

3.   The magnitude of lateral thrust developed by a sand-ice layer increases with an increase of ice saturation.

At a constant porosity, the increase seems to be linear,
with the slope of the straight line being determined by
the rate of temperature change and the initial temperature
of the soil.

4. Two different sands, having the same porosity
and degree of ice saturation, and conditioned to the same
initial temperature, developed almost the same maximum
pressure when subjected to the same rate of temperature
increase. Therefore, it would appear that the maximum
pressure which a sand-ice system can develop is indepen-
dent of the sand's particle shape, size and gradation,
per se.

5. Three general equations were derived:

(a) for predicting the values of lateral pressure exerted
by a restrained 4-in. thick sand-ice layer, at any
selected time after an increase in soil temperature
took place,

(b) for values of maximum pressure developed by a sand-
ice layer,

(c) for period of time required by the sand-ice layer
to reach its maximum pressure.

These equations were derived for frozen sand specimens
tested under conditions of full radial restraint and in
this respect, they define the largest pressures that the
frozen sand layer can exert on rigid retaining structures.

6.   The Maxwell model is a useful analogue for demonstrating and studying the viscoelastic behaviour of a sand-ice system.

7.   The "elastic strain-time" curve of a frozen sand layer resembles in shape its "pressure-time" curve. Maximum elastic strain and maximum pressure occur at the same time. After reaching this time, the elastic strain decreases rapidly and becomes almost negligible when compared with the plastic strain.

8.   Plastic (creep) strain in a restrained frozen sand layer commences immediately after subjecting the frozen sand to a temperature increase. This creeep strain increases continuously with time, reaching its maximum value just before thawing of the ice matrix takes place.

9.   For all practical purposes, the functions of $\eta'(t)$ and $\in_{pl}$ can be derived, by assuming that the modulus of elasticity of a frozen sand layer subjected to lateral stress and to a uniform temperature increase is constant and equal to the initial modulus of elasticity of the frozen sand layer E_0'.

10.   The maximum pressure exerted by a frozen sand layer, having a considerable thickness of one foot or more, can be evaluated by dividing the frozen layer into a number of 4-in. thick horizontal sub-layers. The profile showing the change in the exerted pressure with depth, can be obtained by calculating separately the

maximum pressure exerted by each individual sub-layer, taking into consideration the existing conditions of T_0, Θ, S_i or n.

Recommendations for further work:

1. Lateral thrust exerted by a frozen soil layer should be investigated under different conditions of lateral restraint other than radial.

2. Studies conducted on the magnitude of lateral thrust should be extended to fine-grained soils, where unfrozen water content in a frozen soil will be an important influencing parameter.

3. More work to establish the relationship between air and ground temperature is required, also the influence of the rate of air temperature change on the rate of soil temperature change should be studied in different regions of Canada.

4. Further work should be done on frozen soils to evaluate their coefficients of thermal expansion and the Poisson ratios applicable to plastic and elastic strain components in the frozen soil.

REFERENCES

Aldrich, H.P., (1956), "Frost Penetration Below Highway and Airfield Pavements", Highway Res. Board, Bull. 135, pp 124-144.

Assur, A., (1959), "Maximum Lateral Pressure Exerted by Ice Sheets", I.A.H.R. 8th Congress, Vol. III, p. 22-SI-1.

Brown, E., and Clark, G., (1932), "Ice Thrust in Connection with Hydro-Electric Plant", The Engineering Journal, January, 1932, pp. 18-25.

Brown, R.J.E., (1963), "Relation Between Mean Annual Air and Ground Temperatures in the Permafrost Region of Canada", N.R.C., Canada, Division of Building Research, Research Paper No. 296.

Drouin, M., (1966), "Static Ice Force on Extended Structures", Proceedings of Conference on Ice Pressures Against Structures, held at Laval University, Nov. 1966, N.R.C. No. 9851.

Feigen, M., (1953), "A Note on Poisson's Ratio", Readers' Forum, Journal of the Aeronautical Sciences, July 14, 1953, p. 785.

Gold, L.W., (1958), "Some Observations on the Dependence on Strain on Stress for Ice", Can. J. Phys., Vol. 36, pp. 1265-1275.

Gold, L.W., (1965), "The Initial Creep of Columnar-Grained Ice", Can. J. Phys., Vol. 43, pp. 1414-1434.

Gold., L.W., (1966), "Elastic and Strength Properties of Fresh-Water Ice", Proceedings of Conference on Ice Pressures Against Structures, held at Laval University, Nov. 1966, N.R.C. No. 10401.

Gold, L.W., (1967), "Some Bulk Properties of Ice", N.R.C., Canada, Division of Building Research Technical Paper No. 256.

Goughnour, R.R., and Andersland, O.B., (1968) "Mechanical Properties of a Sand-Ice System", Journal of the Soil Mechanics Division, A.S.C.E., Vol 94, No. SM4, pp. 923-950.

REFERENCES cont'd

Jumikis, A.R. (1966), "Thermal Soil Mechanics", Rutgers
University Press, New Brunswick, New Jersey.

Korzhavin, K.N., (1962), "Influence de la Glace sur les
Ouvrages de Genie", Academie des Sciences de
l'U.R.S.S., Section de la Siberie.

Krausz, A.S., (1966), "Plastic Deformation of Fresh-
Water Ice", Proceedings of Conference on Ice
Pressures Against Structures, held at Laval
University, Nov. 1966, N.R.C. No. 9851.

Lobdell, H.L., Turner, K.A., and Jumikis, A.R., (1957),
"Study of Subsurface Temperature in Six Soils
During the Winter of 1953-1954", Highway Res. Board
Bull. 168, p. 123.

Lofquist, B., (1952), "Ice Pressure Against Dams: Studies
of the Effects of Temperature Variations", Proceedings
A.S.C.E. Vol. 78, Separate No. 160.

McRostie, G.C. and Schriever, W.R., (1967), "Frost Pressures
in the Tie-Back System at the National Arts Centre
Excavation", N.R.C., Canada, Division of Building
Research, Research Paper No. 309.

Monfore, G.E., (1952), "Ice Pressure Against Dams:
Experimental Investigations by the Bureau of
Reclamation", Proceedings, A.S.C.E., Vol. 78,
Technical Separate No. 162.

"Monthly Record", (1952-1969) Meteorological Observations
in Canada, by Department of Transport, Meteorological
Division.

Royen, N., (1922), "Ice Pressure with Temperature"
(Translation from Swedish), SIPRE TR- 45, 1955,
U.S.A. C.R.R.E.L., Hanover, N.H.

Tsytovich, N.A., (1960), "Bases and Foundations on Frozen
Soil", Highway Res. Board, Special Report 58.

Tsytovich. N.A., (1959), "Basic Mechanics of Freezing,
Frozen and Thawing Soils", Academy of Sciences of
the U.S.S.R., N.R.C., Canada, Technical Translation
No. 1239, 1966.

REFERENCES cont'd

Voitkovskii, K.F., and Krylov, M.M., (1959), "Use of Ice,
    Snow and Frozen Soil in Engineering Structures",
    Academy of Sciences of the U.S.S.R., N.R.C., Canada,
    Technical Translation No. 1267, 1967.

Voitkovskii, K.F., (1960), "The Mechanical Properties of
    Ice", Izd. Akad Nauk, SSSR, Moscow. Am. Met. Soc.
    Office of Technical Services, U.S. Dept. of Commerce,
    Washington 25, D.C. Translation, AMS-T-R-391.

Yong, R.N., and Warkentin, B.P., (1966), "Introduction to
    Soil Behaviour", The Macmillan Co., New York.
    pp. 398-405.

A P P E N D I X
F I G U R E S
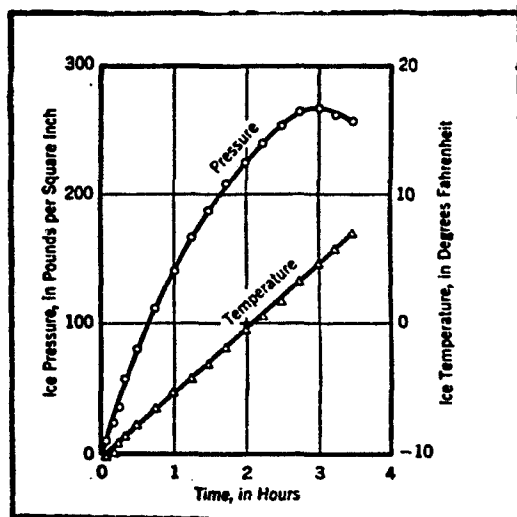
Fig. 1 Typical Ice Pressure Test
(Monfore, 1952)
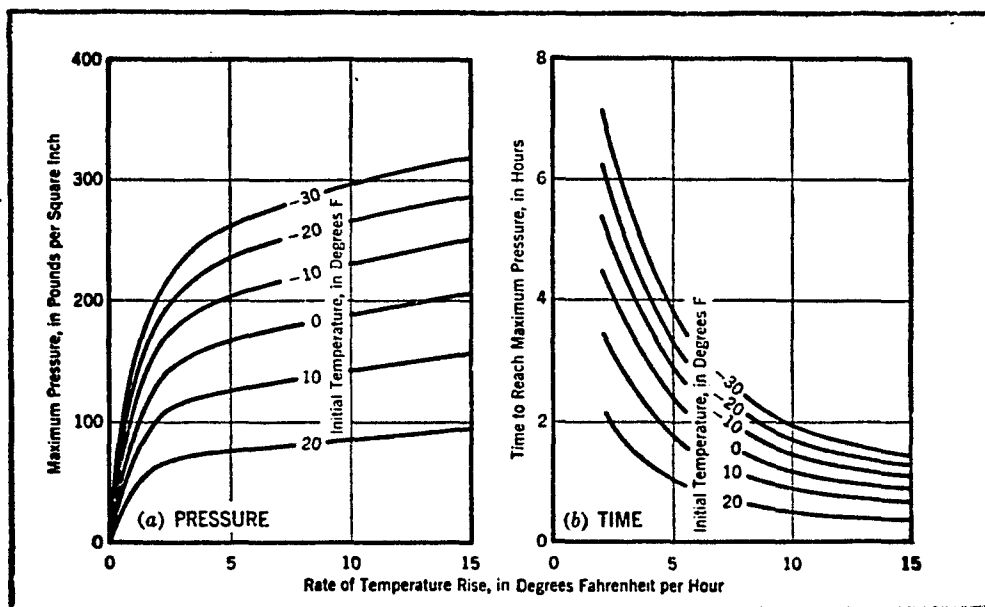
Fig. 2 Maximum Ice Pressure and Time of Temperature
Rise Related to Rate of Ice Temperature Rise
(Monfore, 1952)
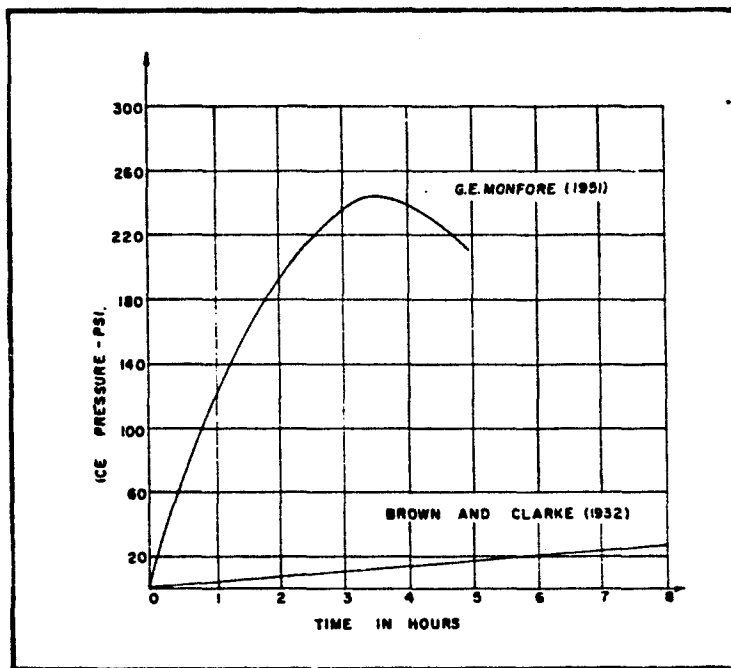
Fig. 3 Comparison Between the Results
of Two Ice Pressure Tests Carried Out
by Brown and Clarke (1932) and Monfore
(1951). (Drouin, 1966)
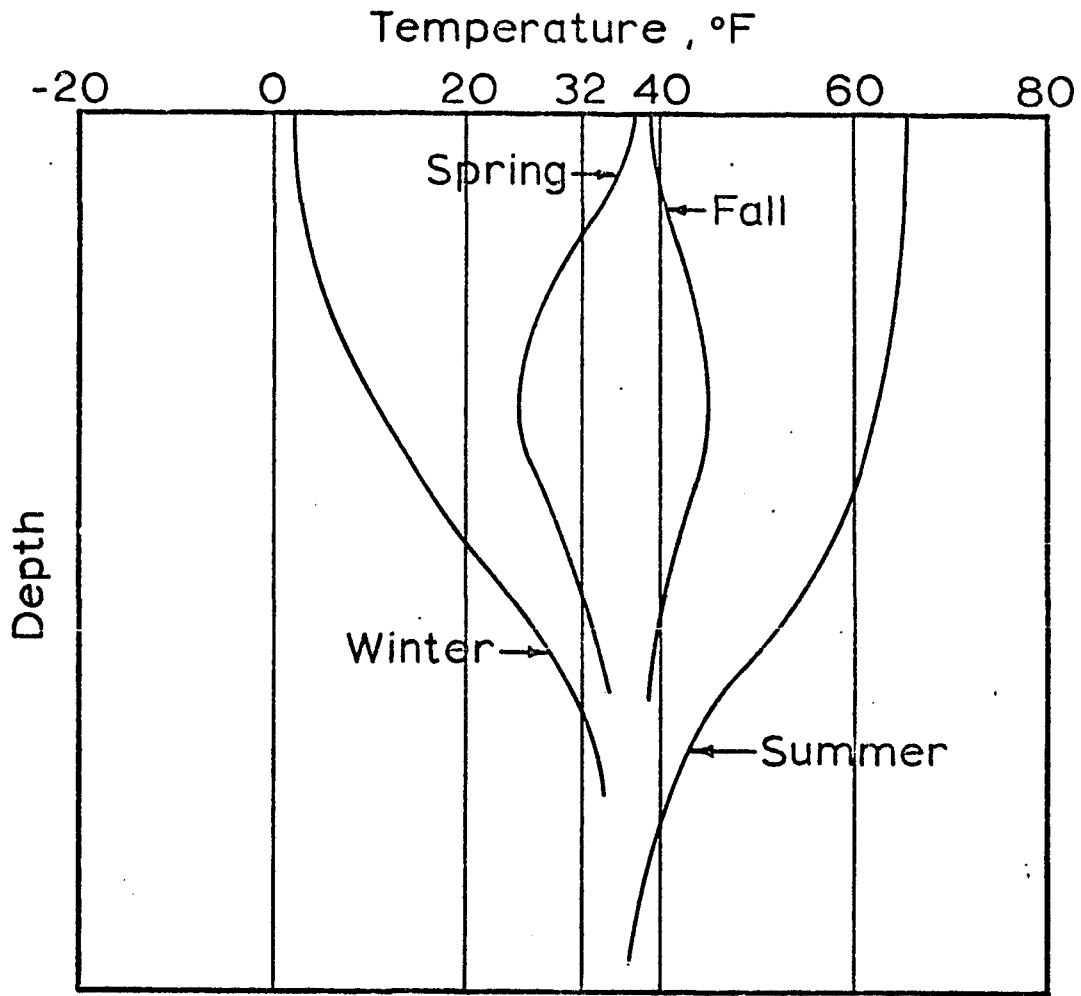
Fig. 4 Generalized Variation of Ground
Temperature with Depth
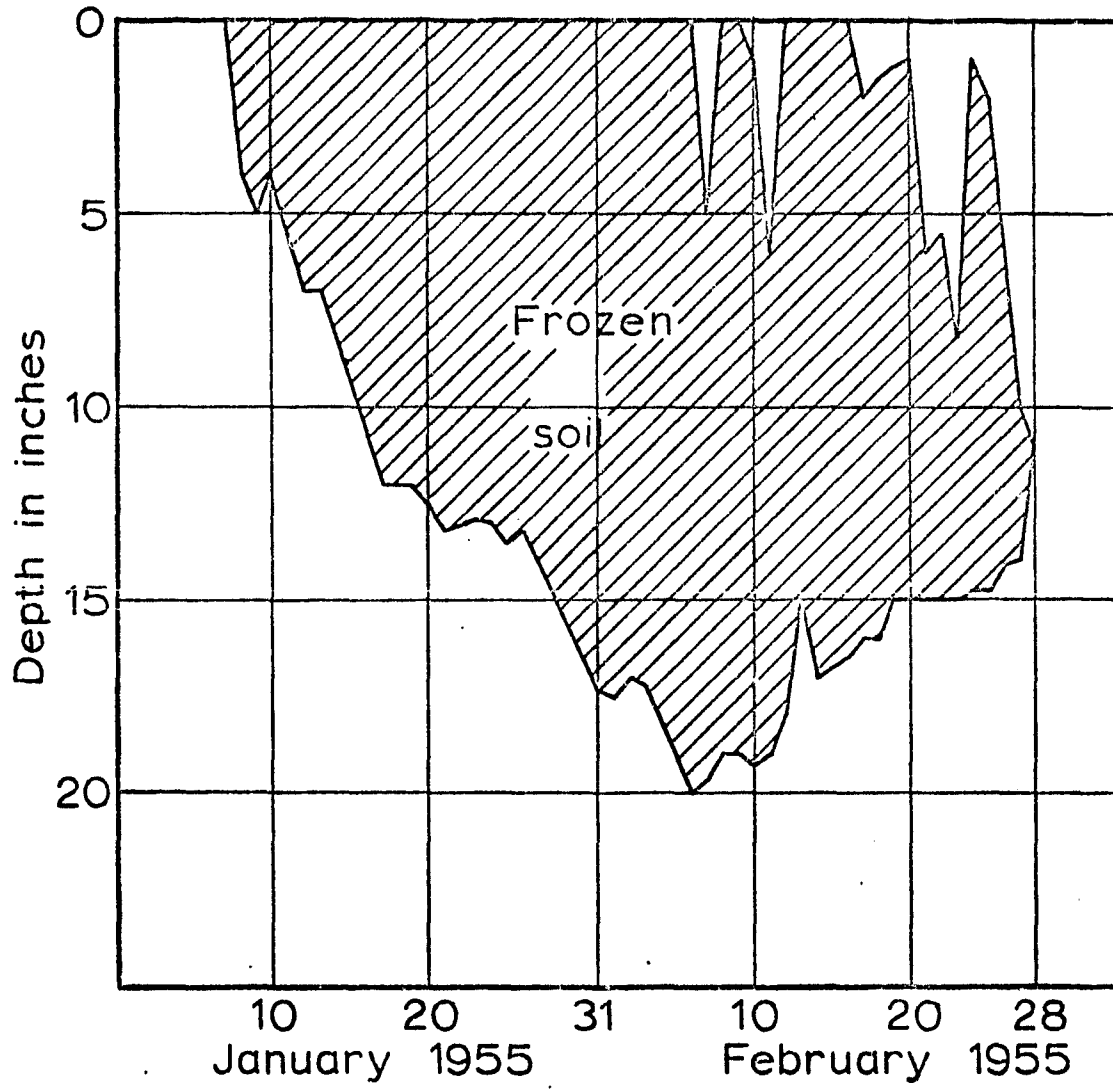
Fig. 5 Depth of $32°F$ Temperature
(Turner and Jumikis, 1956)

TYLER STANDARD SIEVE NUMBERS
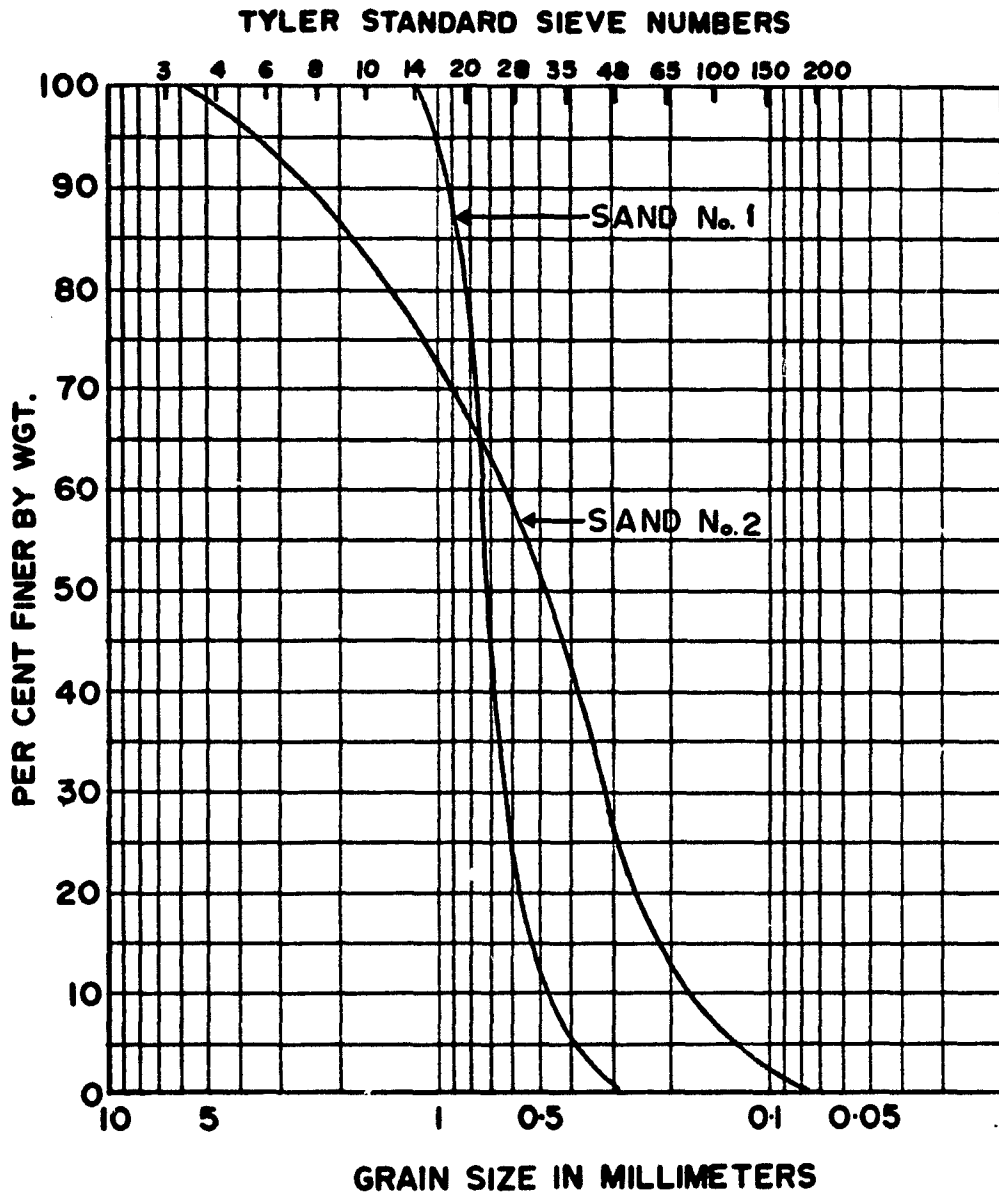
Fig. 6 Grain Size Distribution Diagram
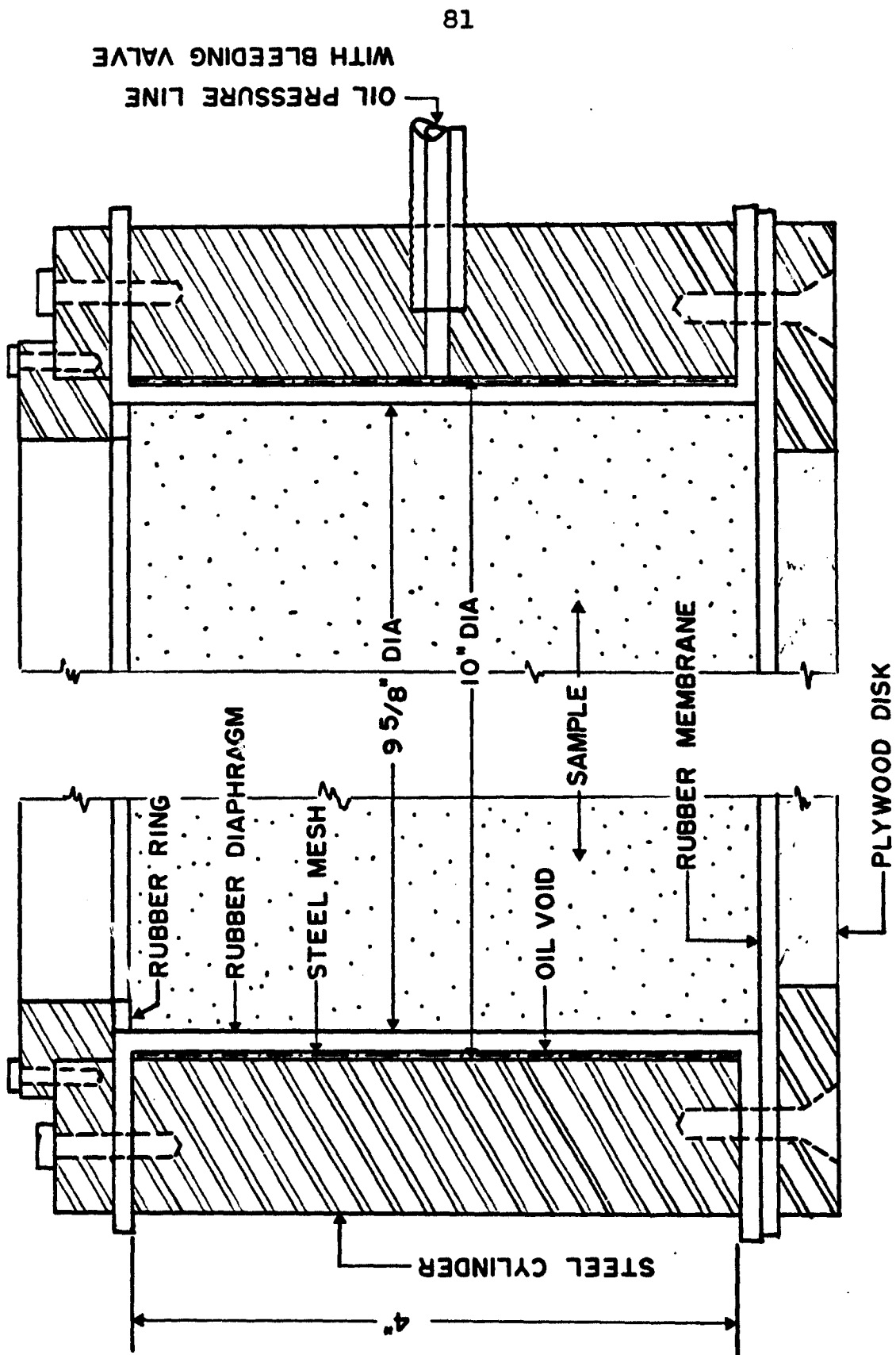
Fig. 7 Steel Cylinder with Rubber Diaphragm
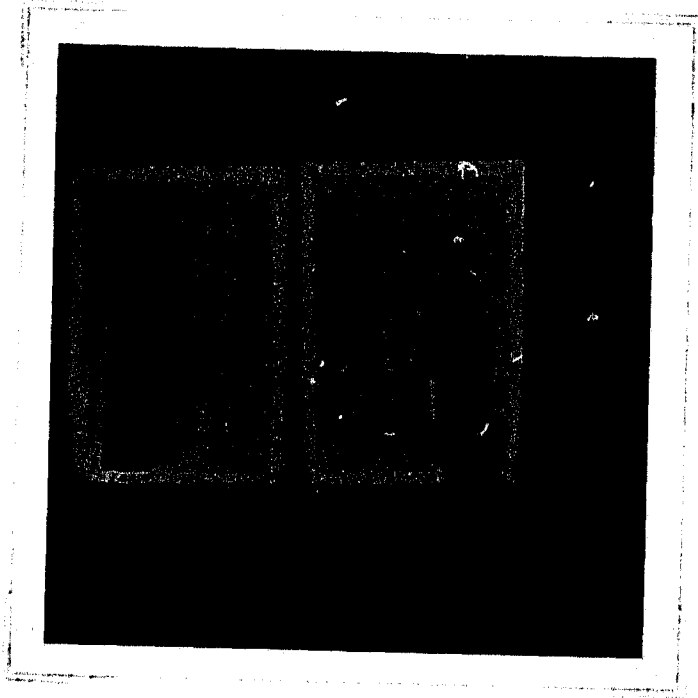
Fig. 8   Strain Gauges Coated with Sand Particles
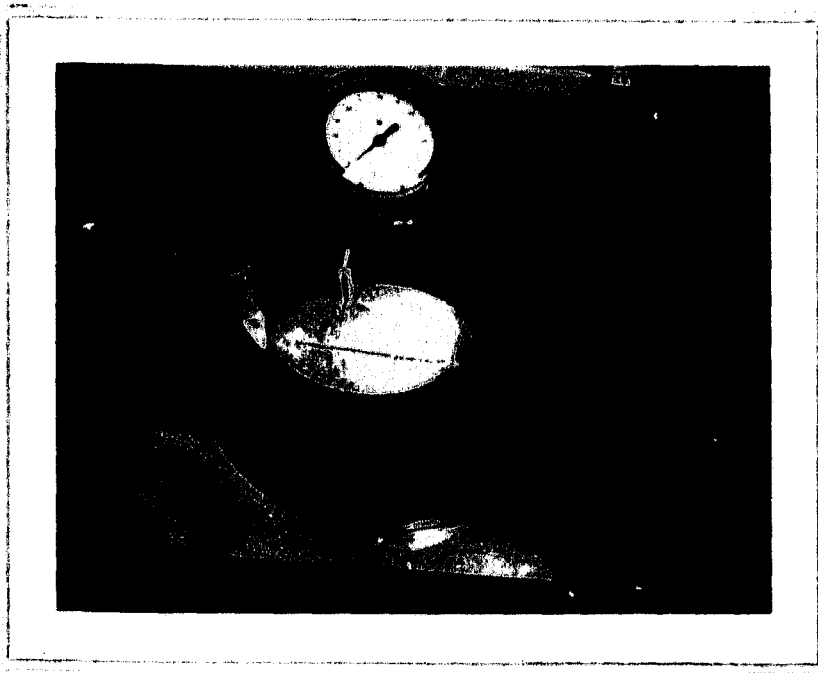
Fig. 9   Strain Gauges Being Placed into the Sample
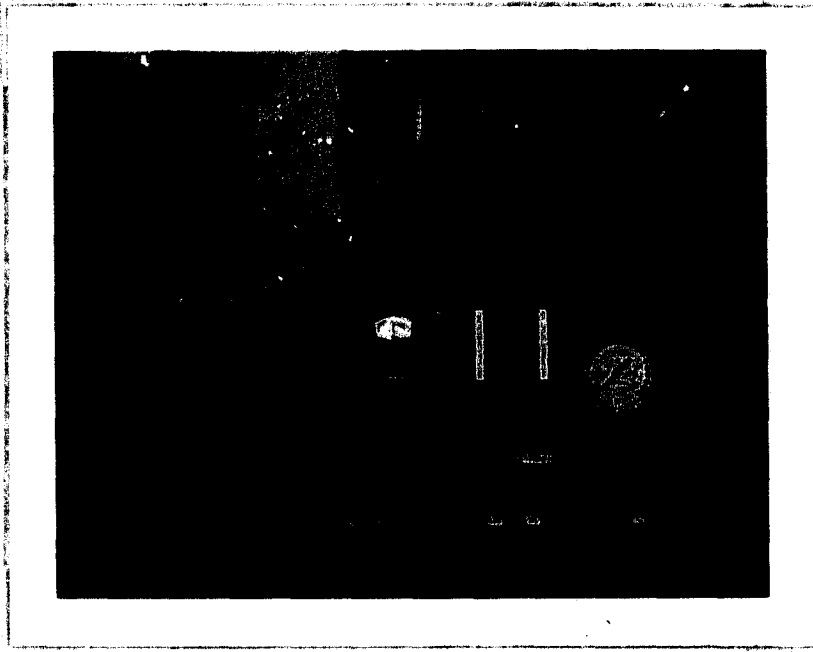
Fig. 10   Equipment and Freezing Chamber Used
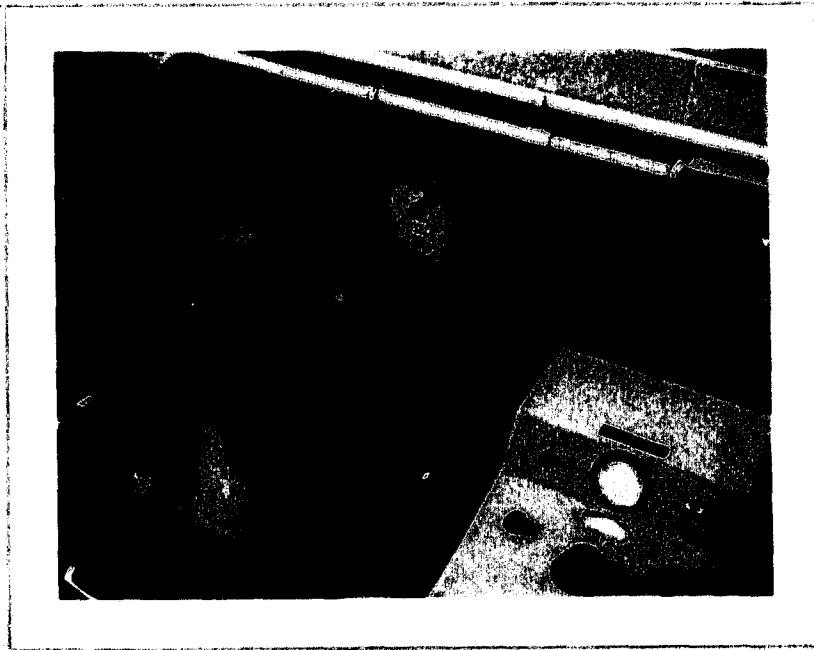
Fig. 11   Maihak Transmitter MDS 53 Placed Inside
Pressure Cylinder
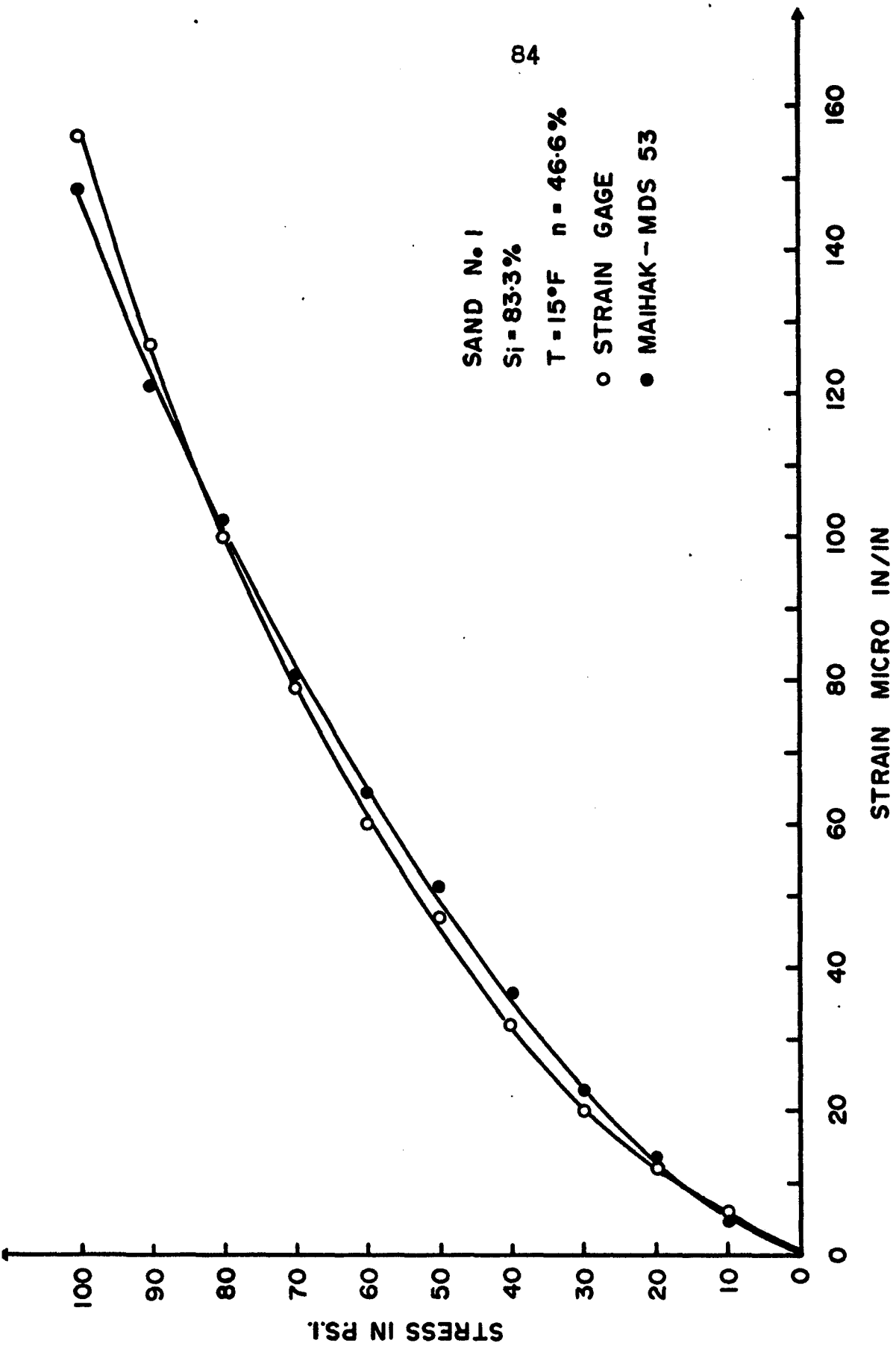
Fig. 12 Comparison Between Stress–Strain Curves Recorded by Strain Gage and
Maihak Transmitter MDS 53, at Constant Temperature of 15°F

SAND N. 1
Si = 83.3%
T = 15°F   n = 46.6%
o STRAIN GAGE
● MAIHAK – MDS 53

STRAIN MICRO IN/IN

STRESS IN P.S.I.
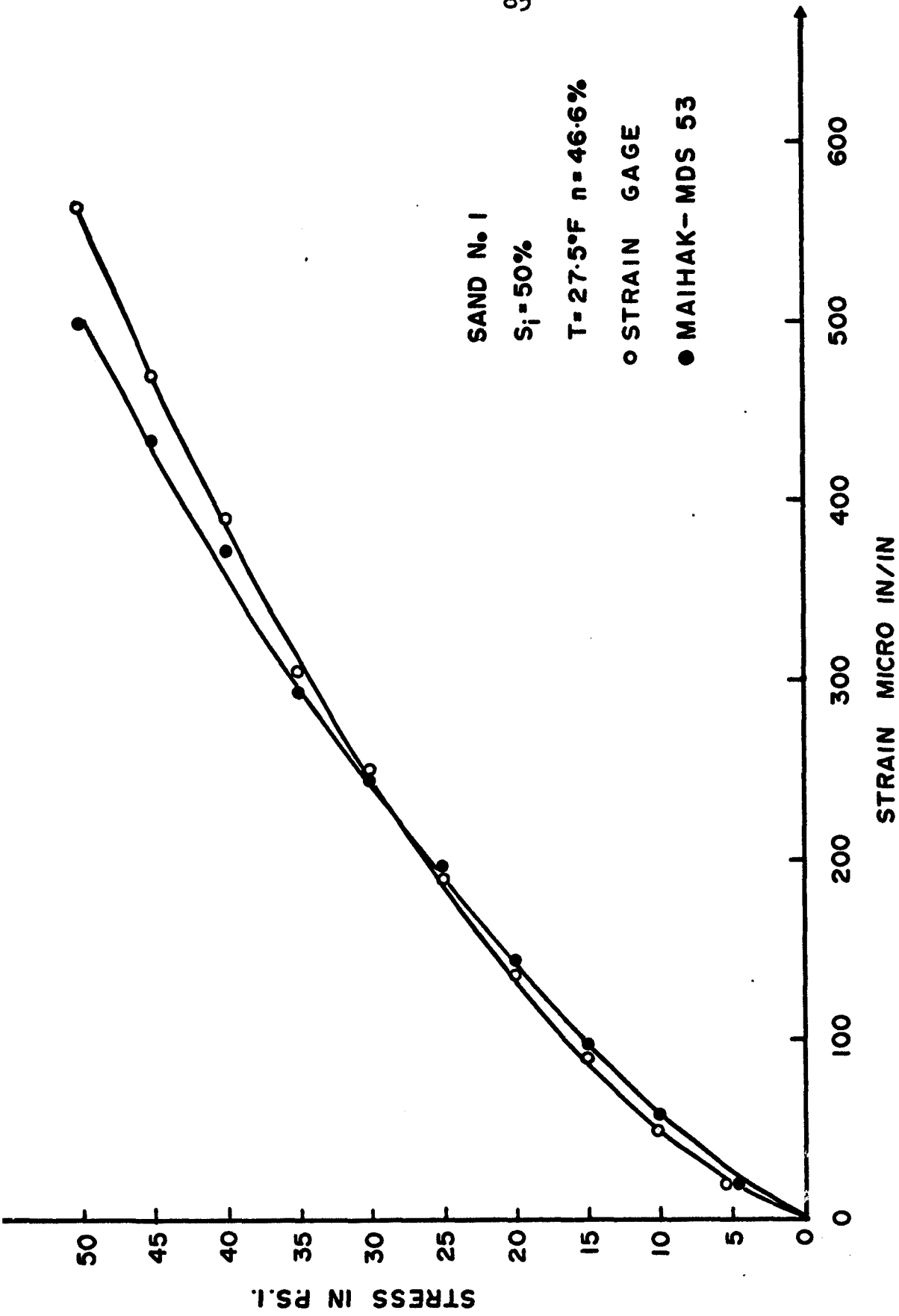
Fig. 13 Comparison Between Stress–Strain Curves Recorded by Strain Gage and
Maihak Transmitter MDS 53, at Constant Temperature of 27.5°F
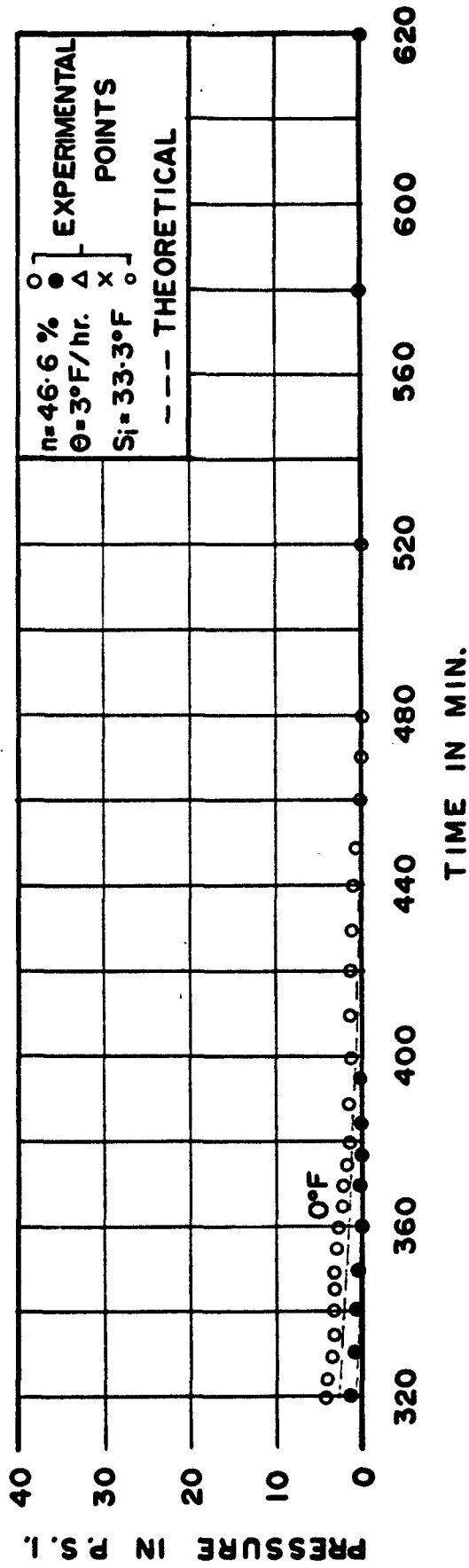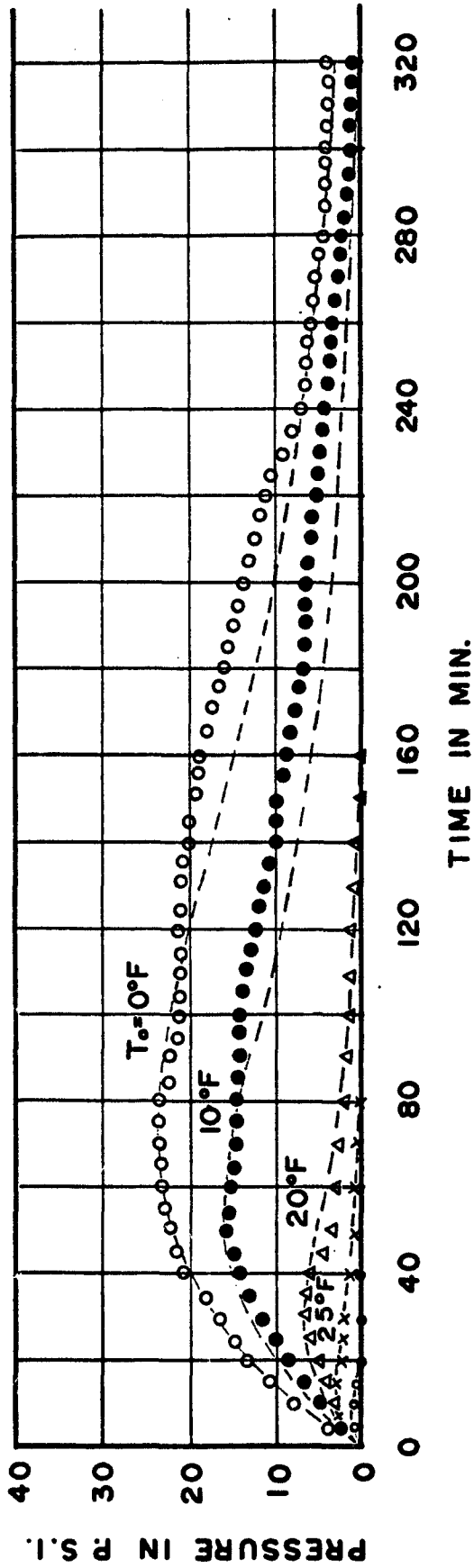
Fig. 14 Pressure-Time Curves for Temperature Rise of $3°F/hr$ and Ice Saturation 33.3% from the Indicated Initial Temperatures
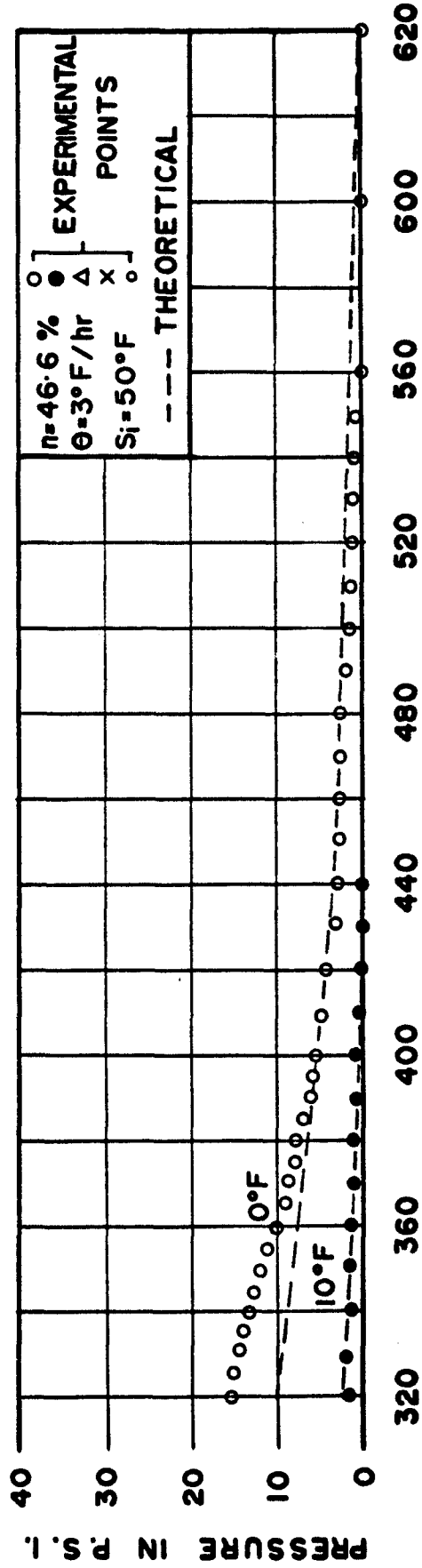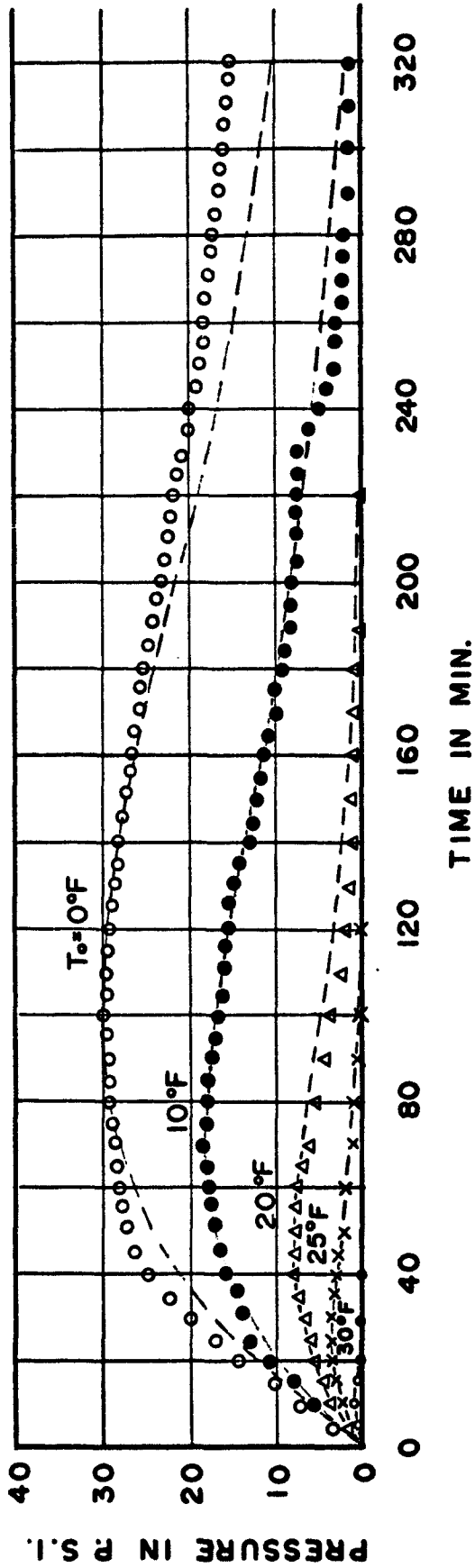
Fig. 15 Pressure-Time Curves for Temperature Rise of 3°F/hr and Ice Saturation 50% from the Indicated Initial Temperatures
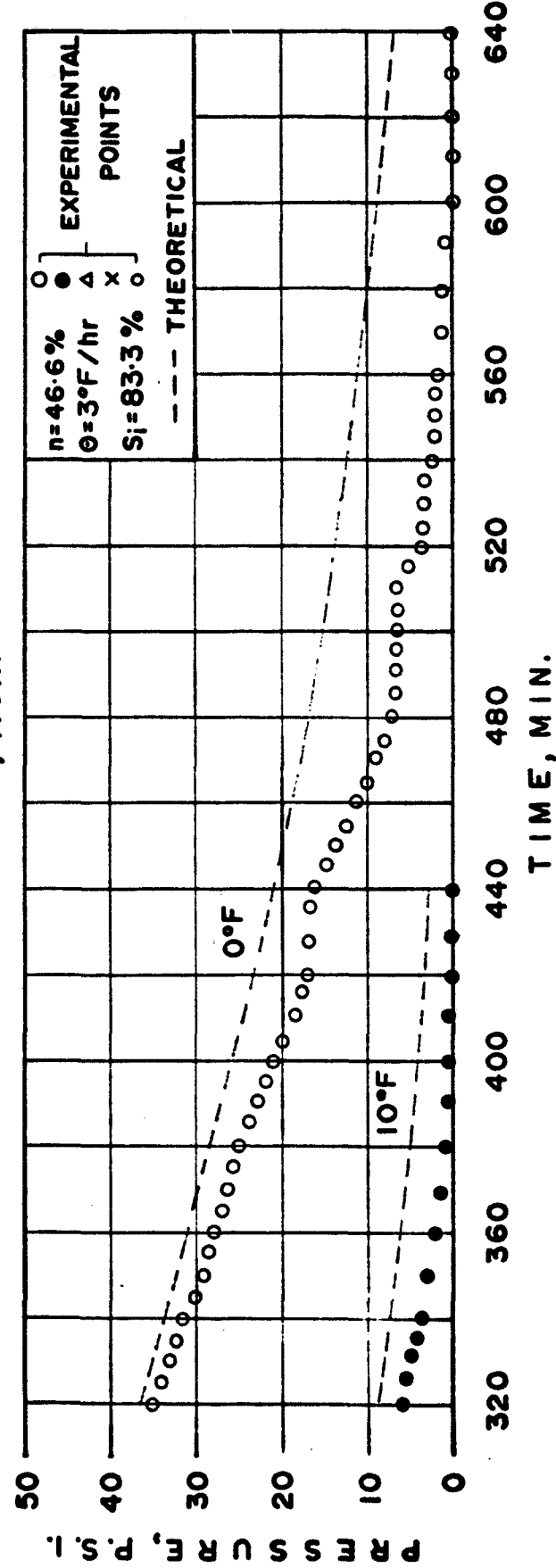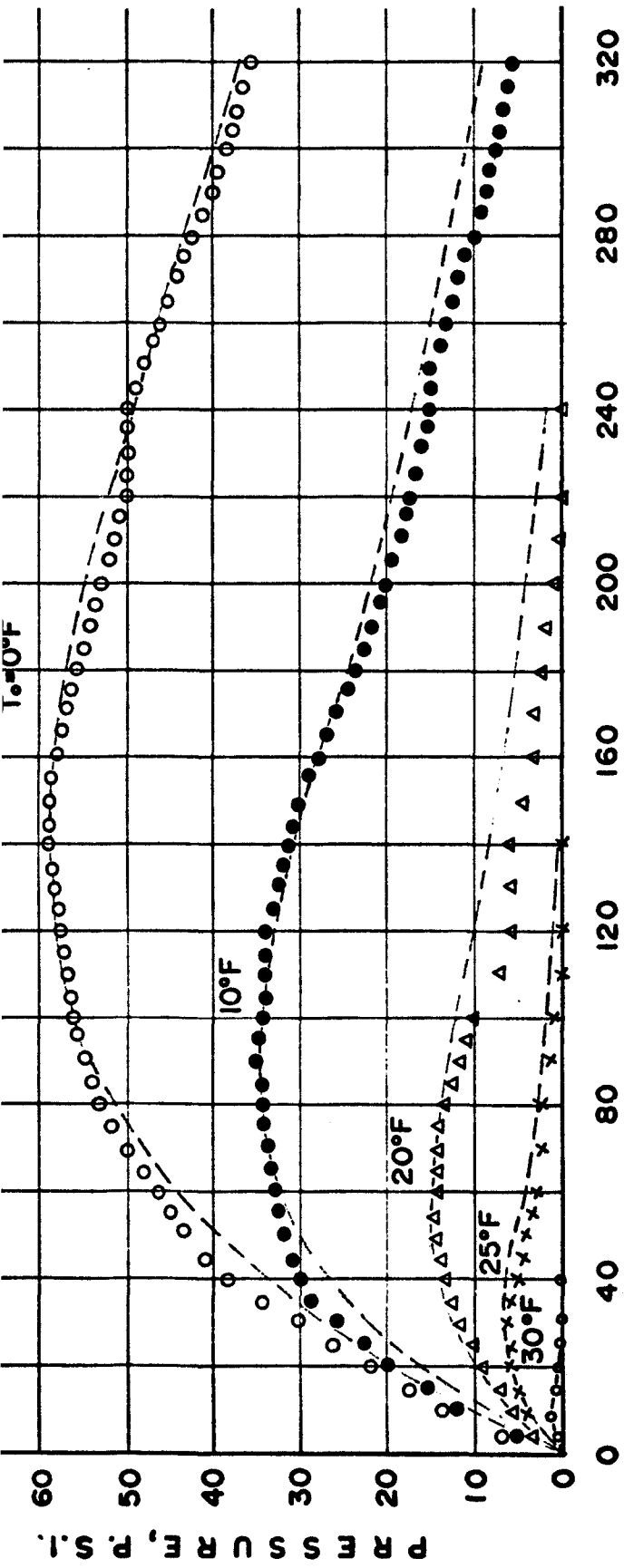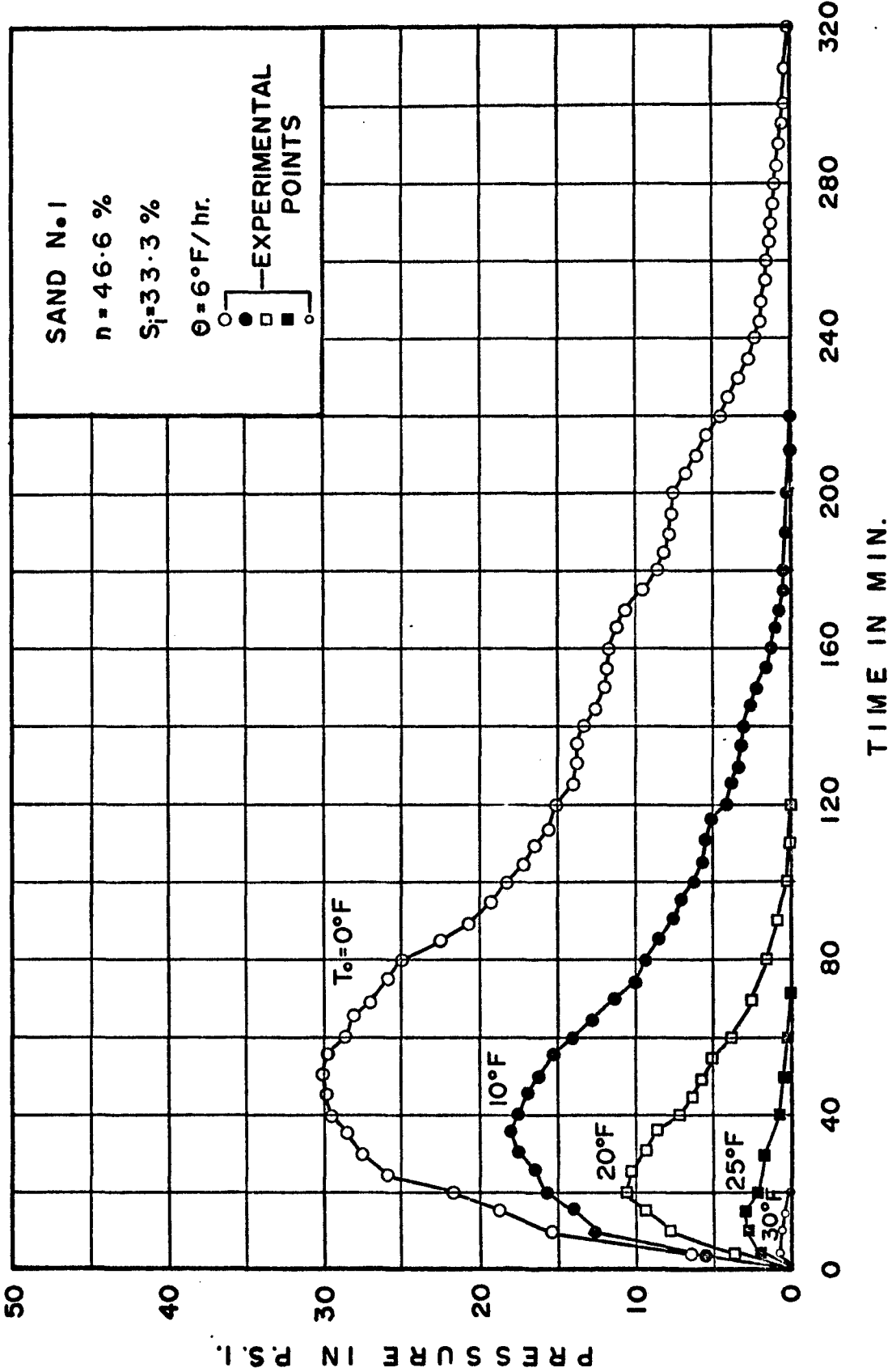
Fig. 16 Pressure-Time Curves for Temperature Rise of 3°F/hr and Ice
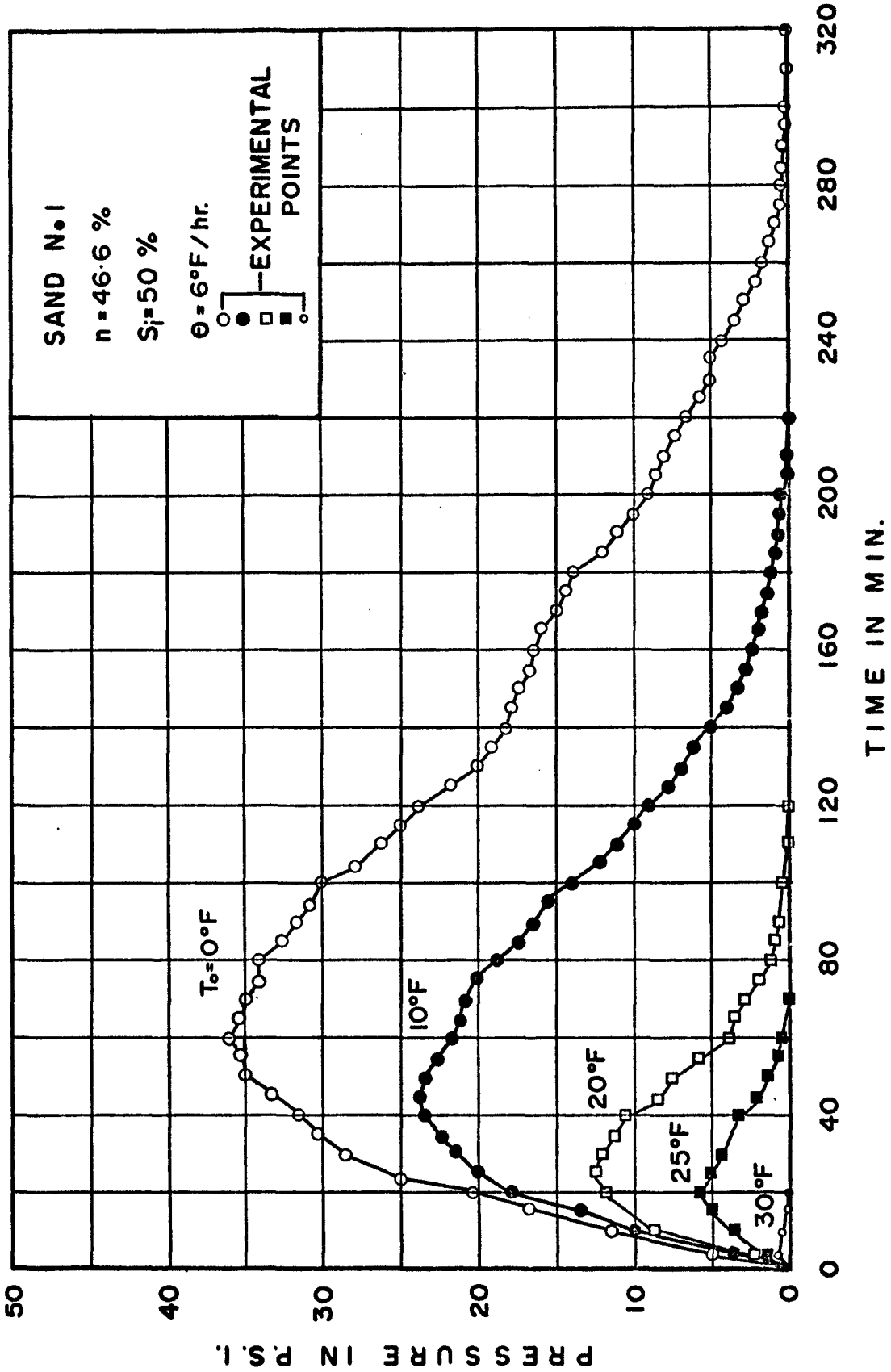Saturation 83.3% from the Indicated Initial Temperatures
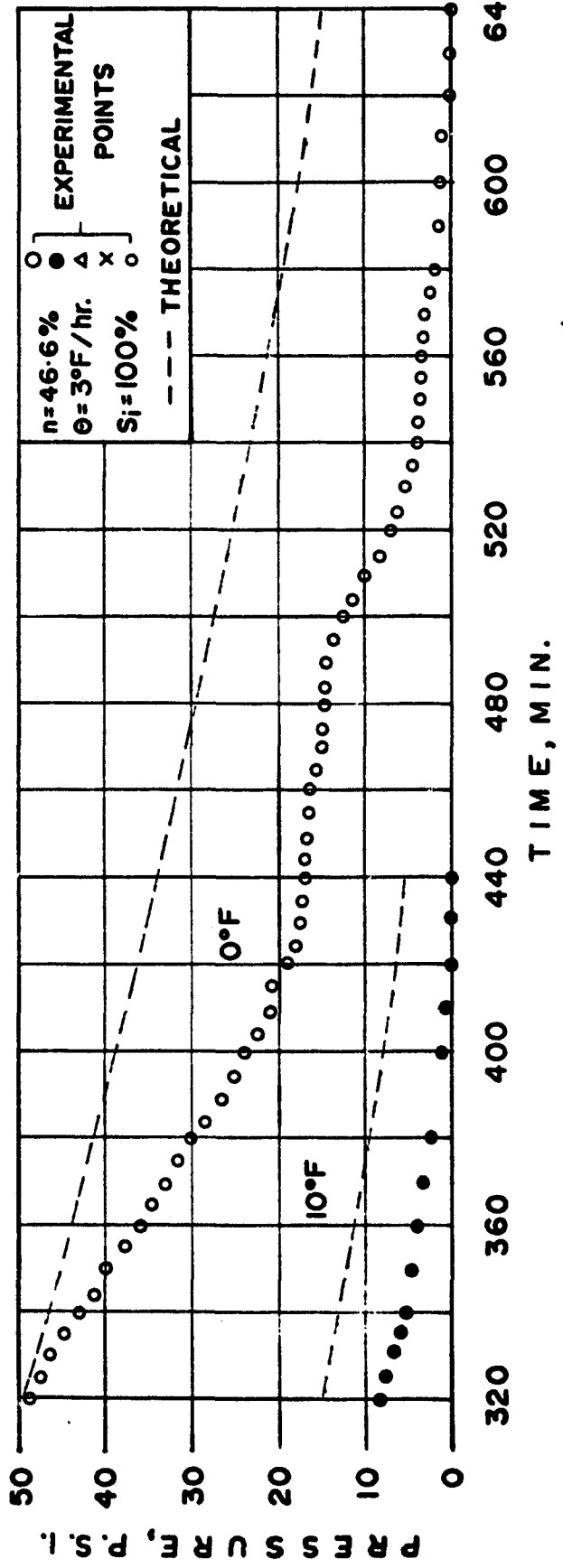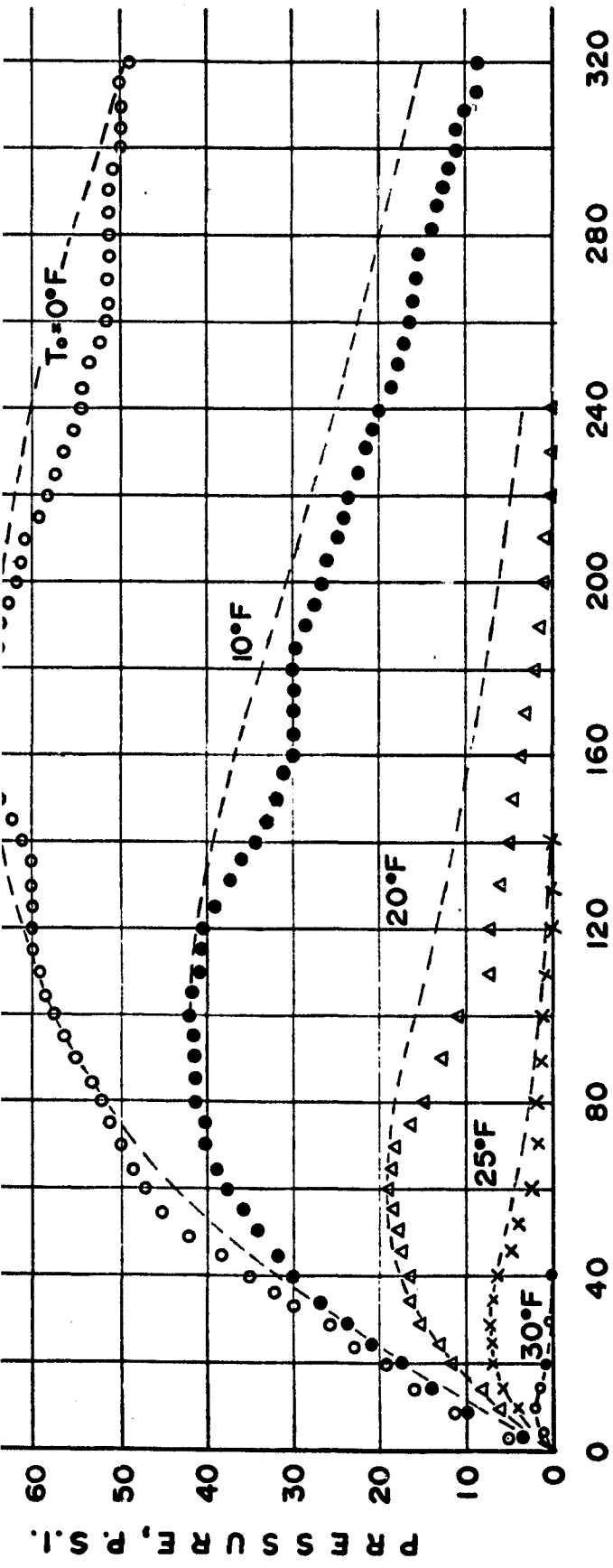
Fig. 17 Pressure-Time Curves for Temperature Rise of 3°F/hr and Ice Saturation 100% from the Indicated Initial Temperatures
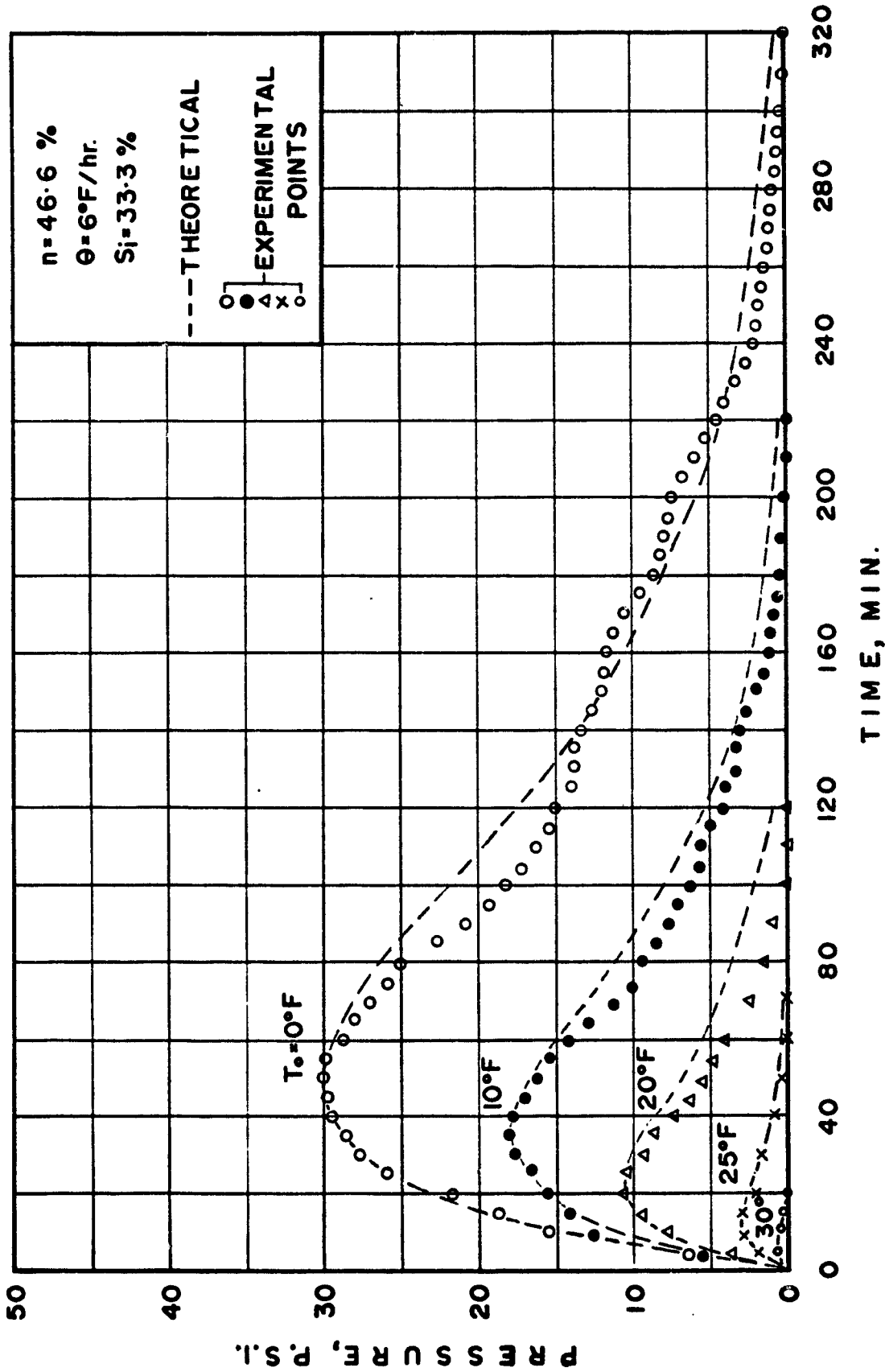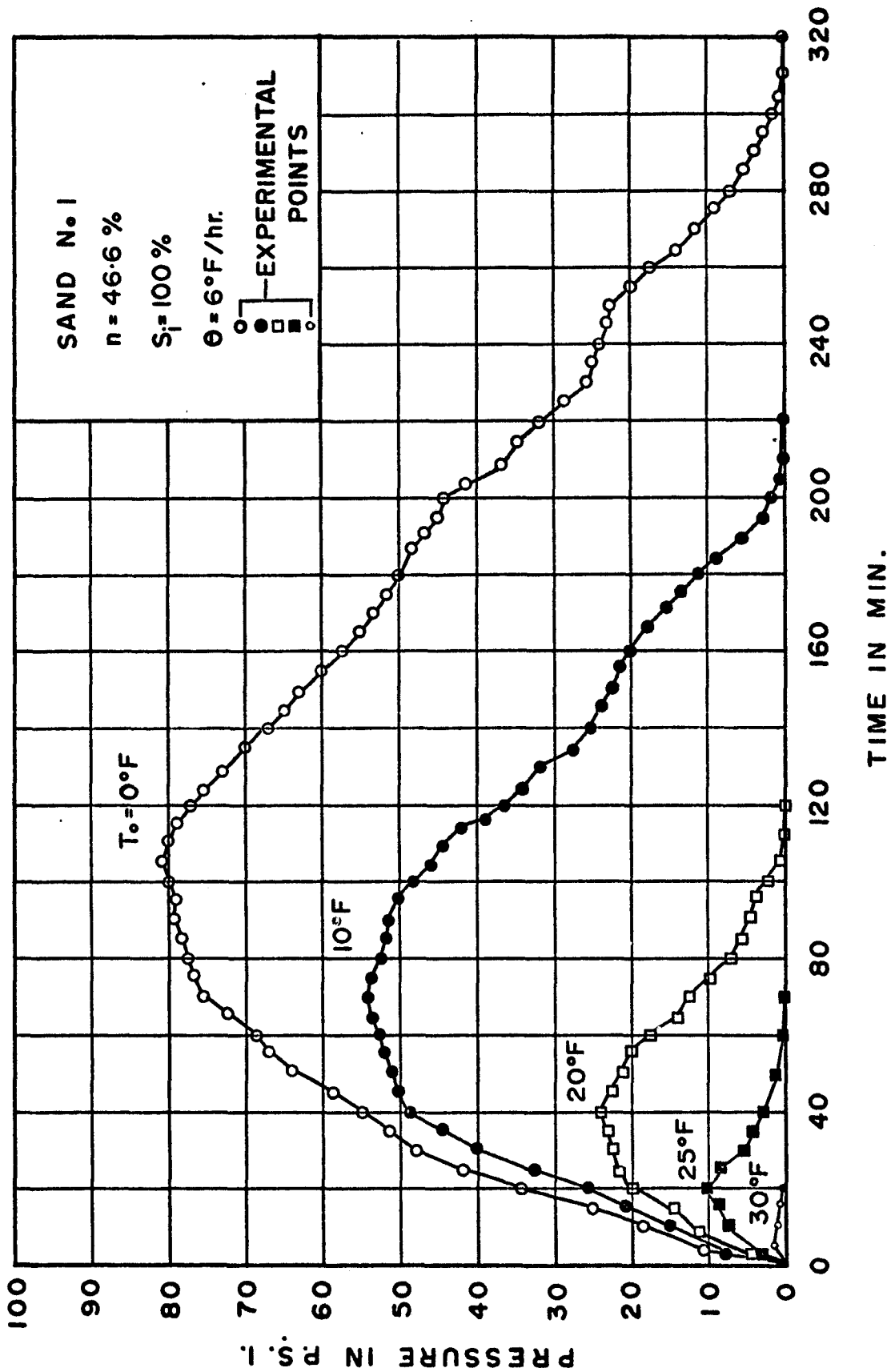
Fig. 18 Pressure-Time Curves for Temperature Rise of 6°F/hr and Ice Saturation 33.3% from the Indicated Initial Temperatures
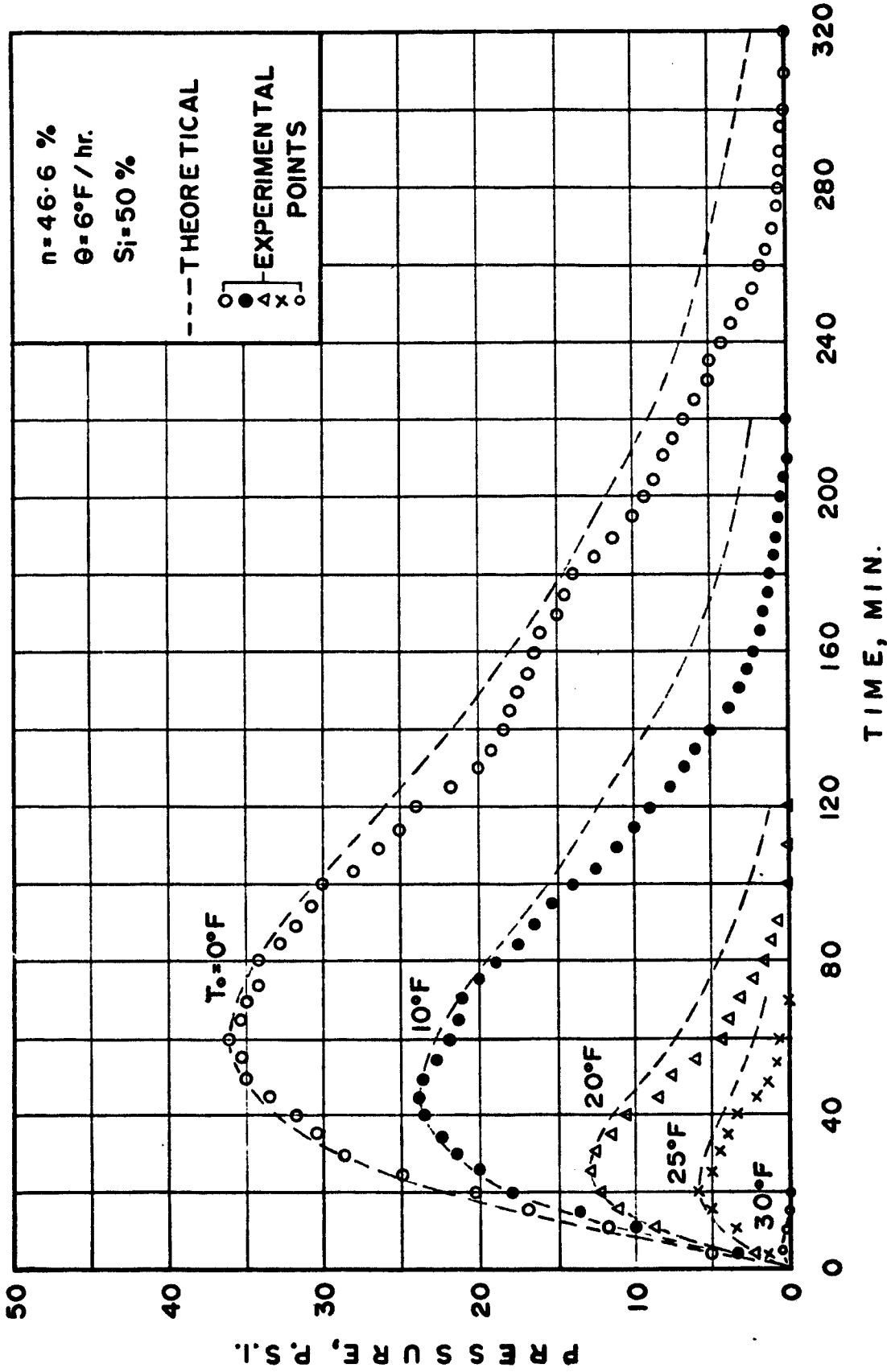
Fig. 19 Pressure-Time Curves for Temperature Rise of 6°F/hr and Ice
Saturation 50% from the Indicated Initial Temperatures
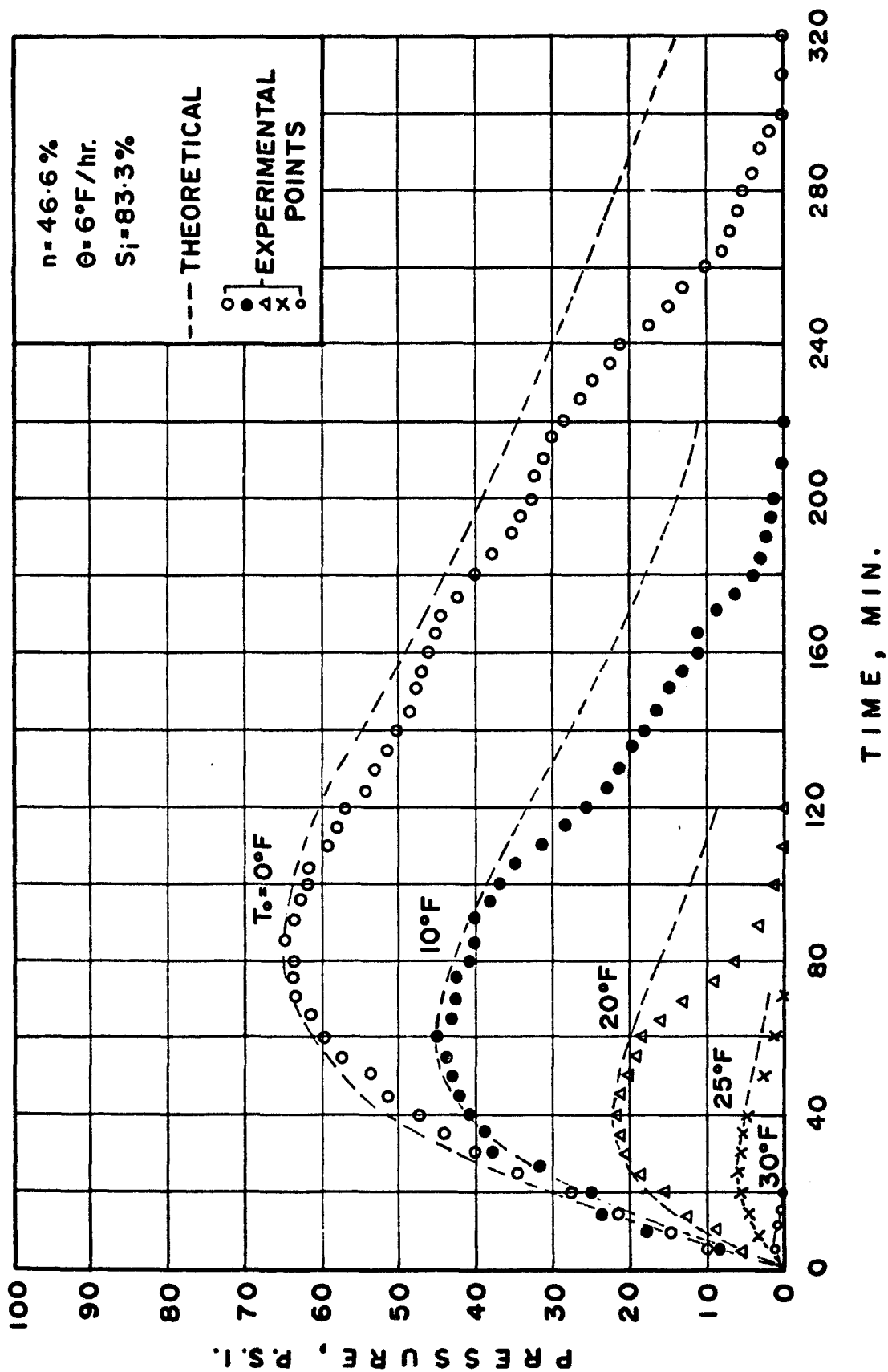
Fig. 20 Pressure-Time Curves for Temperature Rise of 6°F/hr and Ice Saturation 83.3% from the Indicated Initial Temperatures
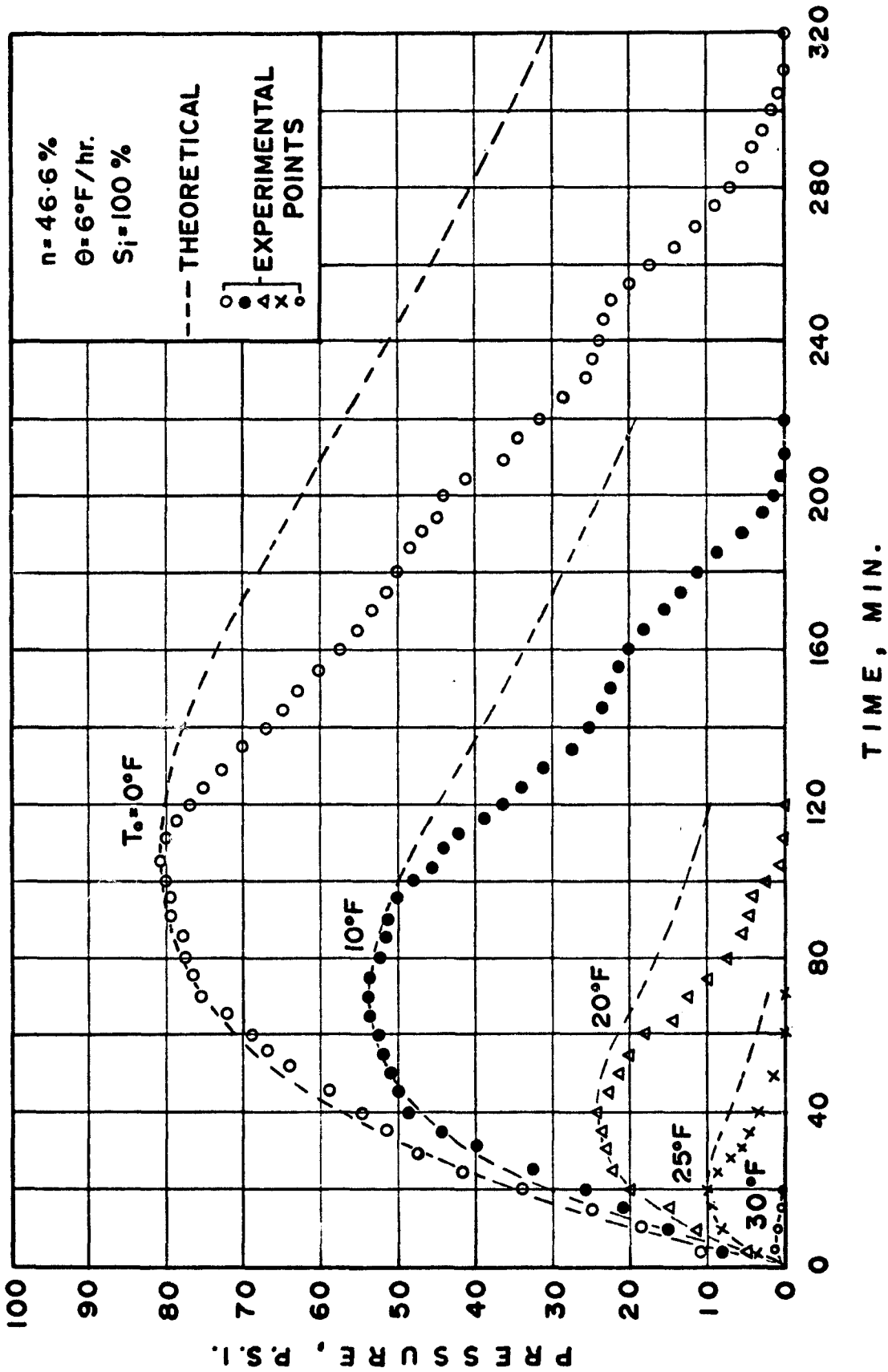
Fig. 21 Pressure-Time Curves for Temperature Rise 6°F/hr and Ice
Saturation 100% from the Indicated Initial Temperatures
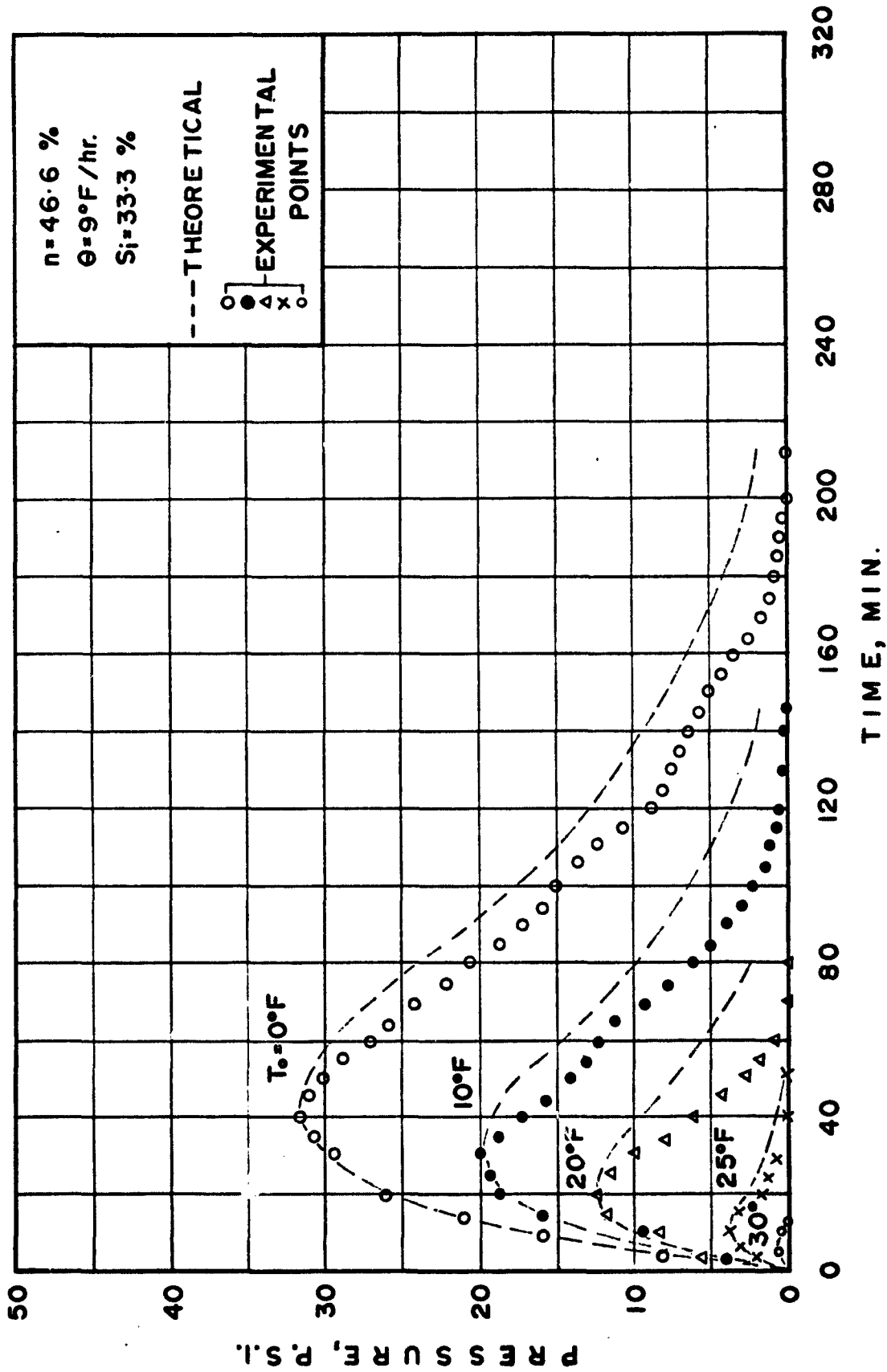
Fig. 22 Pressure-Time Curves for Temperature Rise 9°F/hr and Ice Saturation 33.3% from the Indicated Initial Temperatures
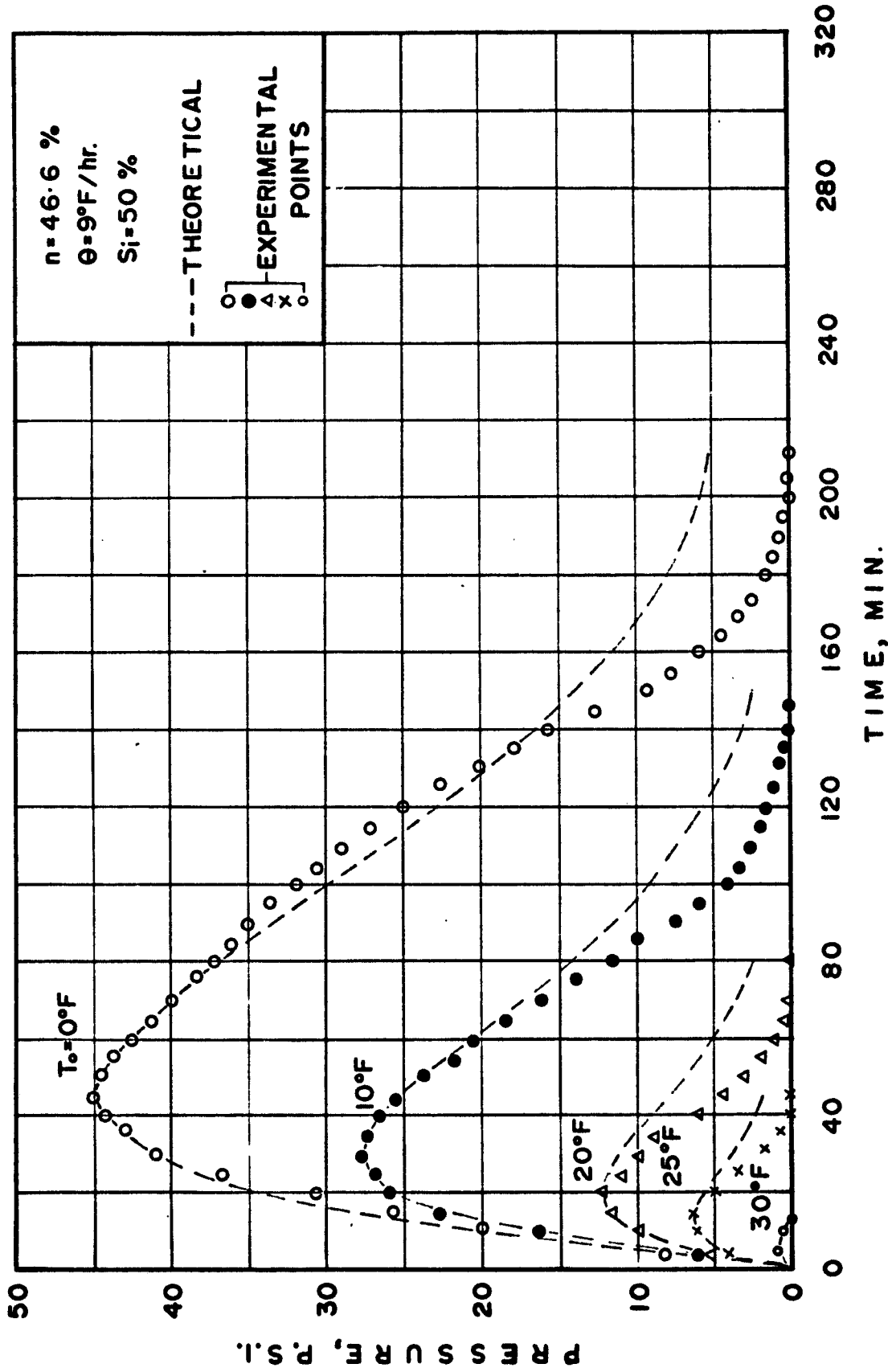
Fig. 23 Pressure-Time Curves for Temperature Rise 9°F/hr and Ice Saturation 50% from the Indicated Initial Temperatures
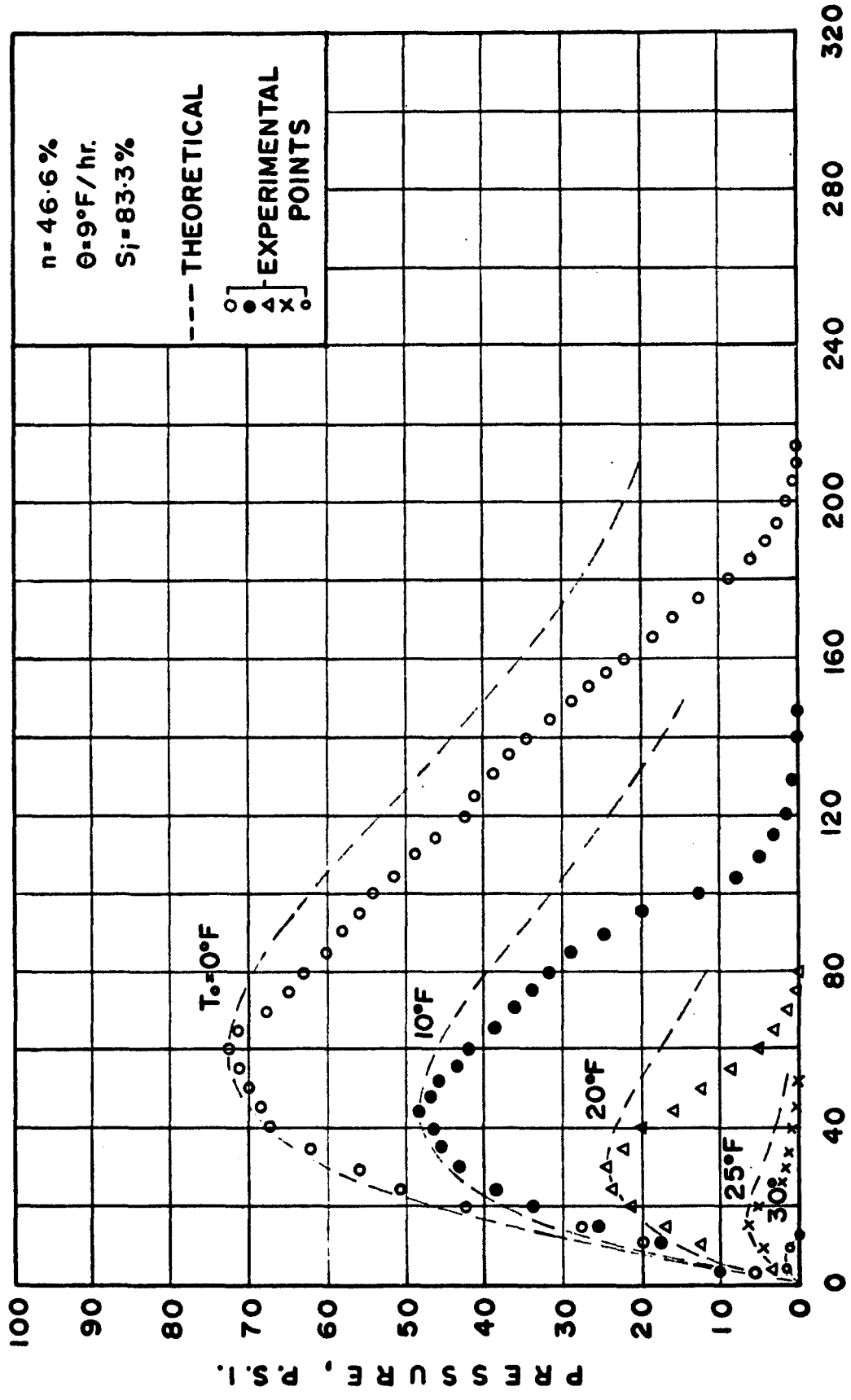
Fig. 24 Pressure-Time Curves for Temperature Rise 9°F/hr and Ice
Saturation 83.3% from the Indicated Initial Temperatures
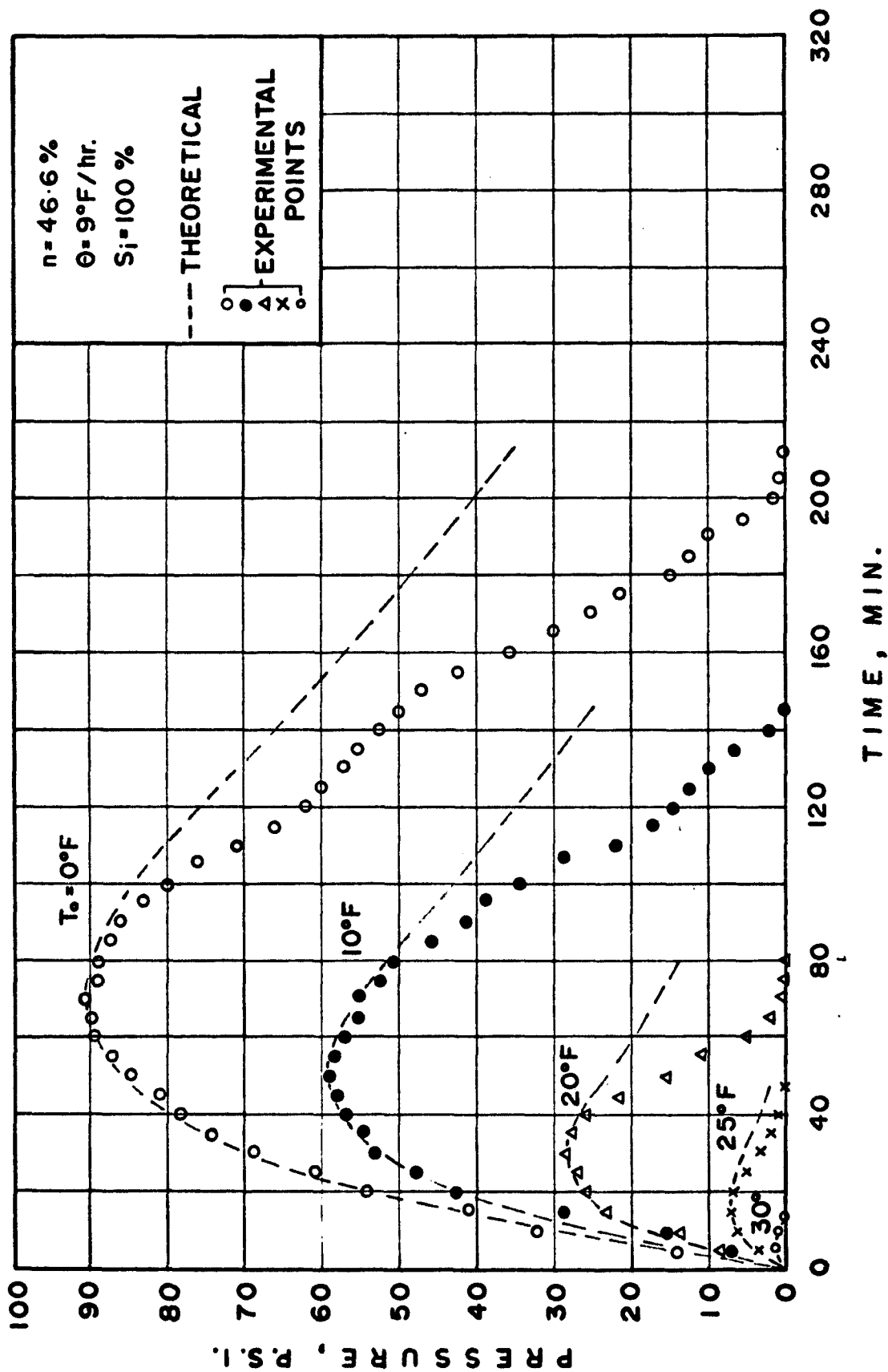
Fig. 25 Pressure-Time Curves for Temperature Rise 9°F/hr and Ice
Saturation 100% from the Indicated Initial Temperatues

Fig. 26 Pressure-Time Curves for Temperature Rise of 6°F/hr and Ice
Saturation 33.3% from the Indicated Initial Temperatures

Fig. 27 Pressure-Time Curves for Temperature Rise of 6°F/hr and Ice Saturation 50% from the Indicated Initial Temperatures

Fig. 28 Pressure-Time Curves for Temperature Rise 6°F/hr and Ice
Saturation 100% from the Indicated Initial Temperatures
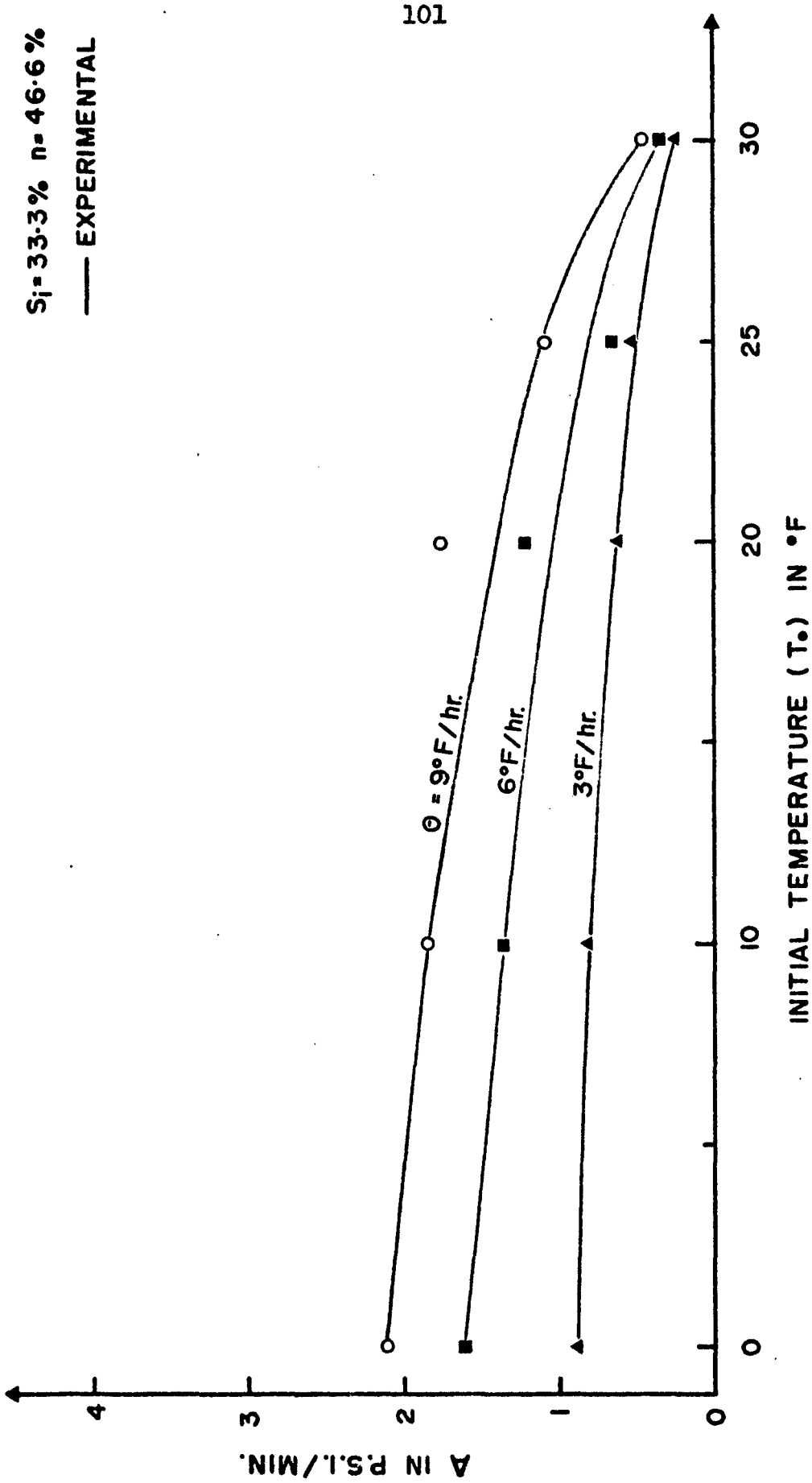
Fig. 29 Coefficient A vs. Initial Frozen Sand Temperatures
for Ice Saturation 33.3%
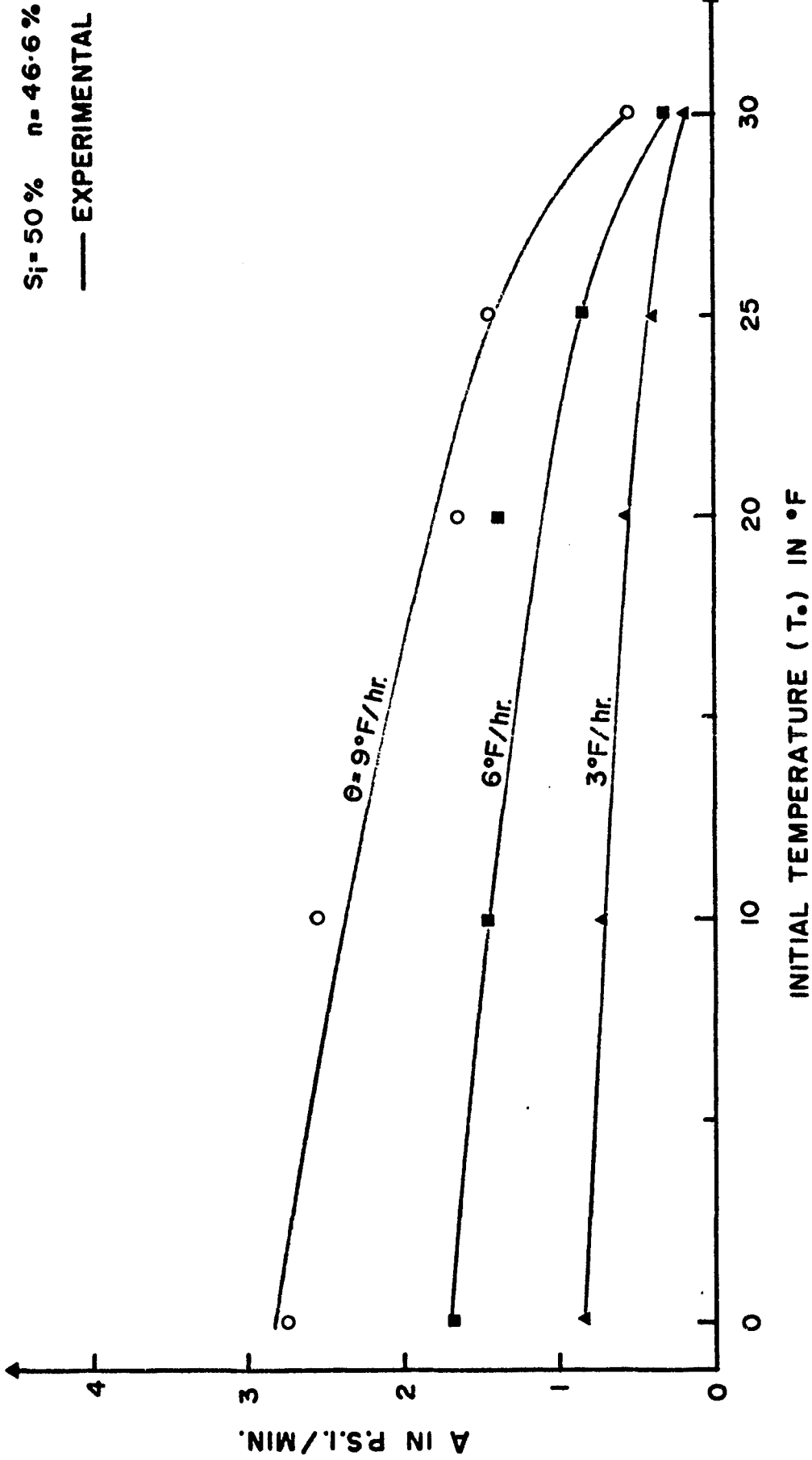
Fig. 30 Coefficient A vs. Initial Frozen Sand Temperature
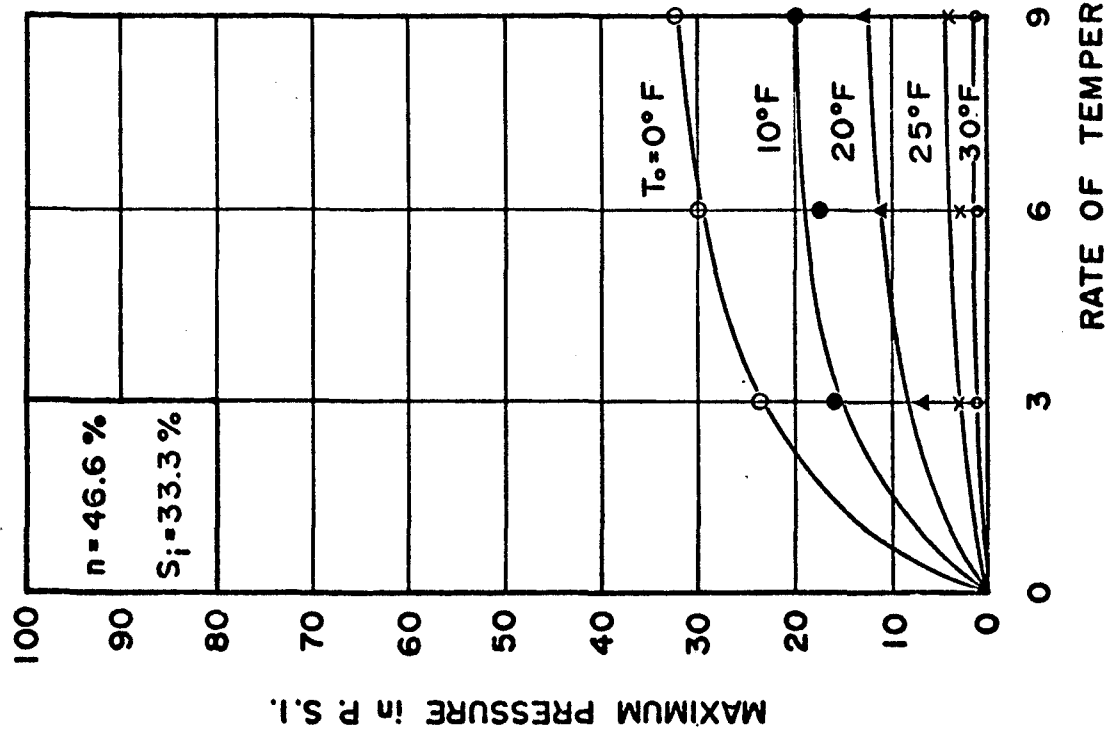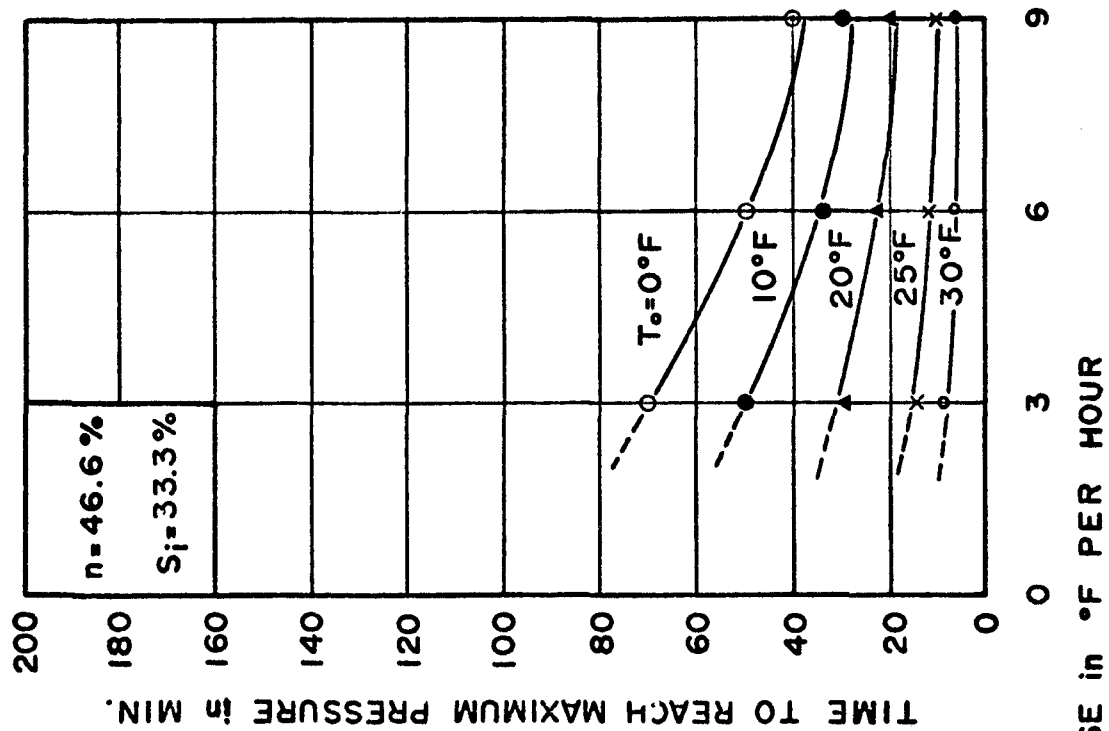for Ice Saturation 50%
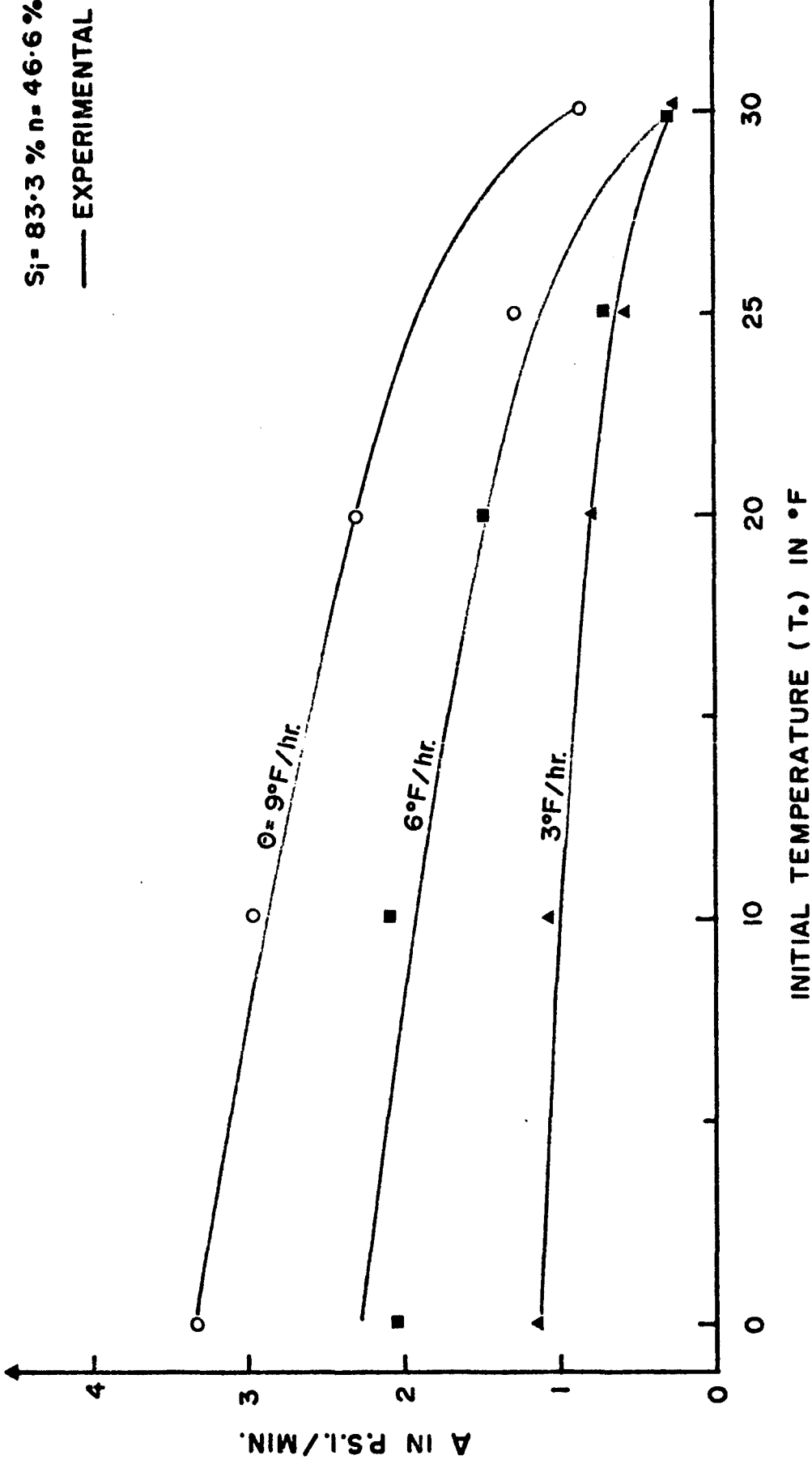
Fig. 31   Coefficient A vs. Initial Frozen Sand Temperature
for Ice Saturation 83.3%
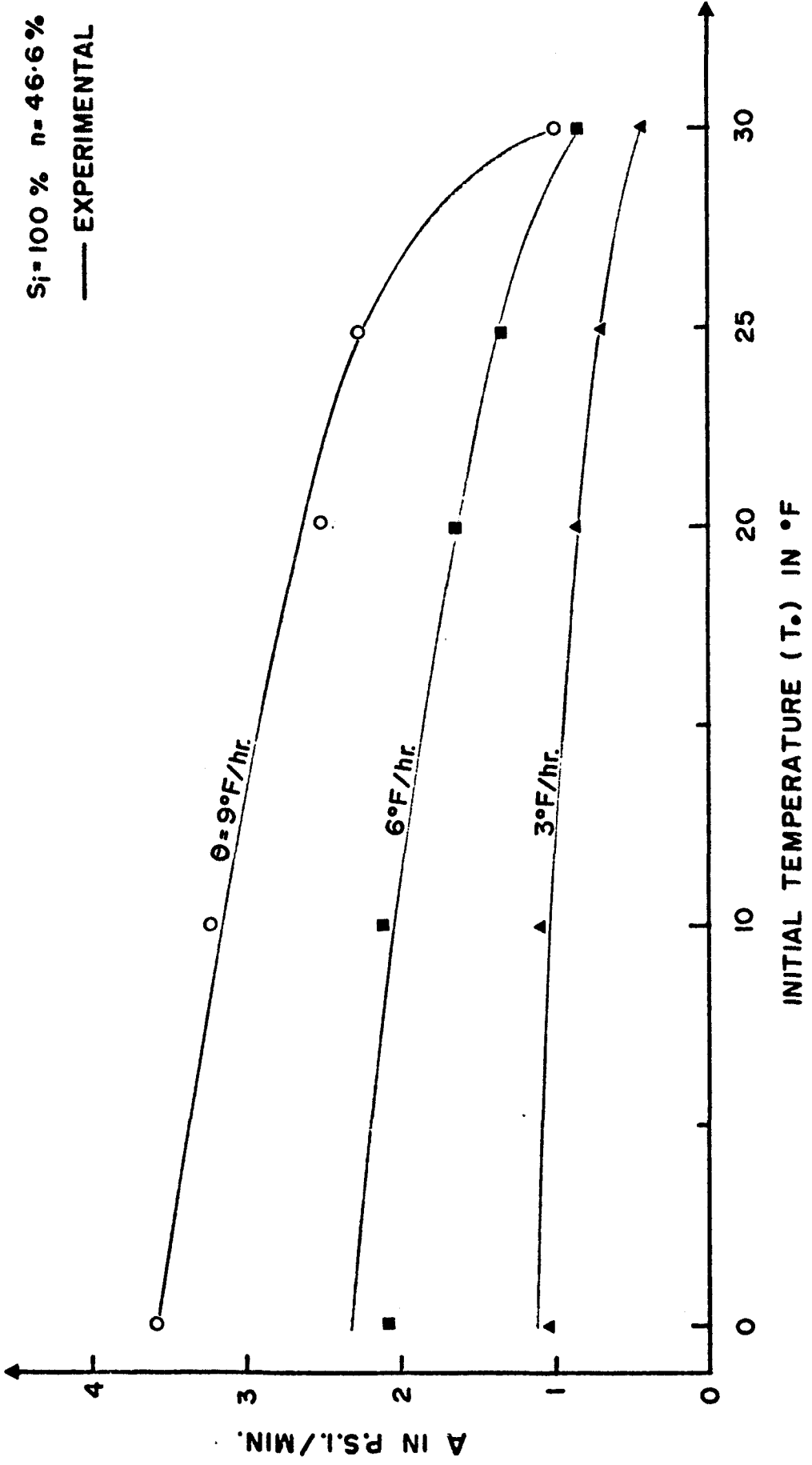
Fig. 32 Coefficient A vs. Initial Frozen Sand Temperature
for Ice Saturation 100%

Fig. 33 Maximum Pressure and Time to Reach Maximum Pressure for Sand No. 1 and Ice Saturation of 33.3% Related to Rate of Temperature Rise
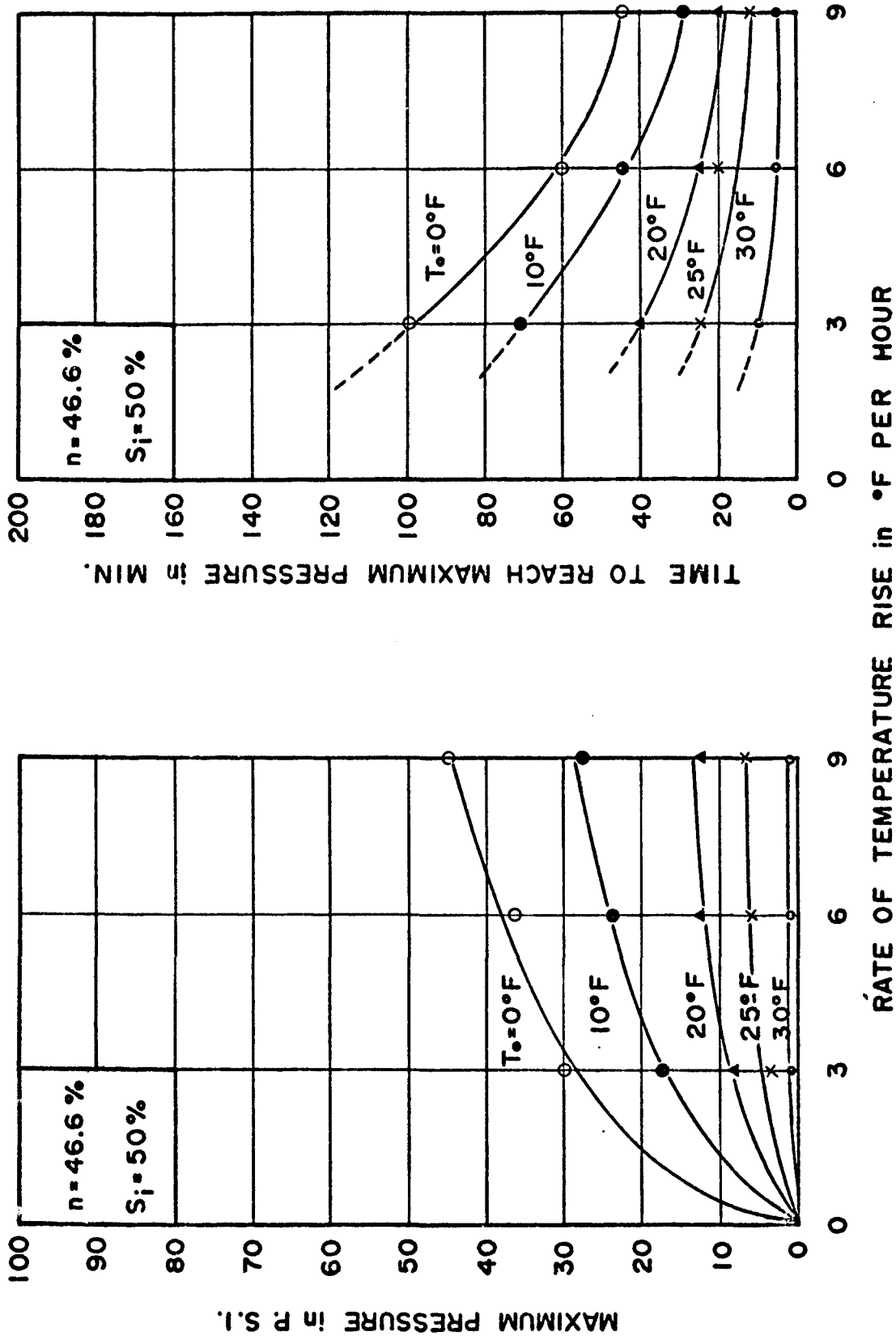
Fig. 34 Maximum Pressure and Time to Reach Maximum Pressure for Sand No. 1 and Ice Saturation of 50% Related to Rate of Temperature Rise
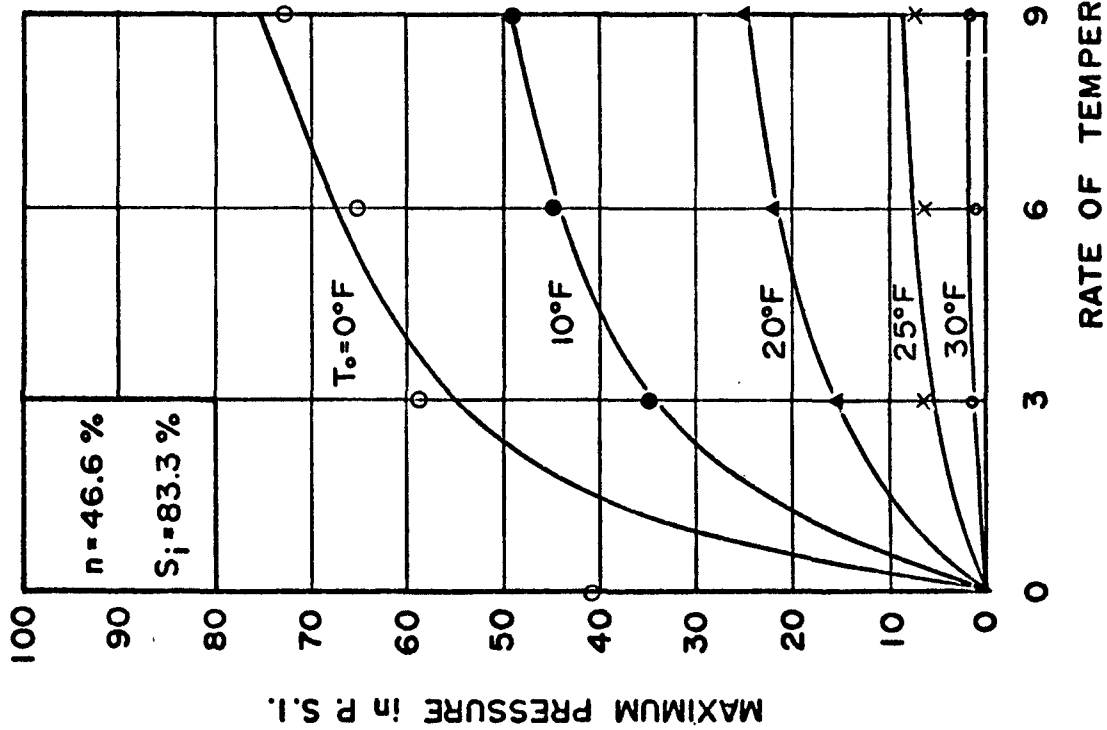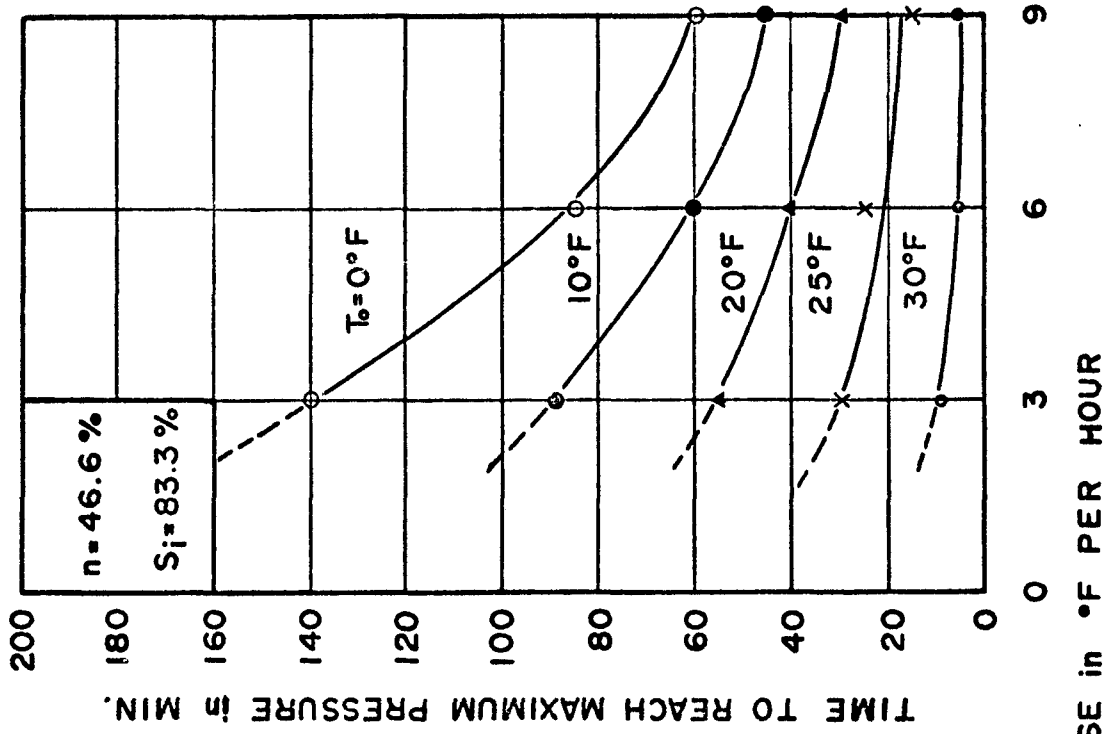
Fig. 35 Maximum Pressure and Time to Reach Maximum Pressure for Sand No. 1 and Ice Saturation of 83.3% Related to Rate of Temperature Rise
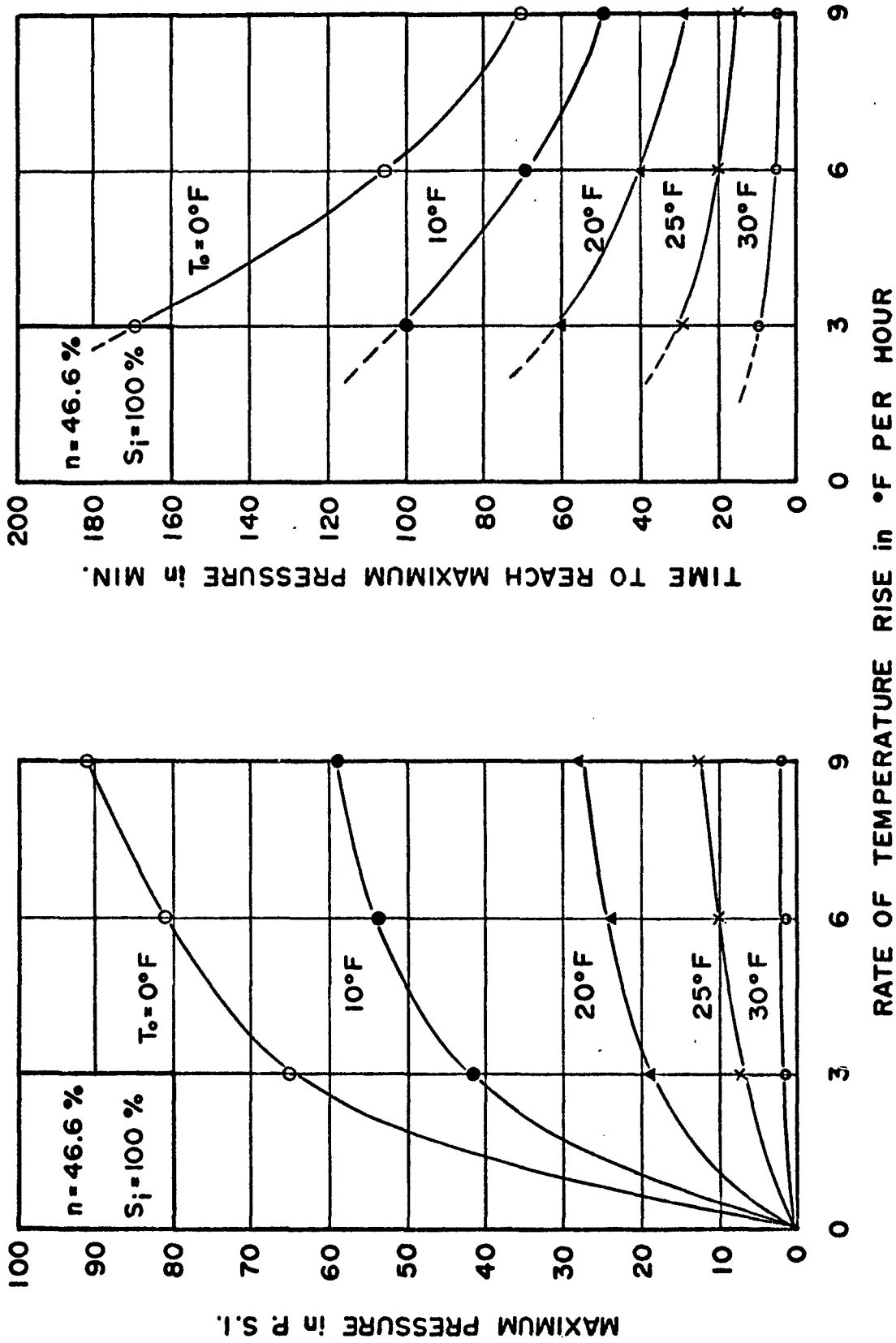
Fig. 36 Maximum Pressure and Time to Reach Maximum Pressure for Sand No. 1
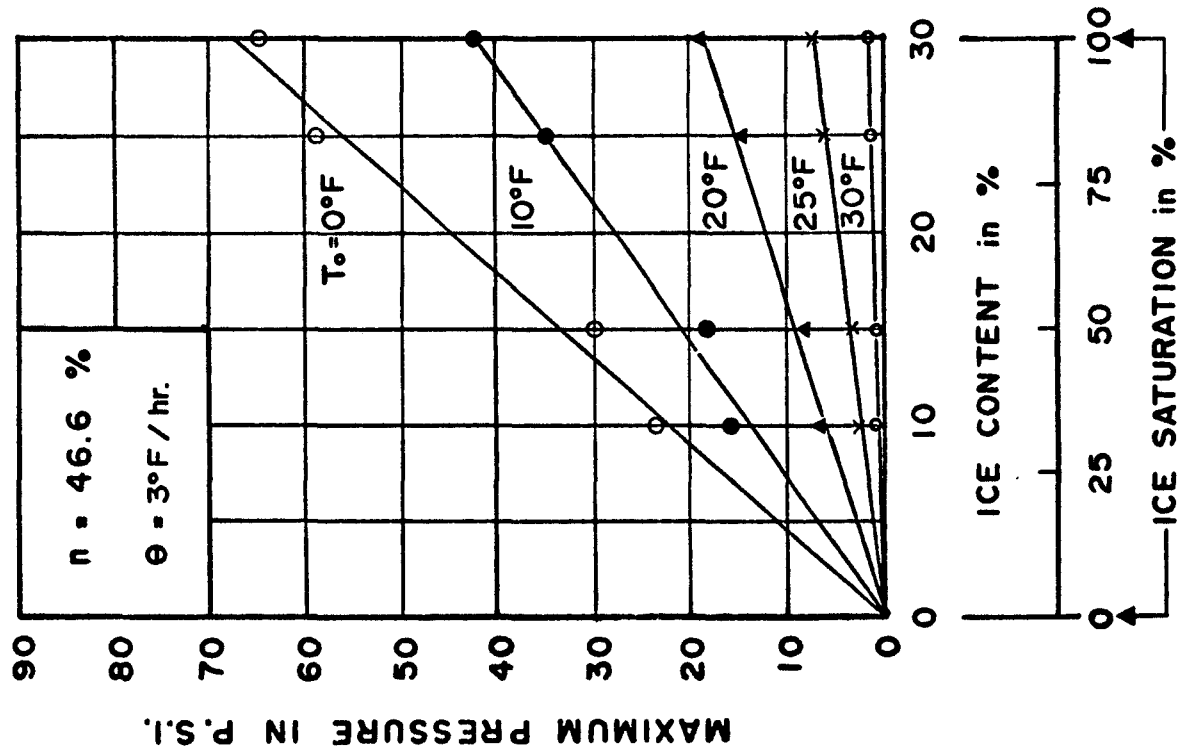and Ice Saturation of 100% Related to Rate of Temperature Rise

Fig. 37 Maximum Pressure and Time to Reach Maximum Pressure Related to Ice Saturation and Rate of Temperature Change 3°F/hr for Sand No. 1

Fig. 38 Maximum Pressure and Time to Reach Maximum Pressure Related to
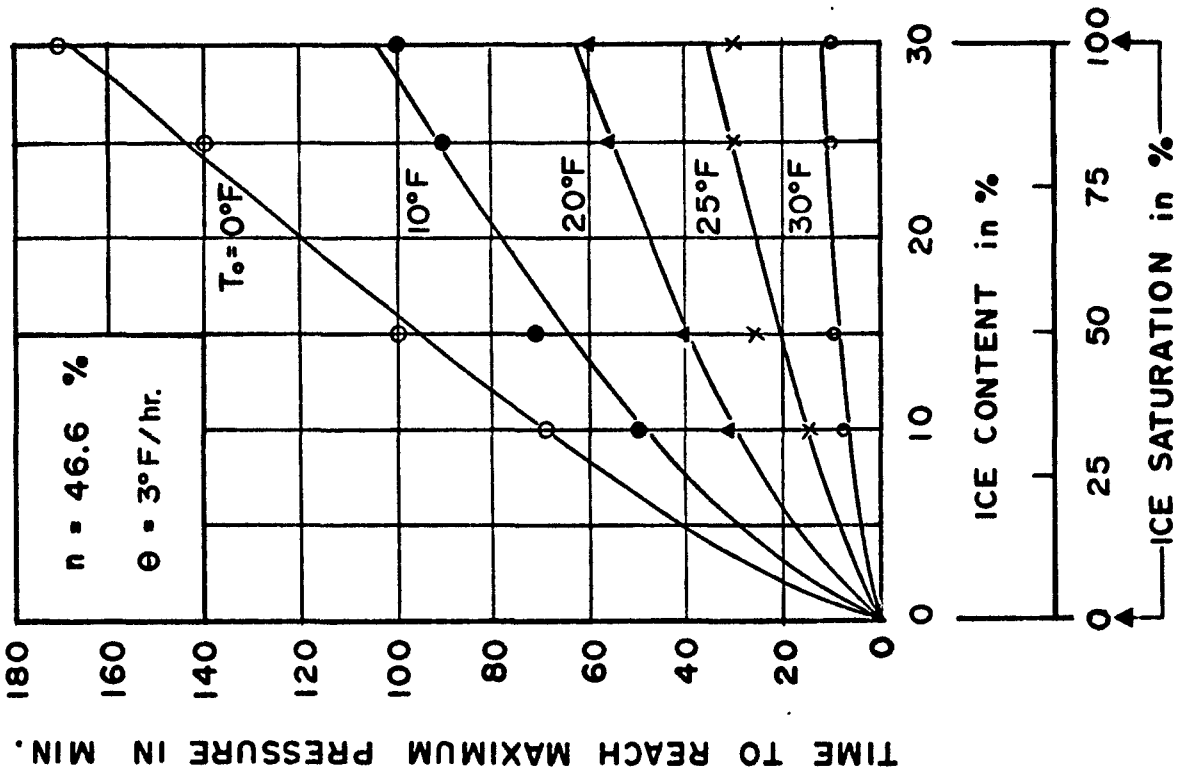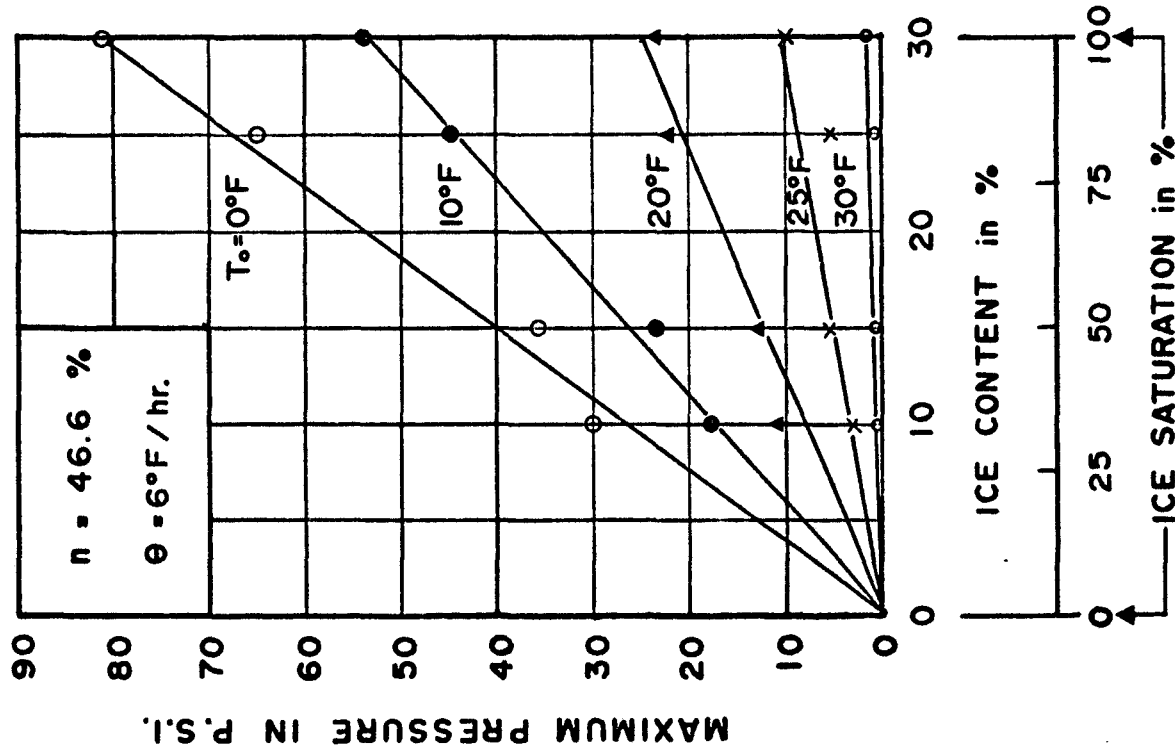Ice Saturation and Rate of Temperature Change 6°F/hr for Sand No. 1

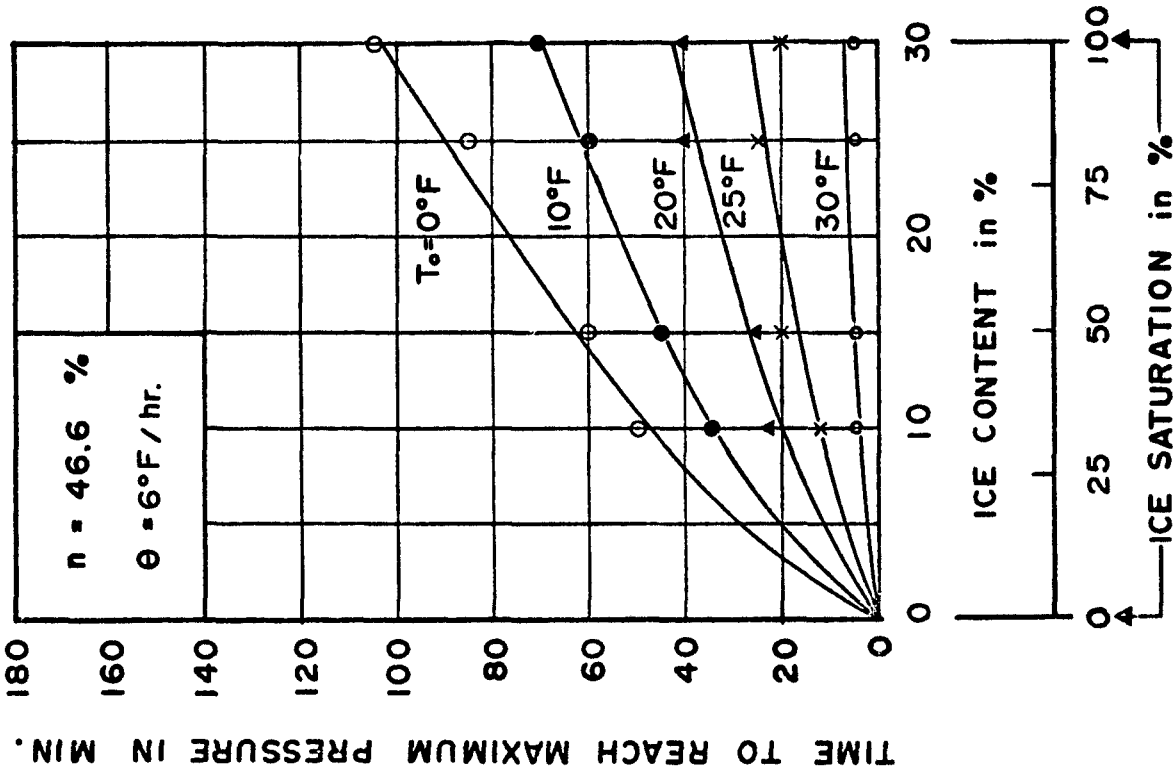Fig. 39 Maximum Pressure and Time to Reach Maximum Pressure Related to
Ice Saturation and Rate of Temperature Change 9°F/hr for Sand No. 1

Fig. 40 Comparison Between Experimental and Calculated Values of Maximum Pressure and Time to Reach Maximum Pressure for Sand No. 1 and Ice Saturation of 33.3% Related to Rate of Temperature Rise.

Fig. 41 Comparison Between Experimental and Calculated Values of Maximum Pressure and Time to Reach Maximum Pressure for Sand No. 1 and Ice Saturation of 50% Related to Rate of Temperature Rise.

Fig. 42 Comparison Between Experimental and Calculated Values of Maximum Pressure and Time to Reach Maximum Pressure for Sand No. 1 and Ice Saturation of 83.3% Related to Rate of Temperature Rise

Fig. 43 Comparison Between Experimental and Calculated Values of Maximum Pressure and Time to Reach Maximum Pressure for Sand No. 1 and Ice Saturation of 100% Related to Rate of Temperature Rise

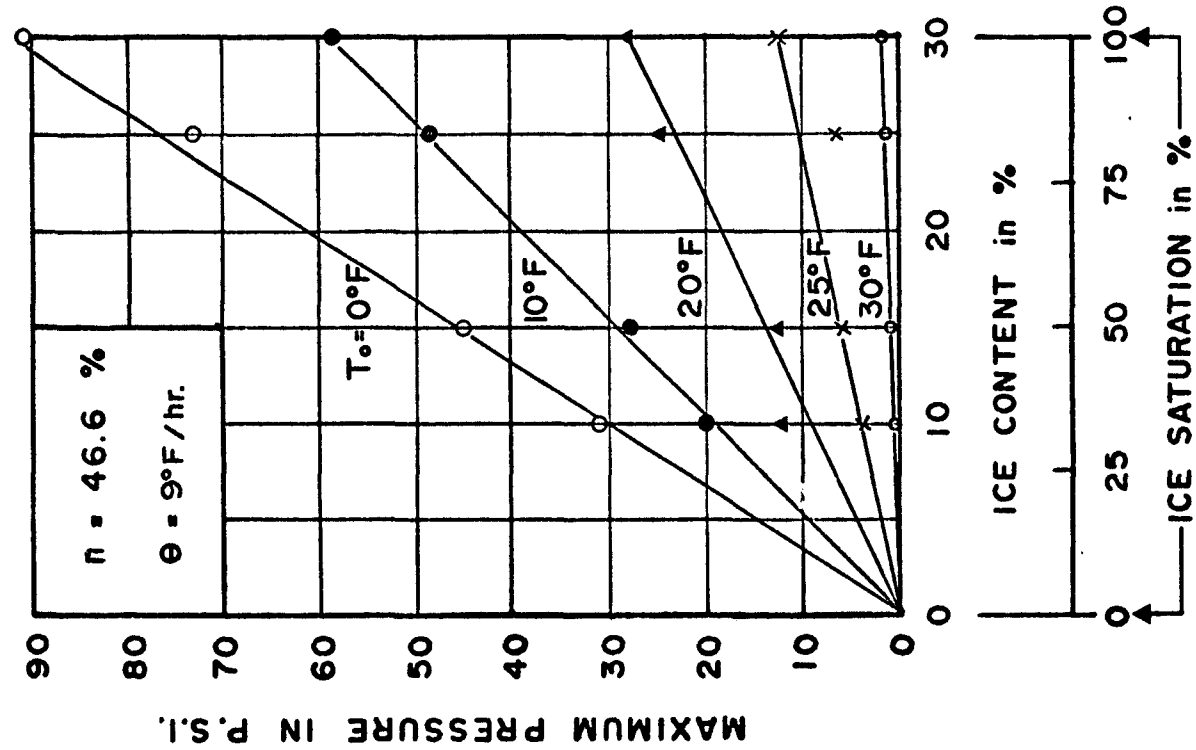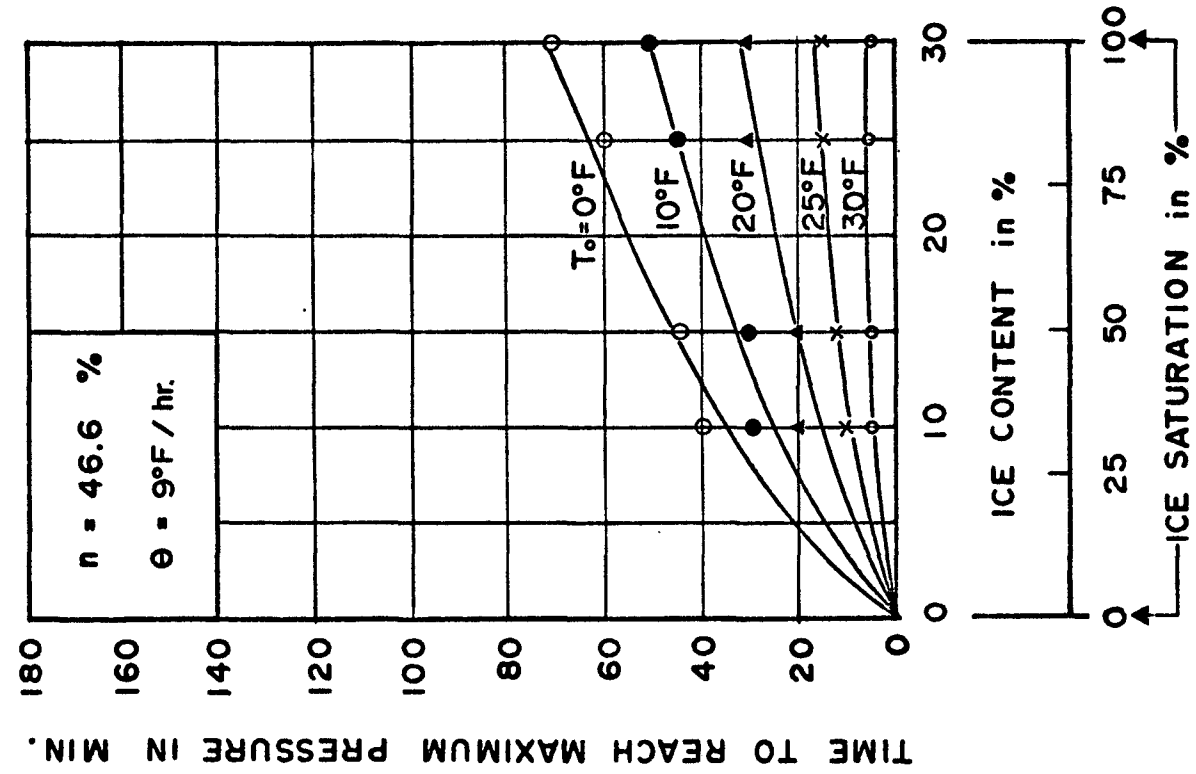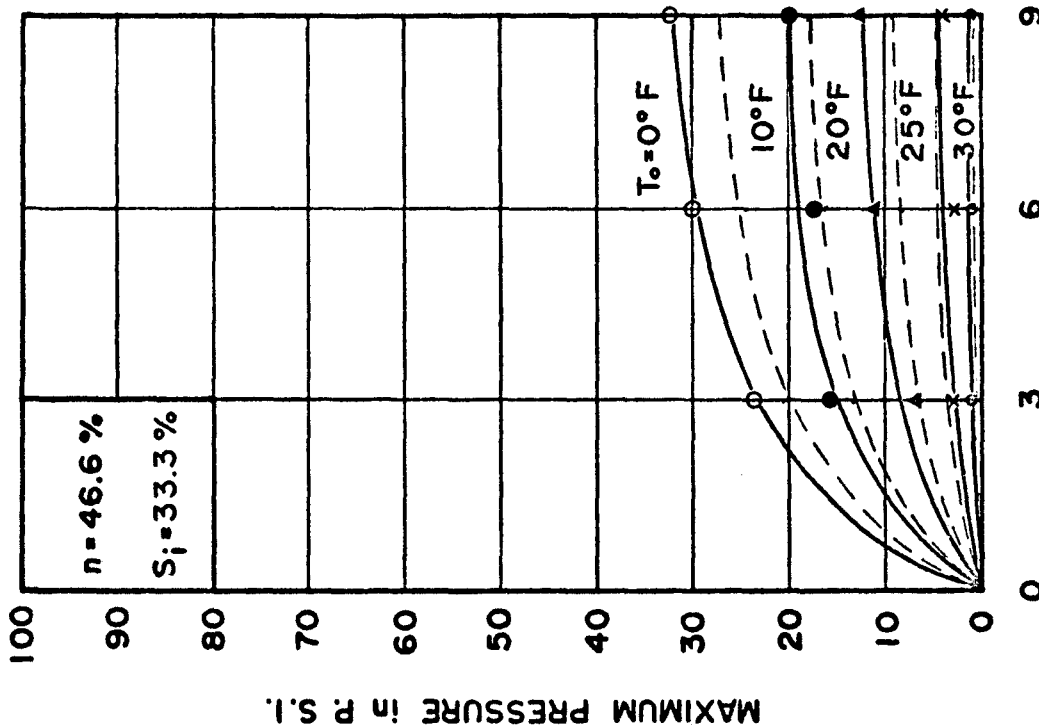**Fig. 44** Comparison Between Experimental and Calculated Values of Maximum Pressure and Time to Reach Maximum Pressure Related to Ice Saturation and Rate of Temperature Change 3°F/hr for Sand No. 1
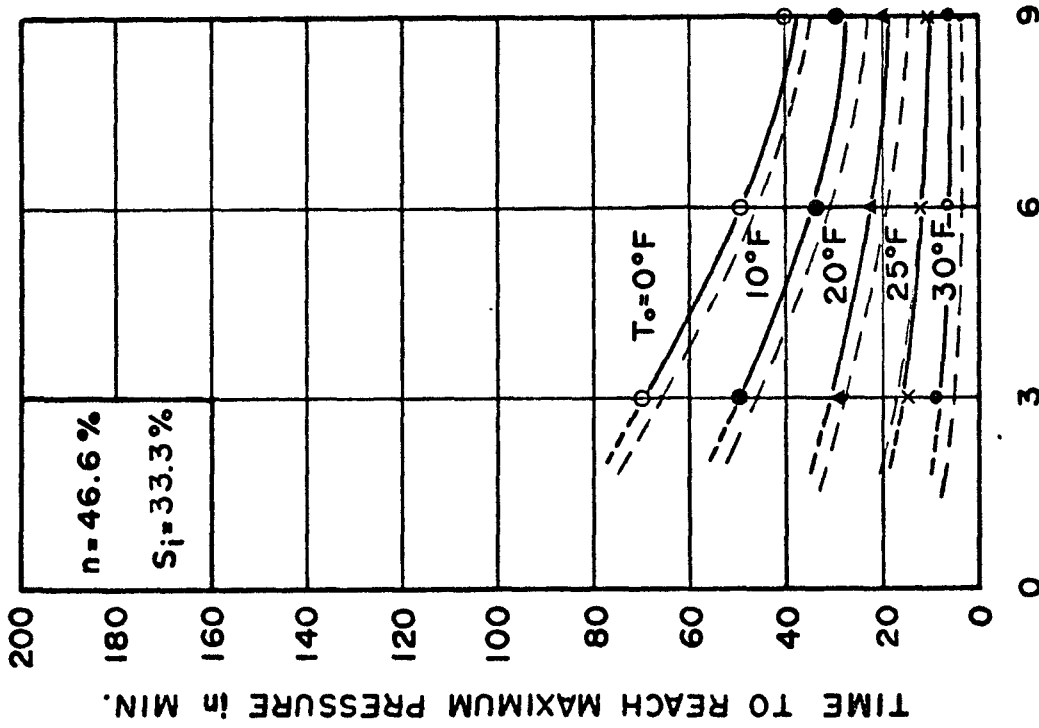
——— Experimental
— — — Theoretical (Calculated)

Fig. 45 Comparison Between Experimental and Calculated Values of Maximum Pressure and Time to Reach Maximum Pressure Related to Ice Saturation and Rate of Temperature Change 6°F/hr for Sand No. 1
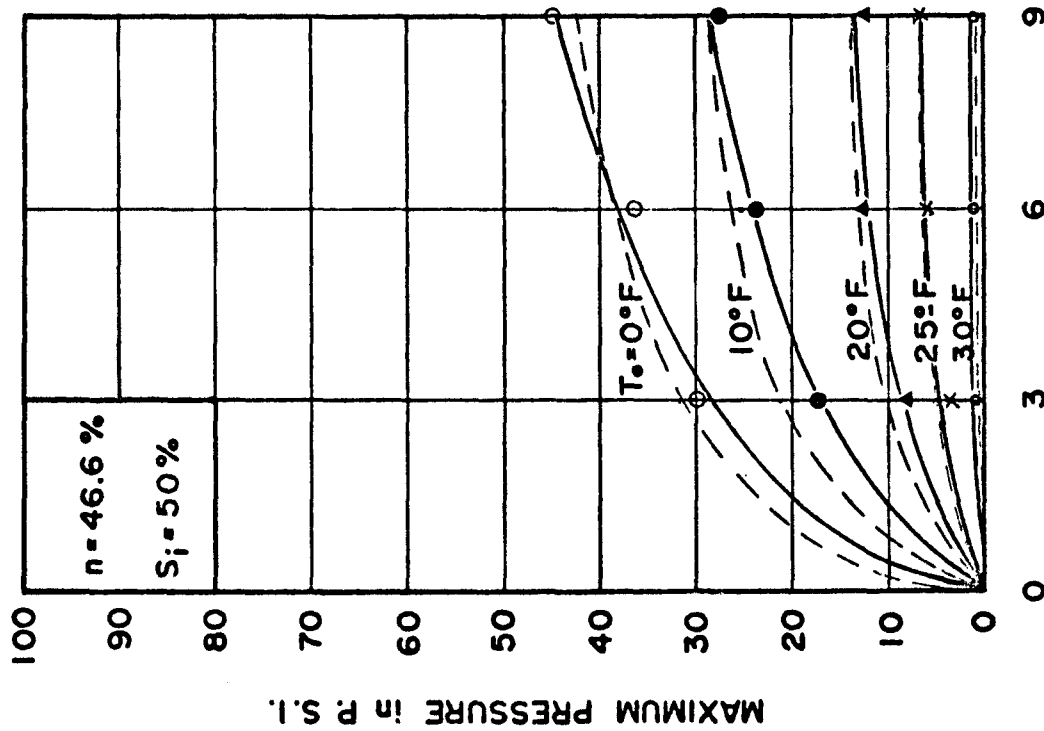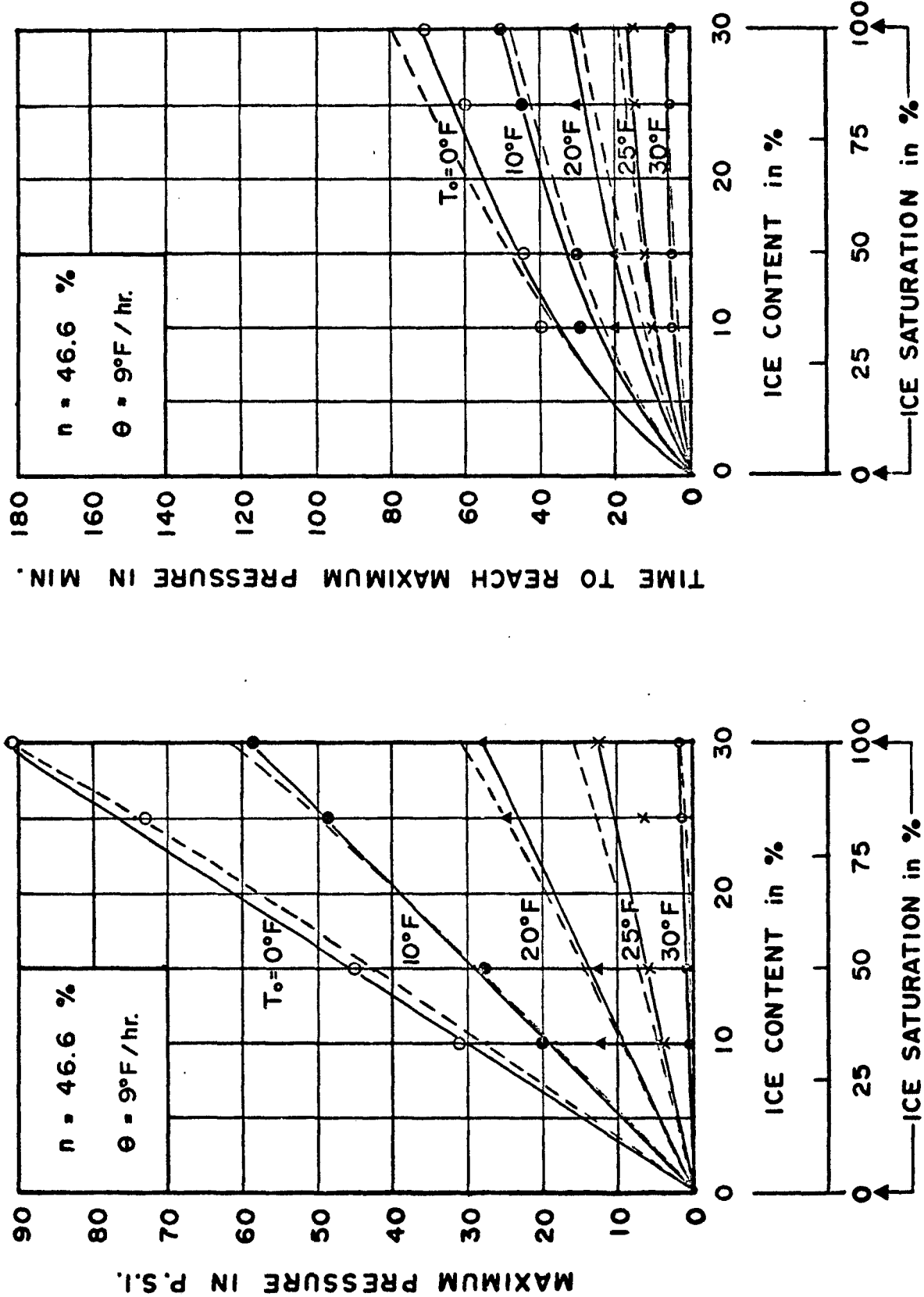
——————— Experimental
– – – – – – Theoretical (Calculated)
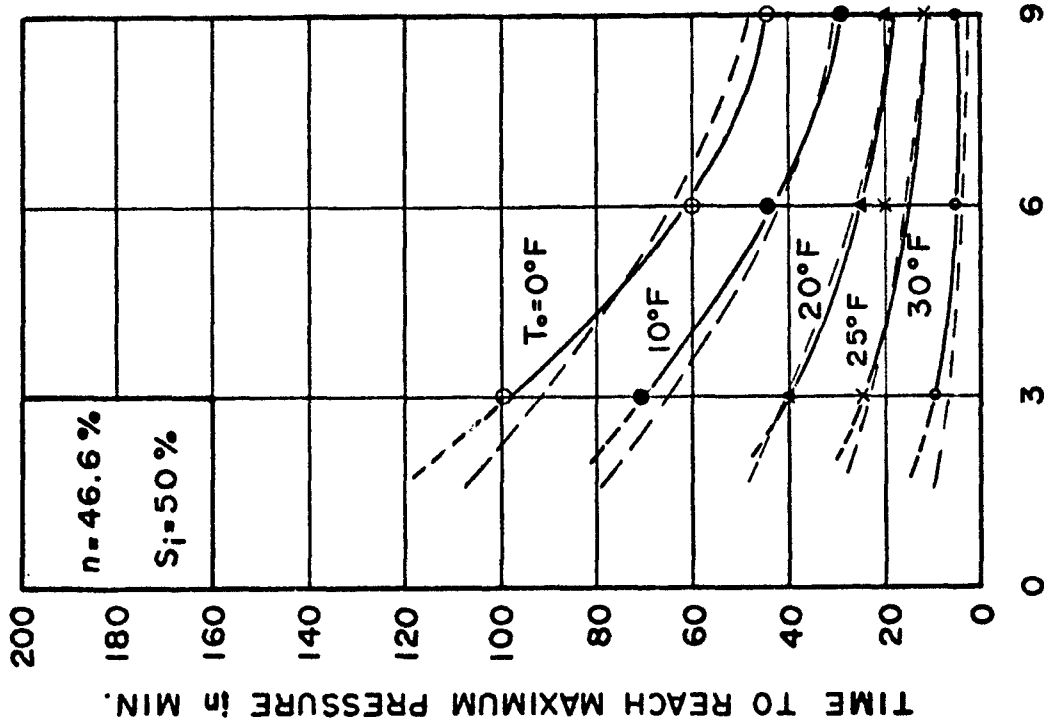
Fig. 46 Comparison Between Experimental and Calculated Values of Maximum Pressure and Time to Reach Maximum Pressure Related to Ice Saturation and Rate of Temperature Change 9°F/hr for Sand No. 1

Fig. 47 Maximum Pressure vs. Porosity for Sand No. 1 and No. 2 at Ice
Saturation of 50%
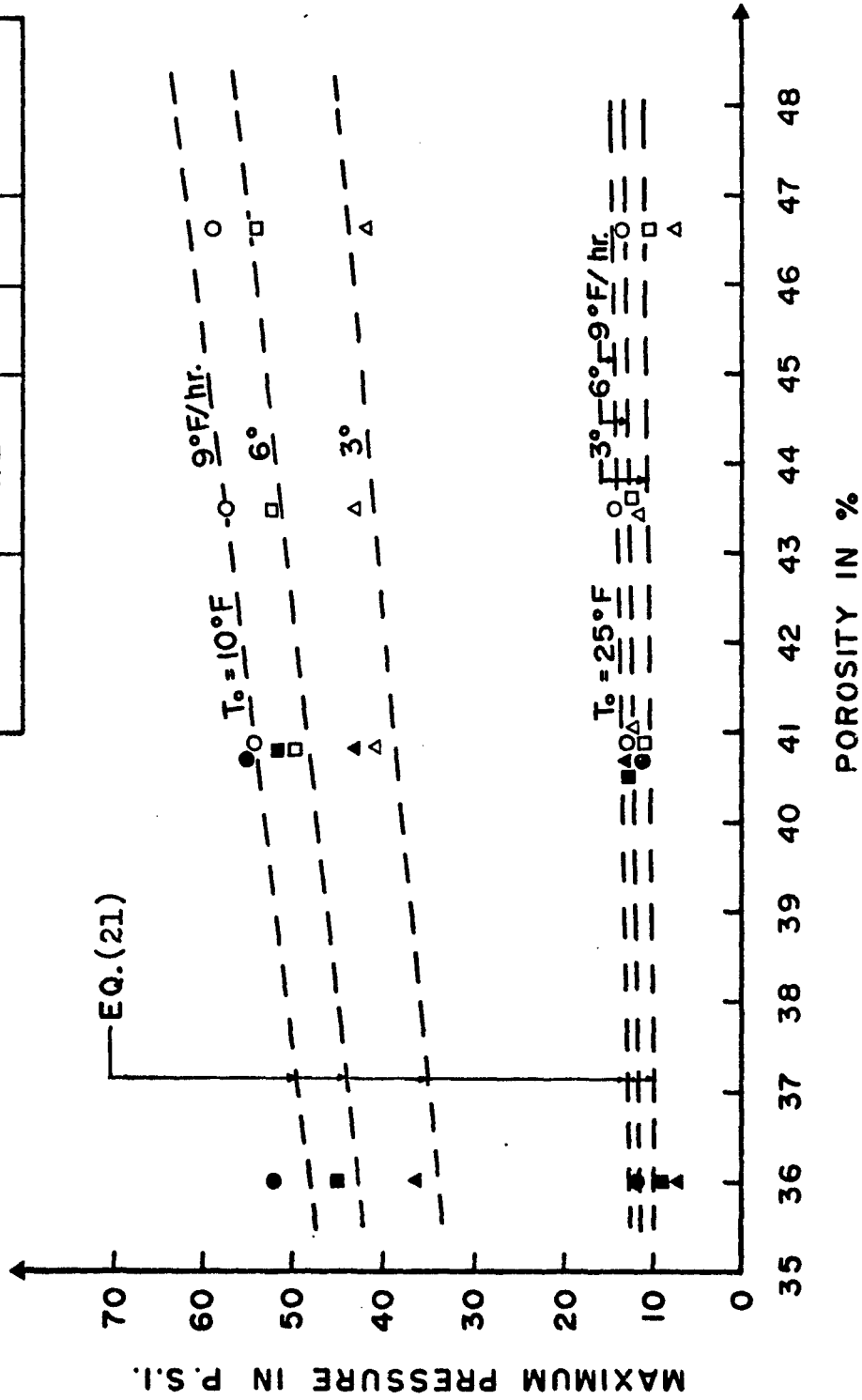
Fig. 48 Maximum Pressure vs. Porosity for Sand No. 1 and No. 2 at Ice
Sauration of 100%
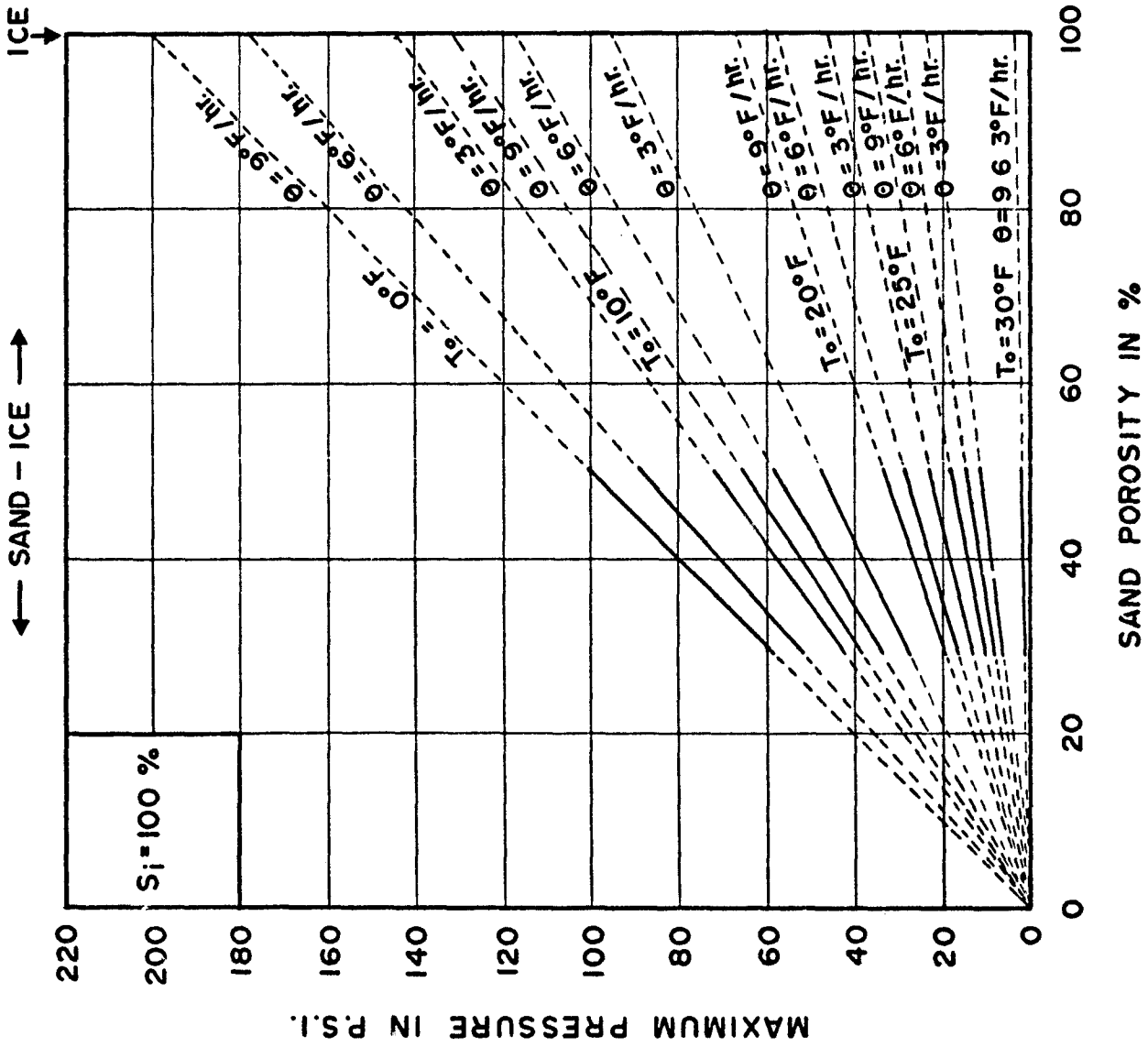
Fig. 49 Maximum Pressure vs. Porosity for 100% Saturated Sand-Ice System
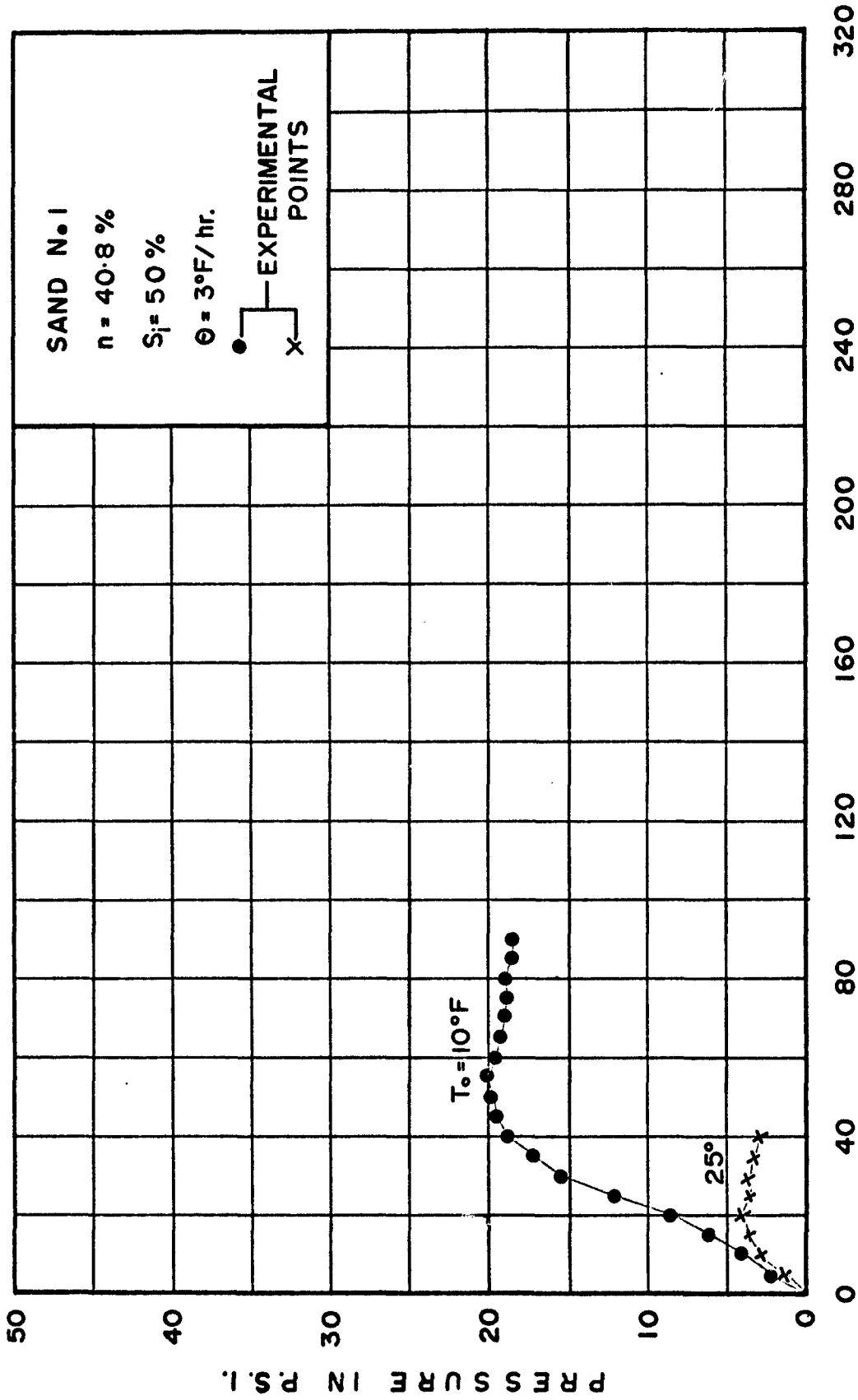
Fig. 50 Pressure-Time Curves for Temperature Rise of 3°F/hr and Ice Saturation of 50% for Initial Soil Temperature of 10° and 25°F
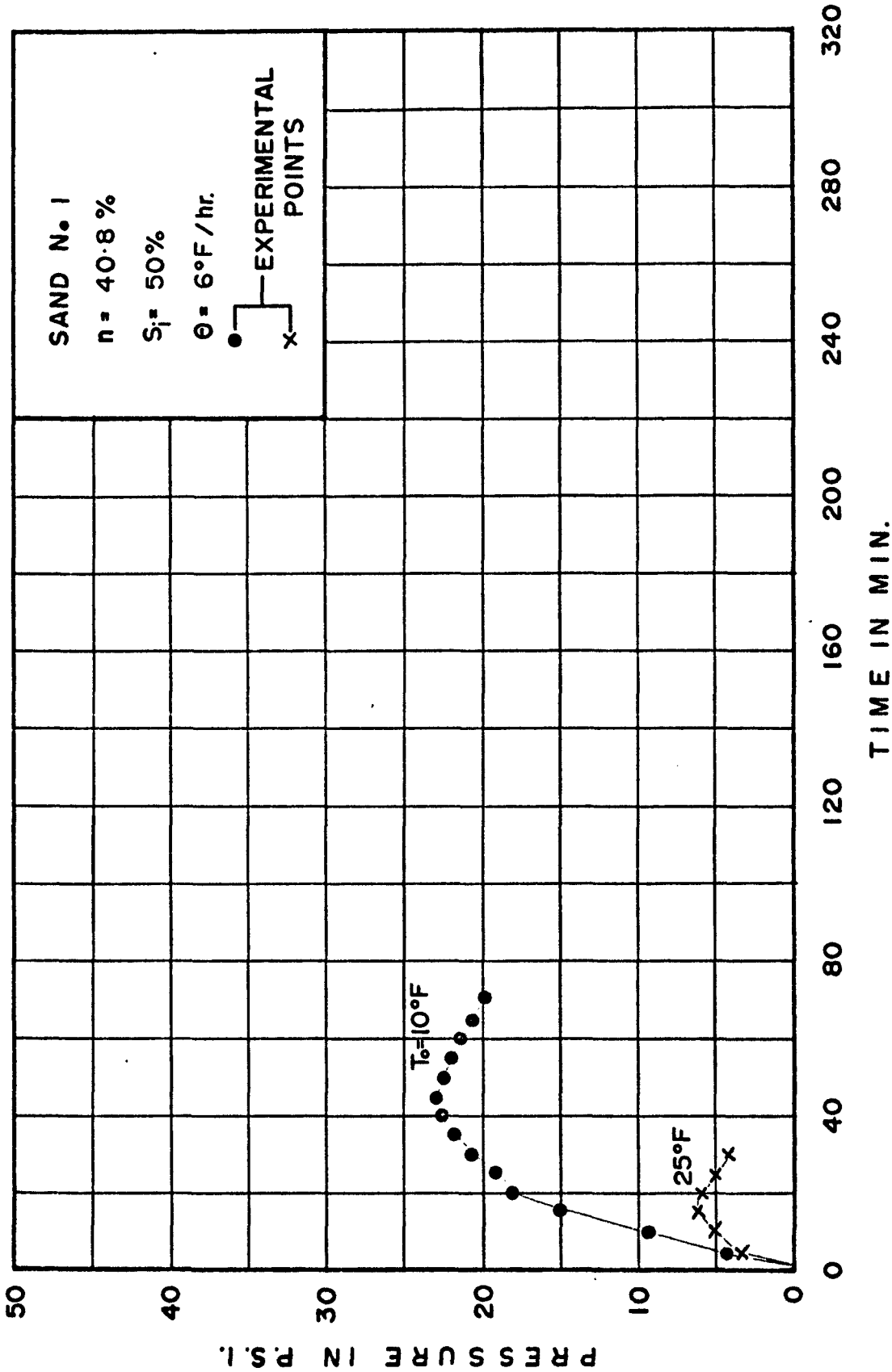
Fig. 51 Pressure-Time Curves for Temperature Rise of 6°F/hr and Ice Saturation of 50% for Initial Soil Temperatures of 10° and 25°F
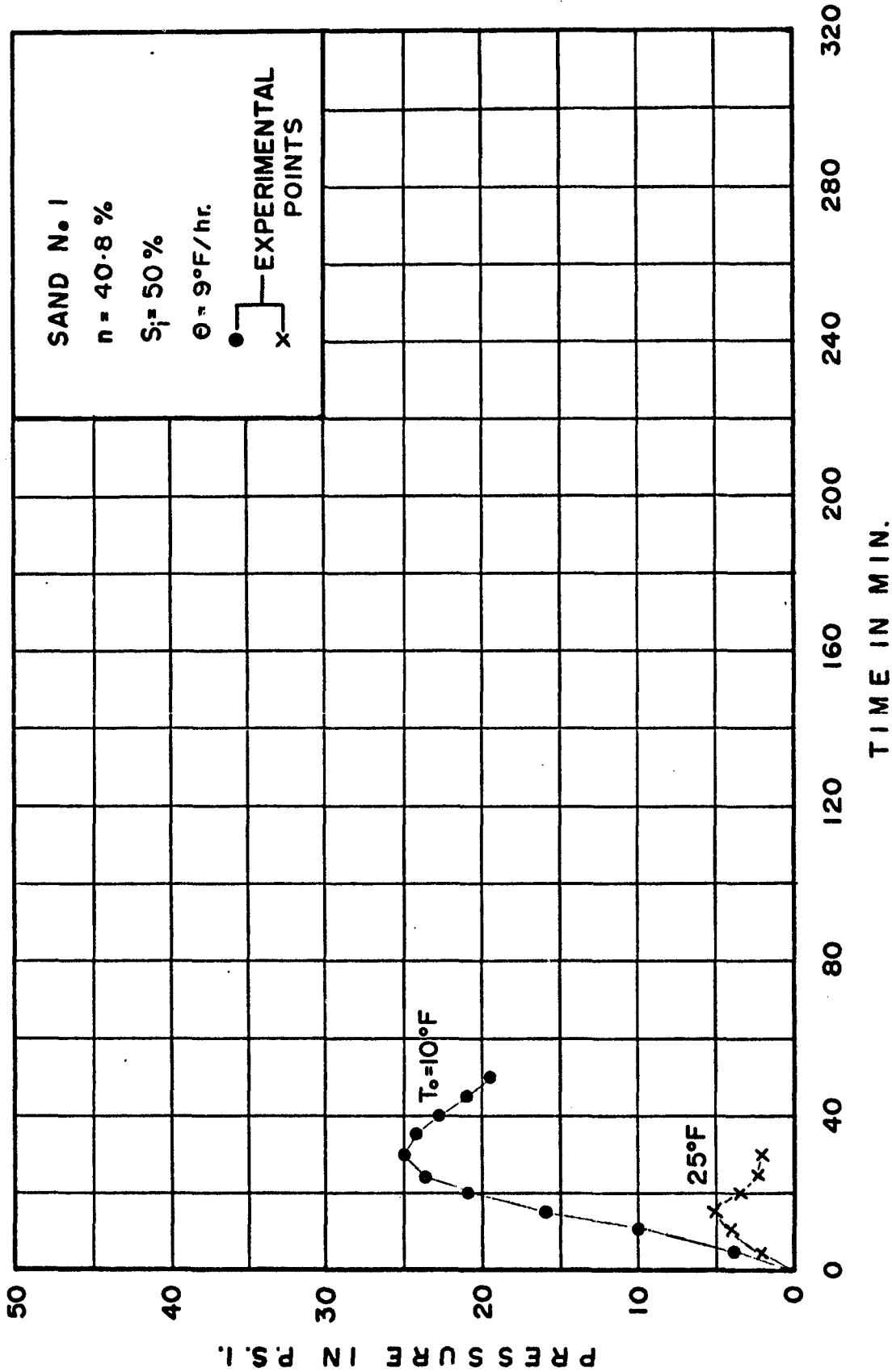
Fig. 52 Pressure-Time Curves for Temperature Rise of 9°F/hr and Ice
Saturation of 50% for Initial Soil Temperatures of 10° and 25°F
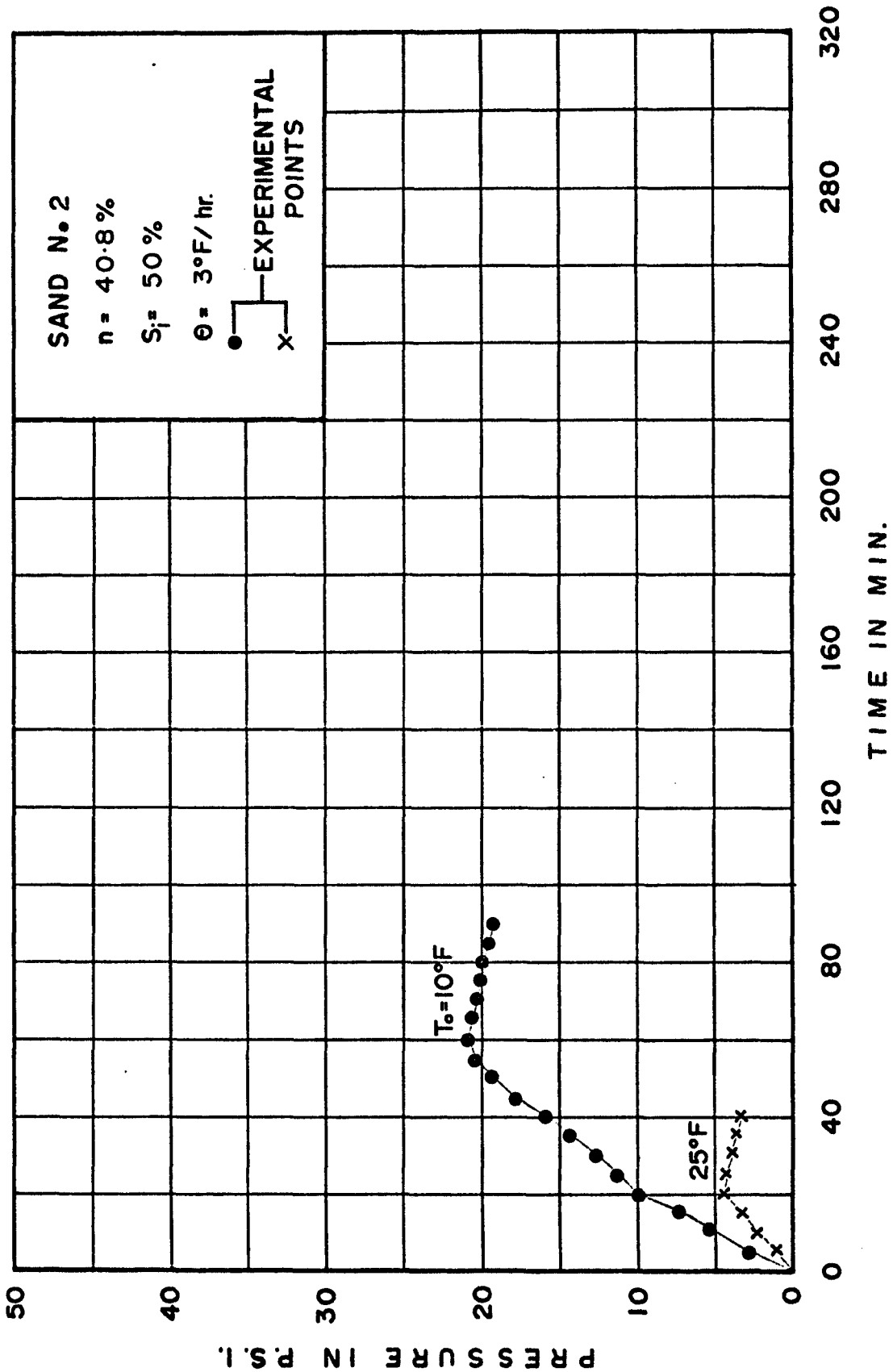
Fig. 53 Pressure-Time Curves for Temperature Rise of $3°F/hr$ and Ice Saturation of 50% for Initial Soil Temperatures of $10°$ and $25°F$
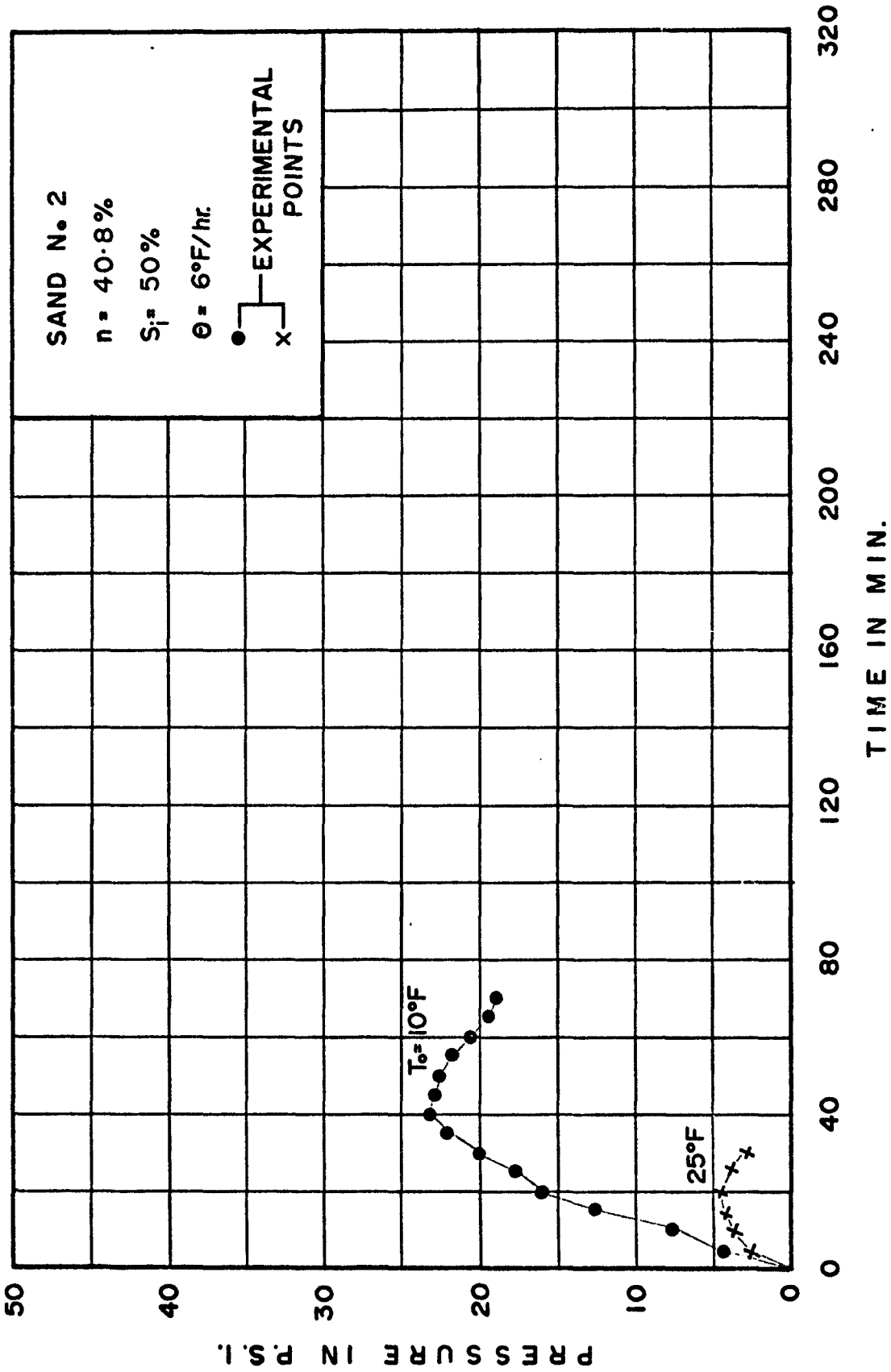
Fig. 54 Pressure-Time Curves for Temperature Rise of 6°F/hr and Ice Saturation of 50% for Initial Soil Temperatures of 10 and 25°F
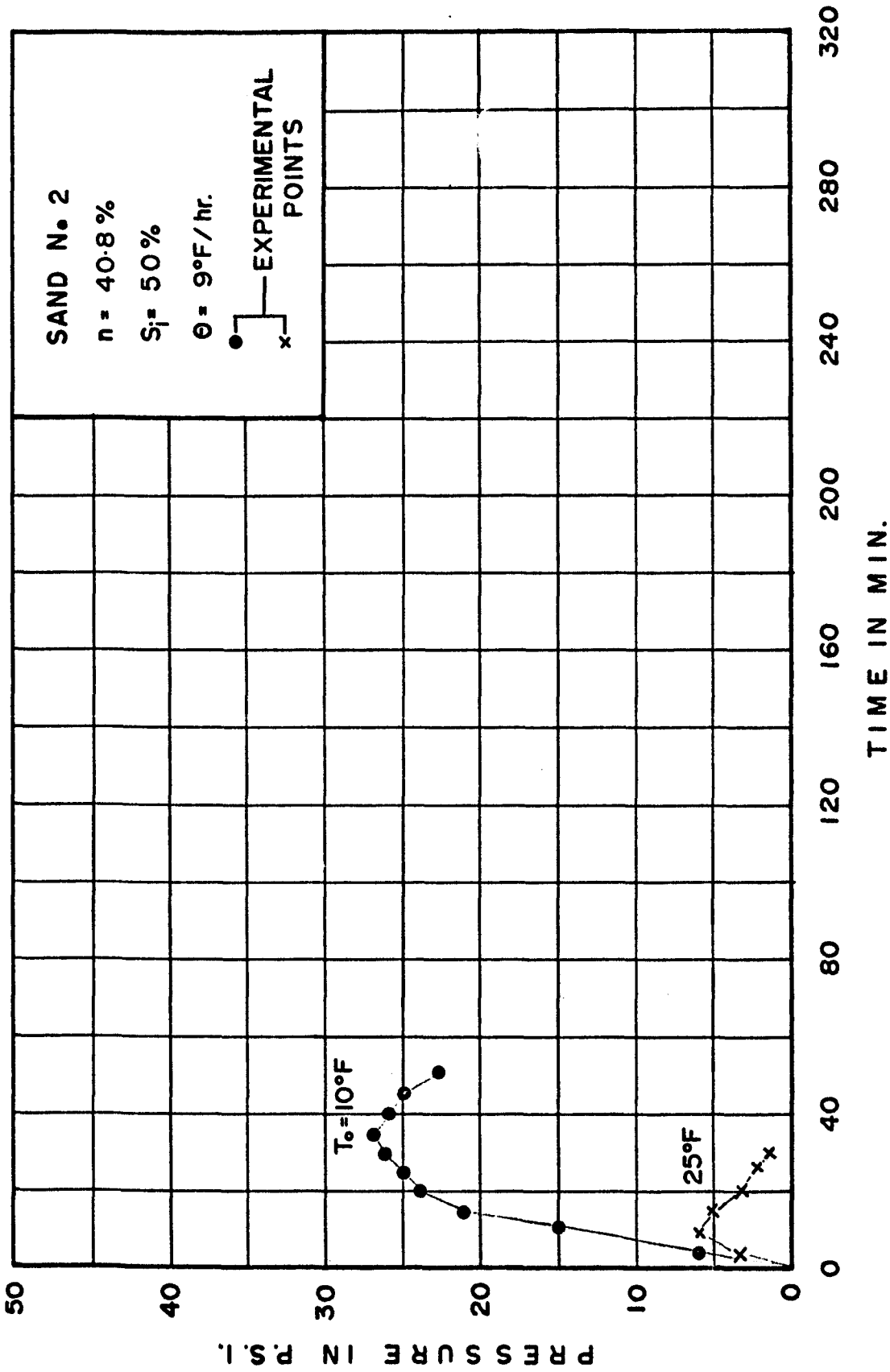
Fig. 55 Pressure-Time Curves for Temperature Rise of 9°F/hr and Ice
Saturation of 50% for Initial Soil Temperatures of 10° and 25°F
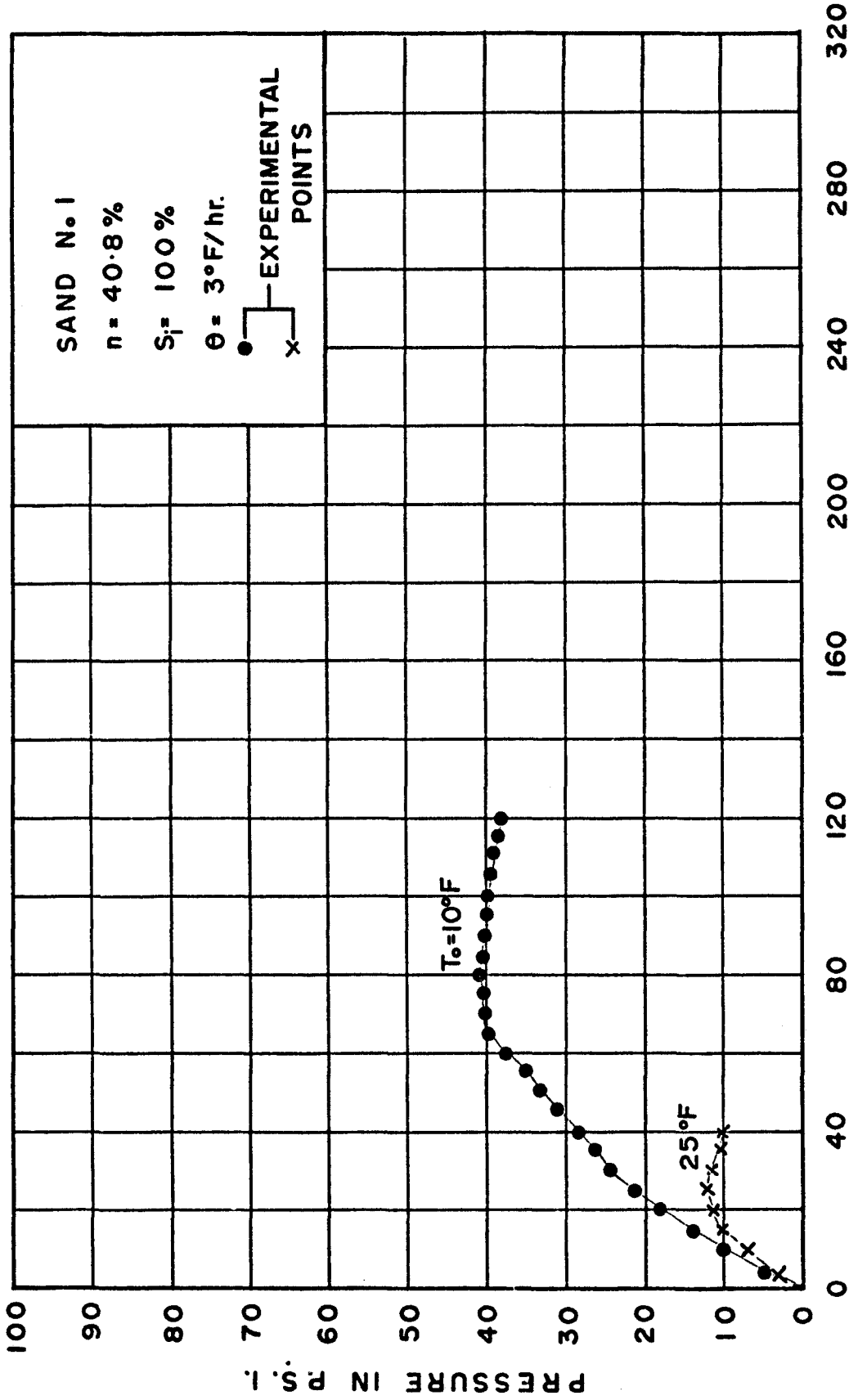
Fig. 56 Pressure-Time Curves for Temperature Rise of 3°F/hr and Ice Saturation of 100% for Initial Soil Temperatures of 10° and 25°F
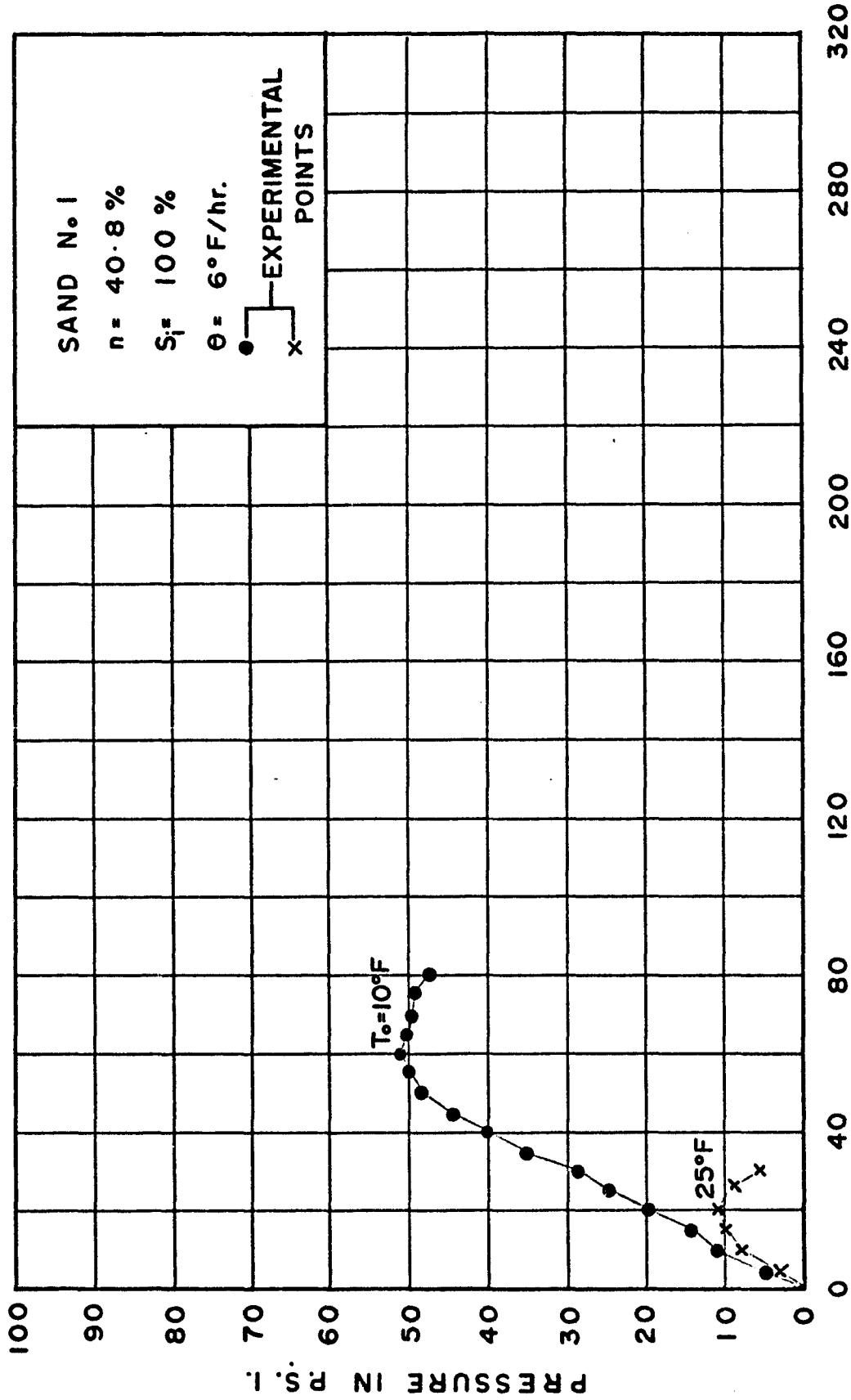
Fig. 57 Pressure-Time Curves for Temperature Rise of 6°F/hr and Ice
Saturation of 100% for Initial Soil Temperatures of 10° and 25°F
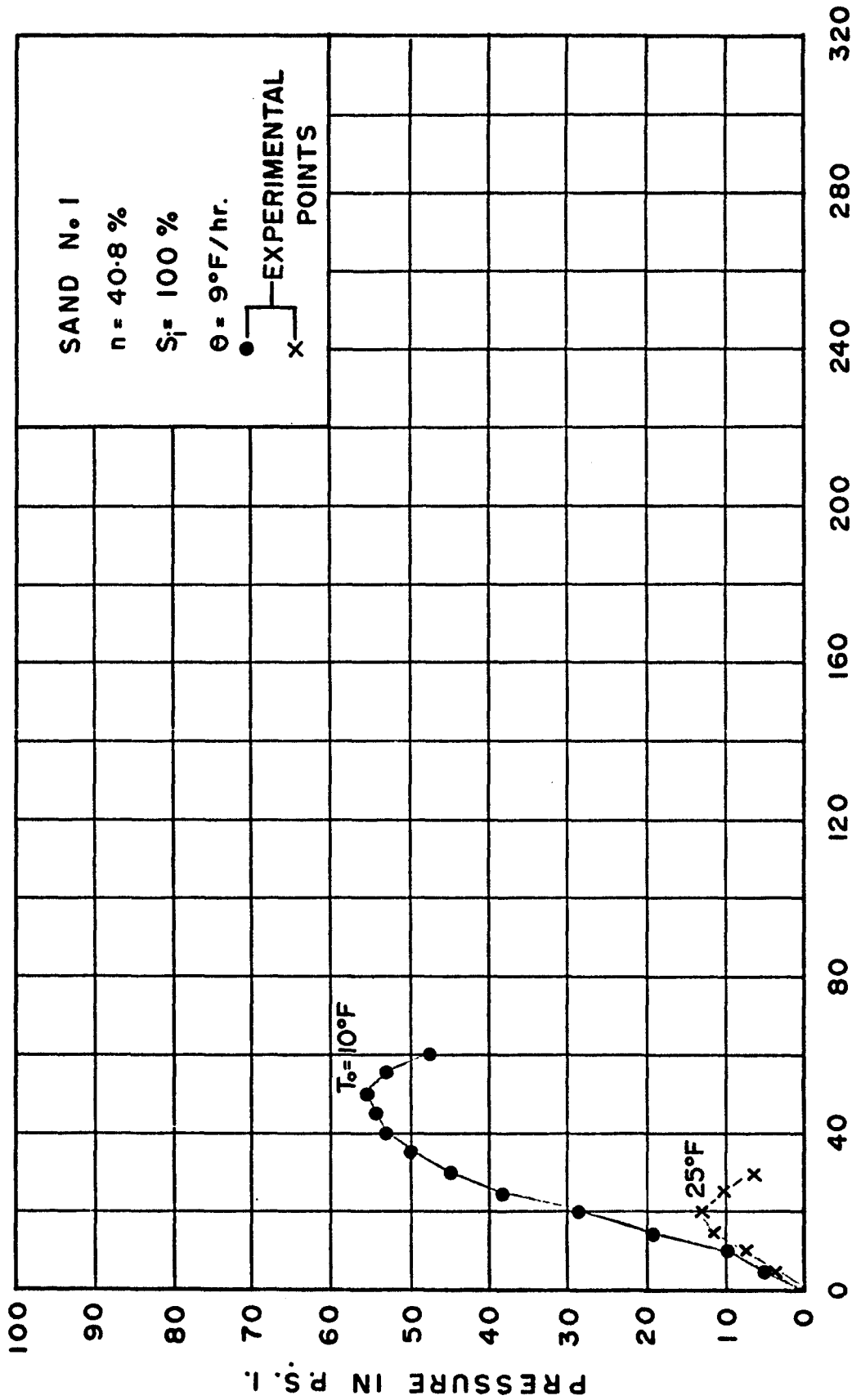
Fig. 58 Pressure-Time Curves for Temperature Rise of 9°F/hr and Ice Saturation of 100% for Initial Soil Temperatures of 10° and 25°F
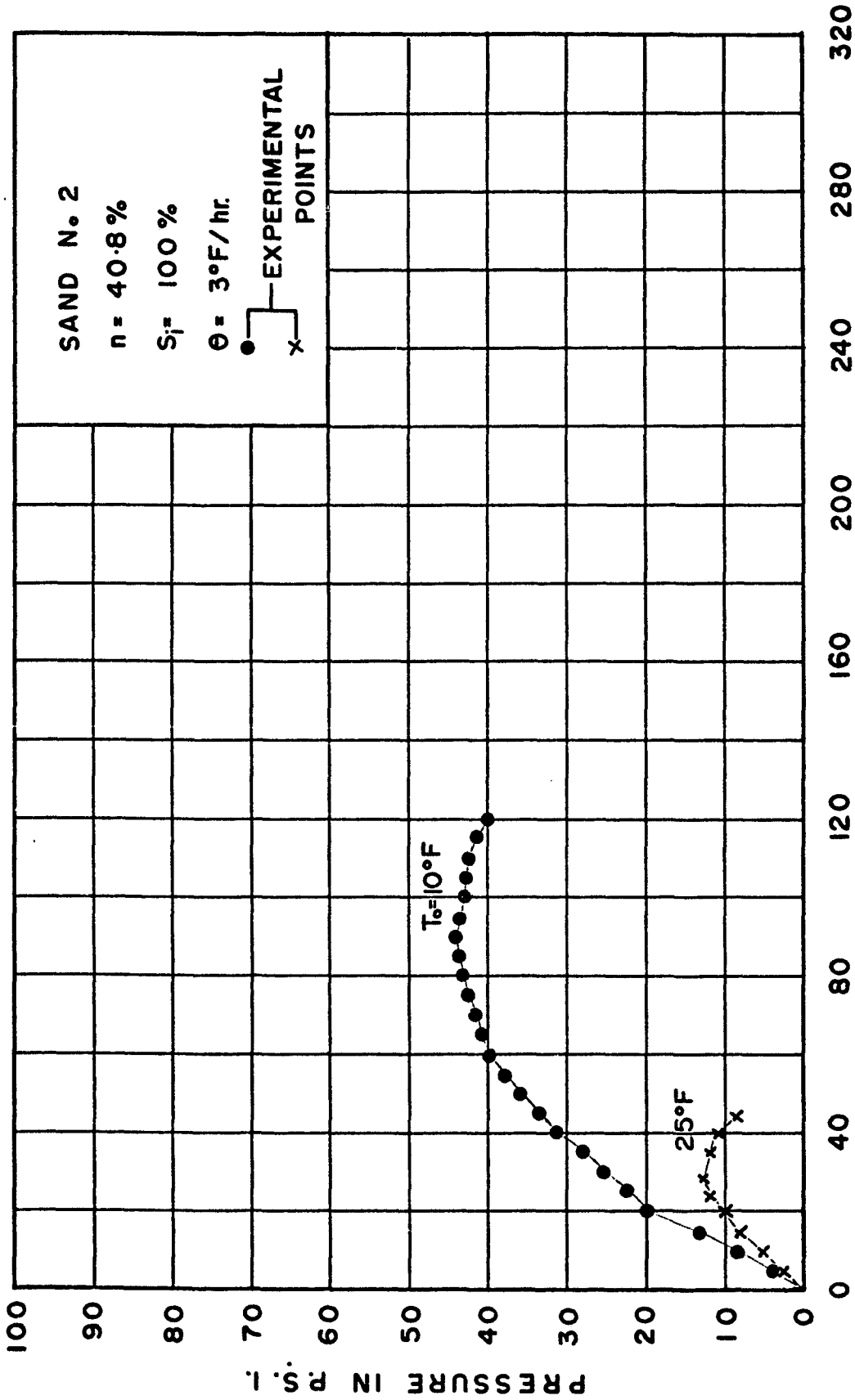
Fig. 59 Pressure-Time Curves for Temperature Rise of 3°F/hr and Ice Saturation of 100% for Initial Soil Temperatures of 10° and 25°F
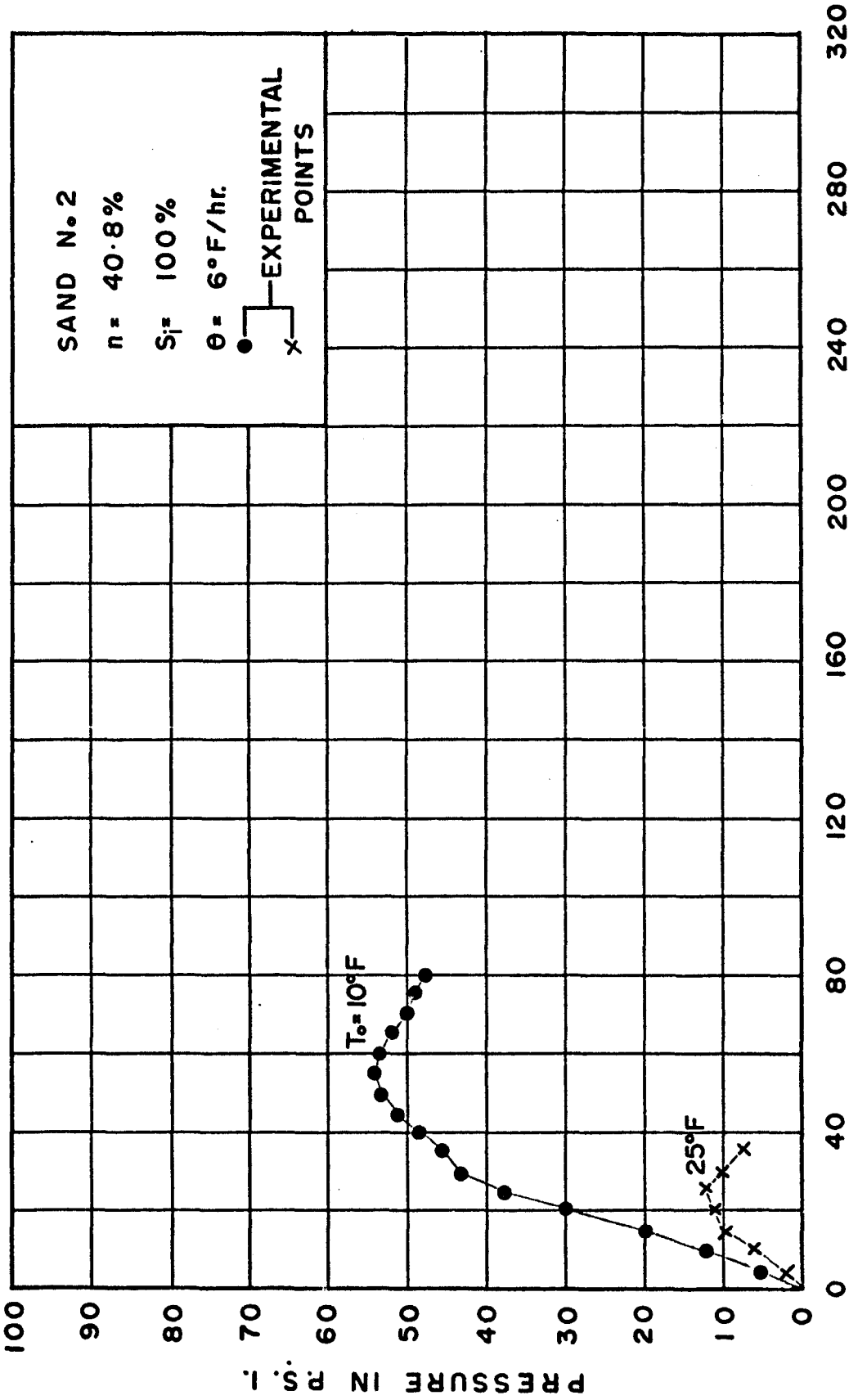
Fig. 60 Pressure-Time Curves for Temperature Rise of 6°F/hr and Ice
Saturation of 100% for Initial Soil Temperatures of 10° and 25°F
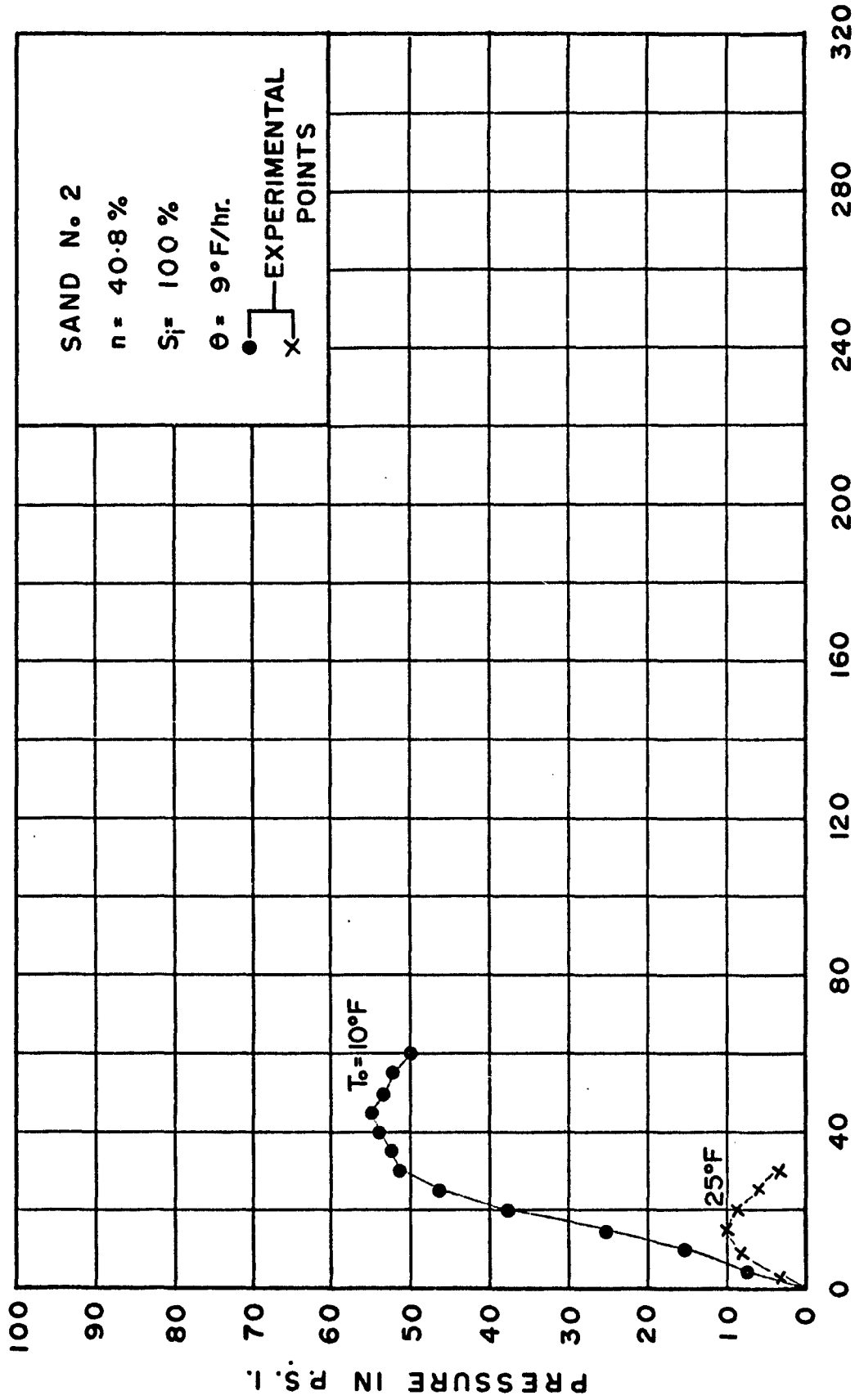
Fig. 61 Pressure-Time Curves for Temperature Rise of 9°F/hr and Ice Saturation of 100% for Initial Soil Temperatures of 10° and 25°F
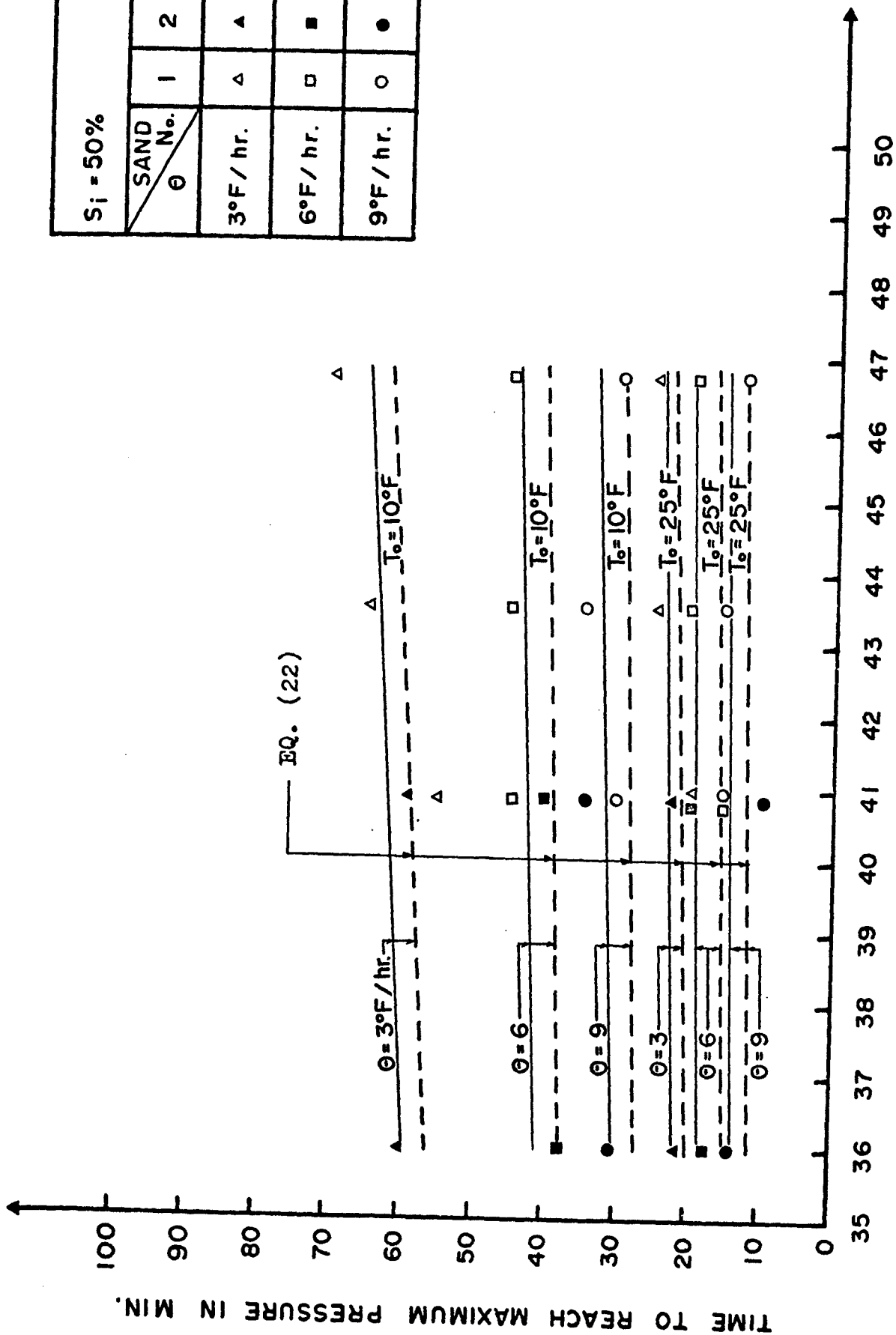
Fig. 62 Required Time to Reach Maximum Pressure vs. Porosity for Sands No. 1 and 2 at Ice Saturation 50%
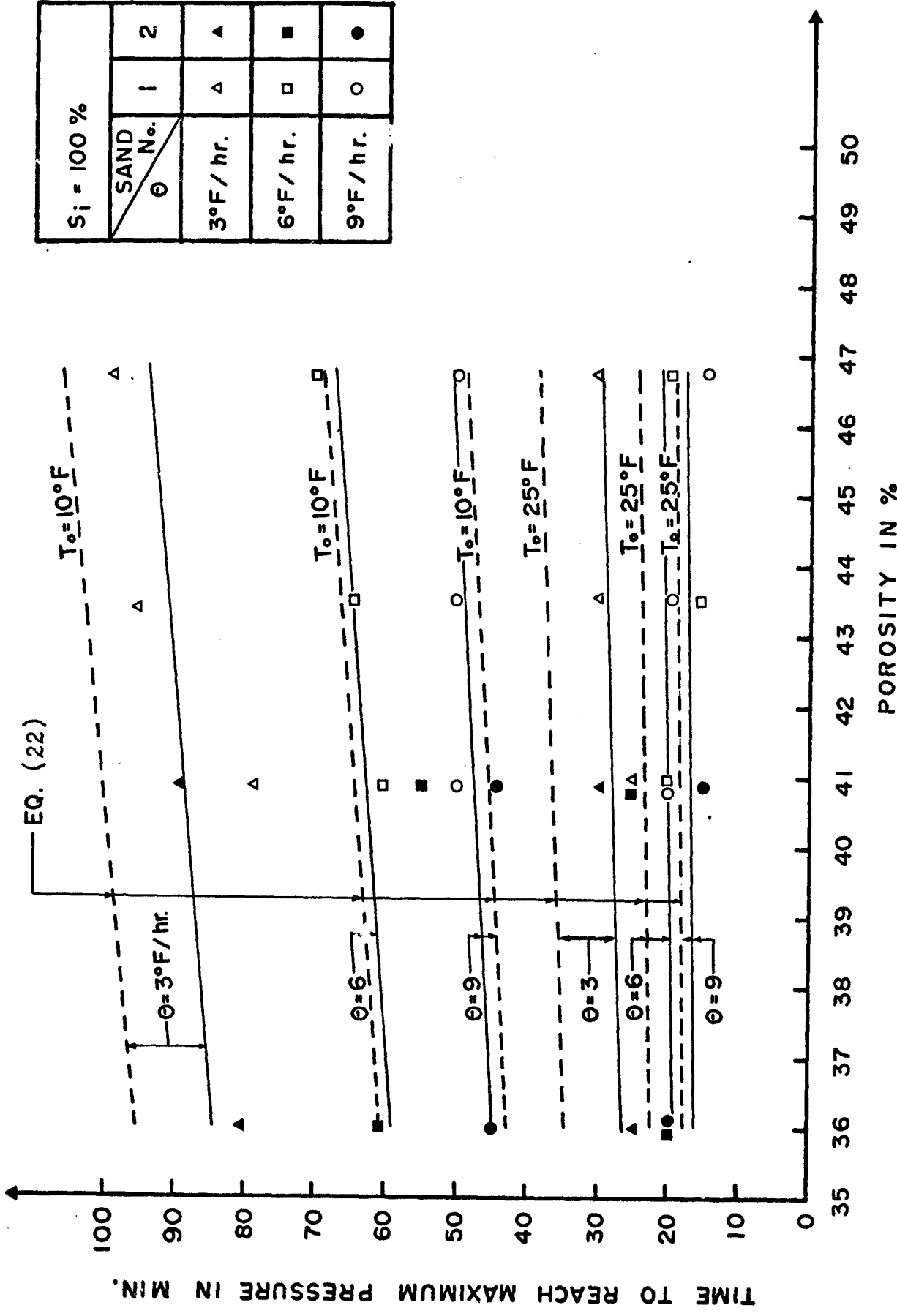
Fig. 63   Required Time to Reach Maximum Pressure vs. Porosity for Sands No. 1 and 2 at Ice Saturation 100%
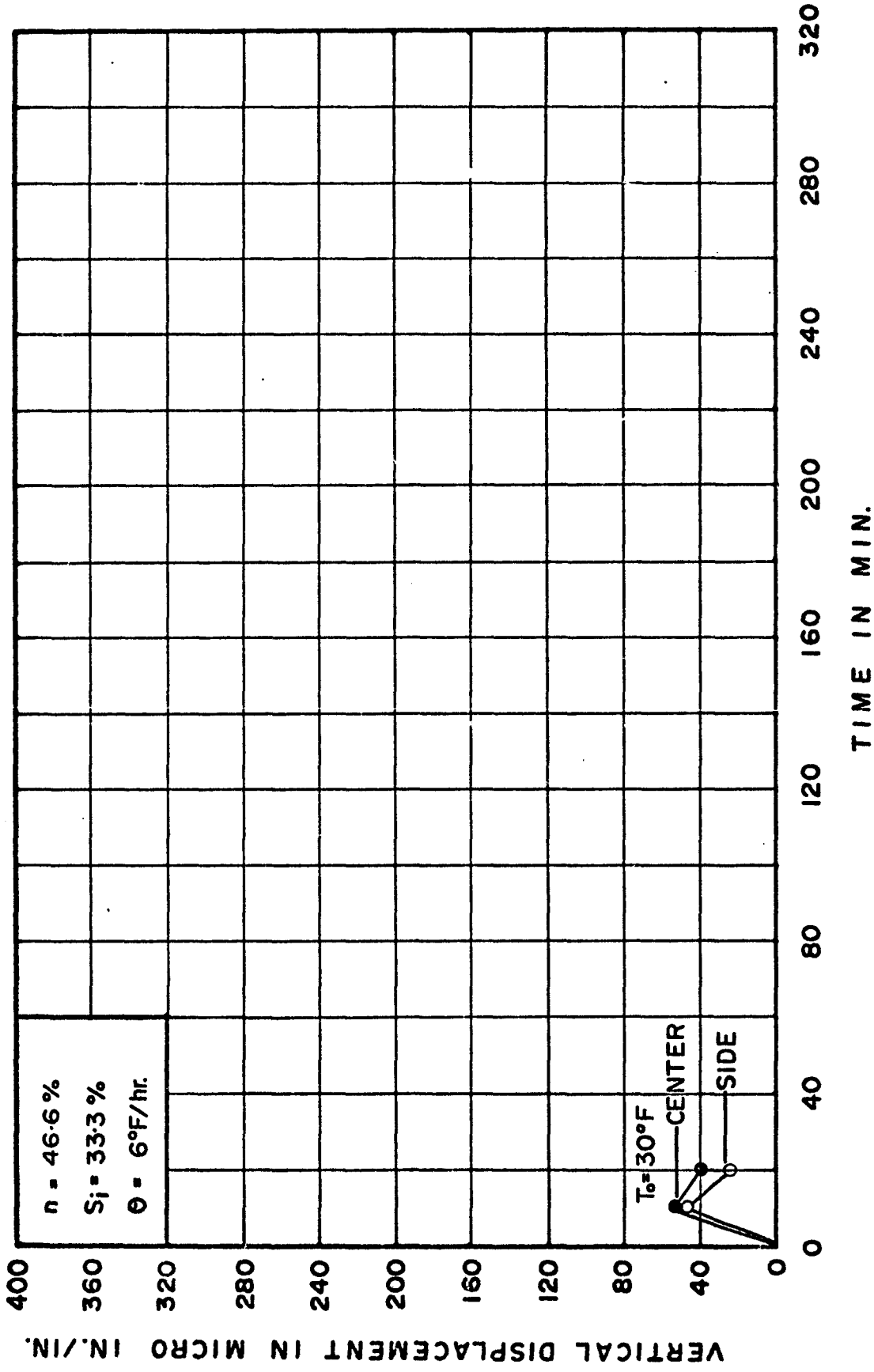
Fig. 64 Vertical Displacement-Time Curves for Sand No. 1 at Initial
Temperature 30°F and Ice Saturation 33.3%
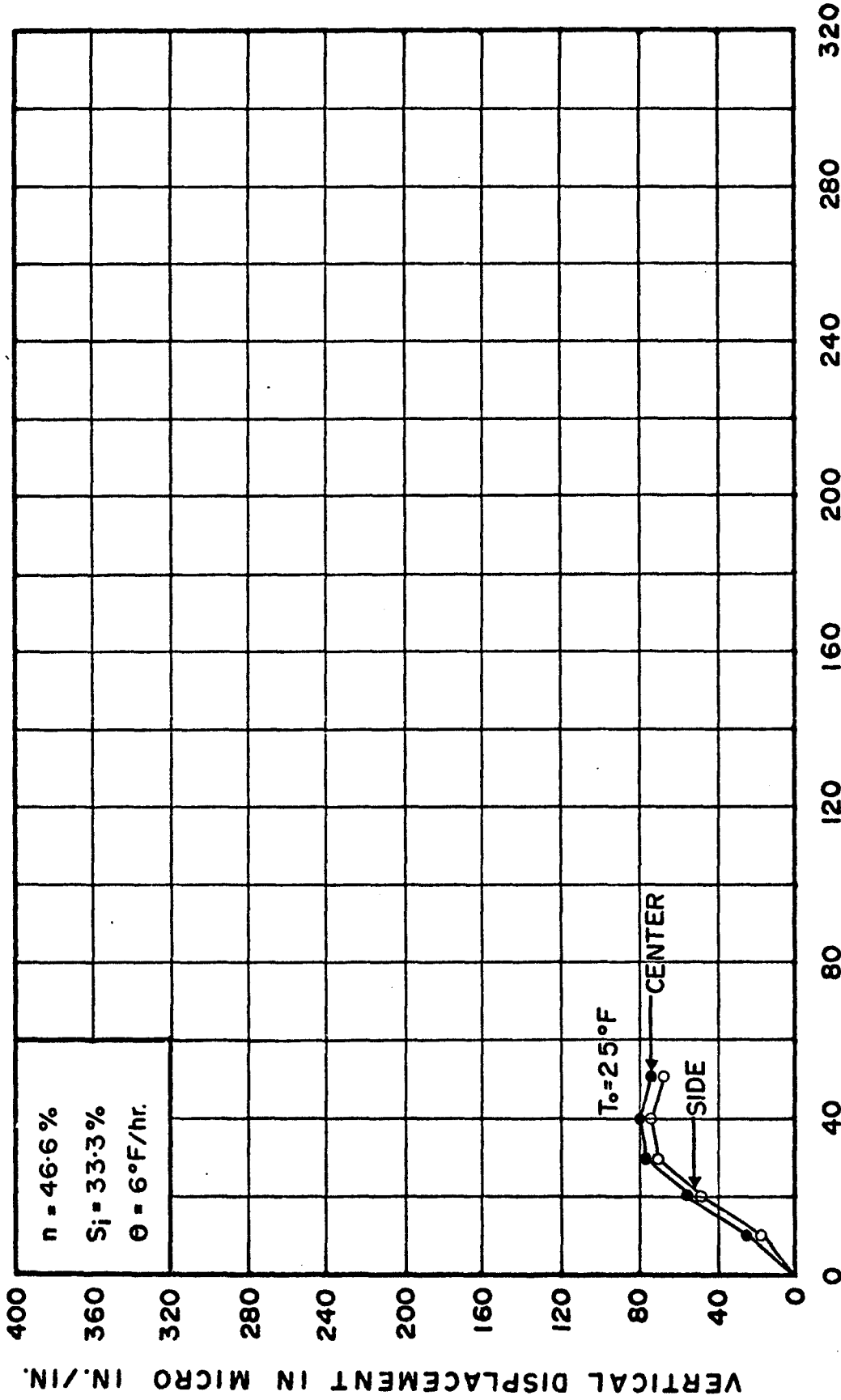
Fig. 65 Vertical Displacement—Time Curve for Sand No. 1 at Initial
Temperature 25°F and Ice Saturation 33.3%
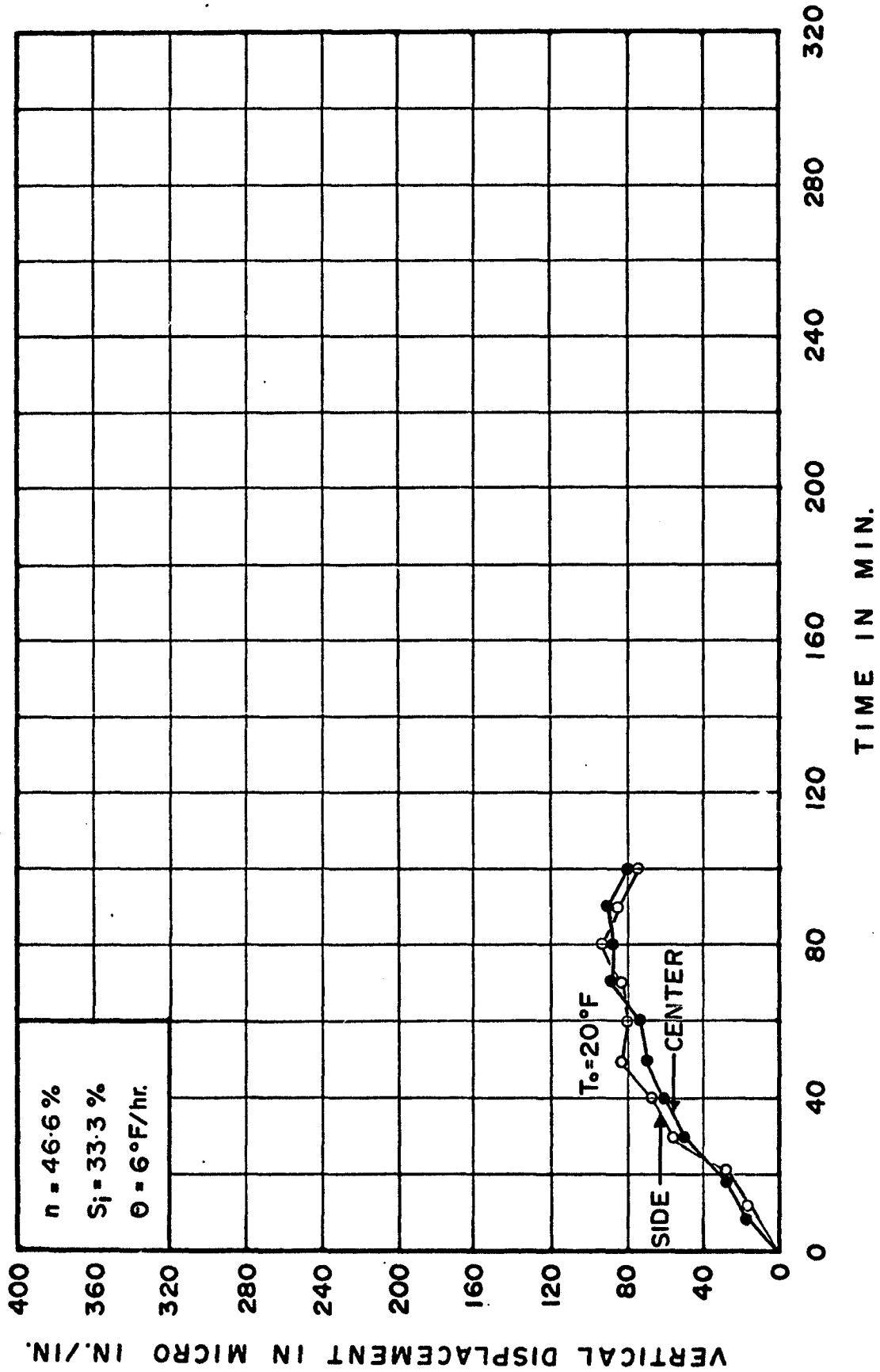
Fig. 66 Vertical Displacement-Time Curves for Sand No. 1 at Initial
Temperature 20°F and Ice Saturation 33.3%
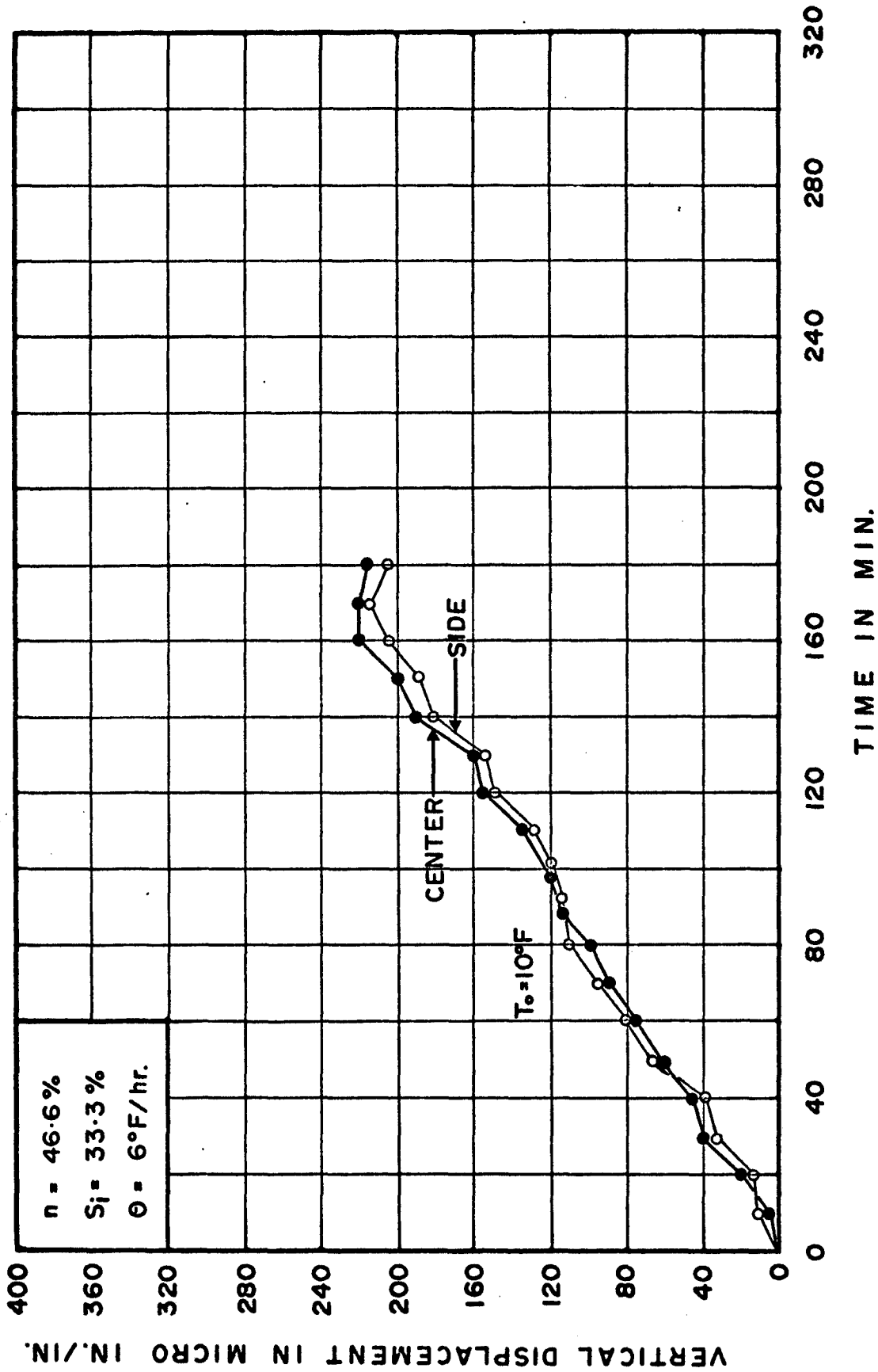
Fig. 67 Vertical Displacement-Time Curves for Sand No. 1 at Initial
Temperature 10°F and Ice Saturation 33.3%
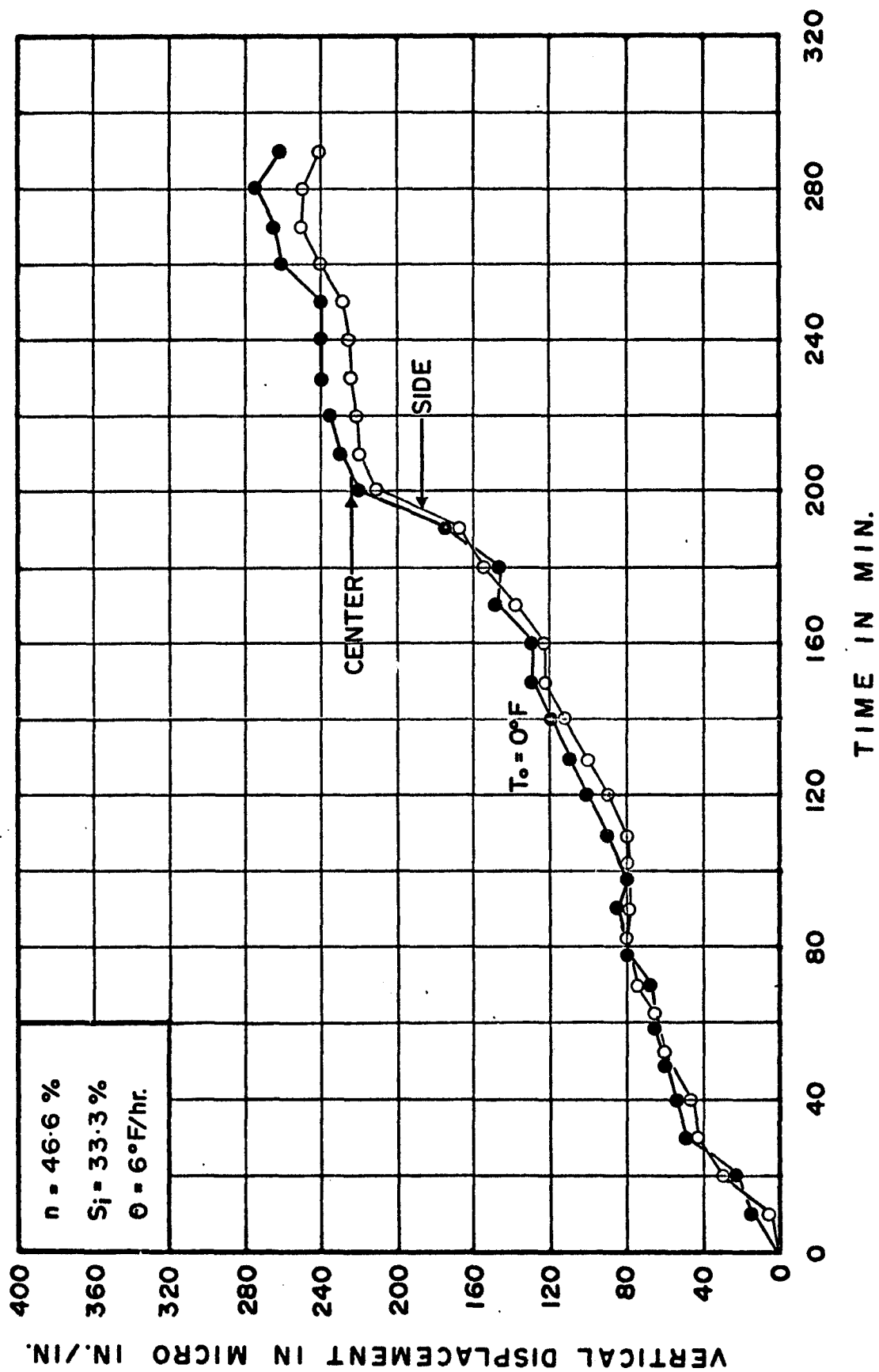
Fig. 68 Vertical Displacement-Time Curves for Sand No. 1 at Initial
Temperature 0°F and Ice Saturation 33.3%
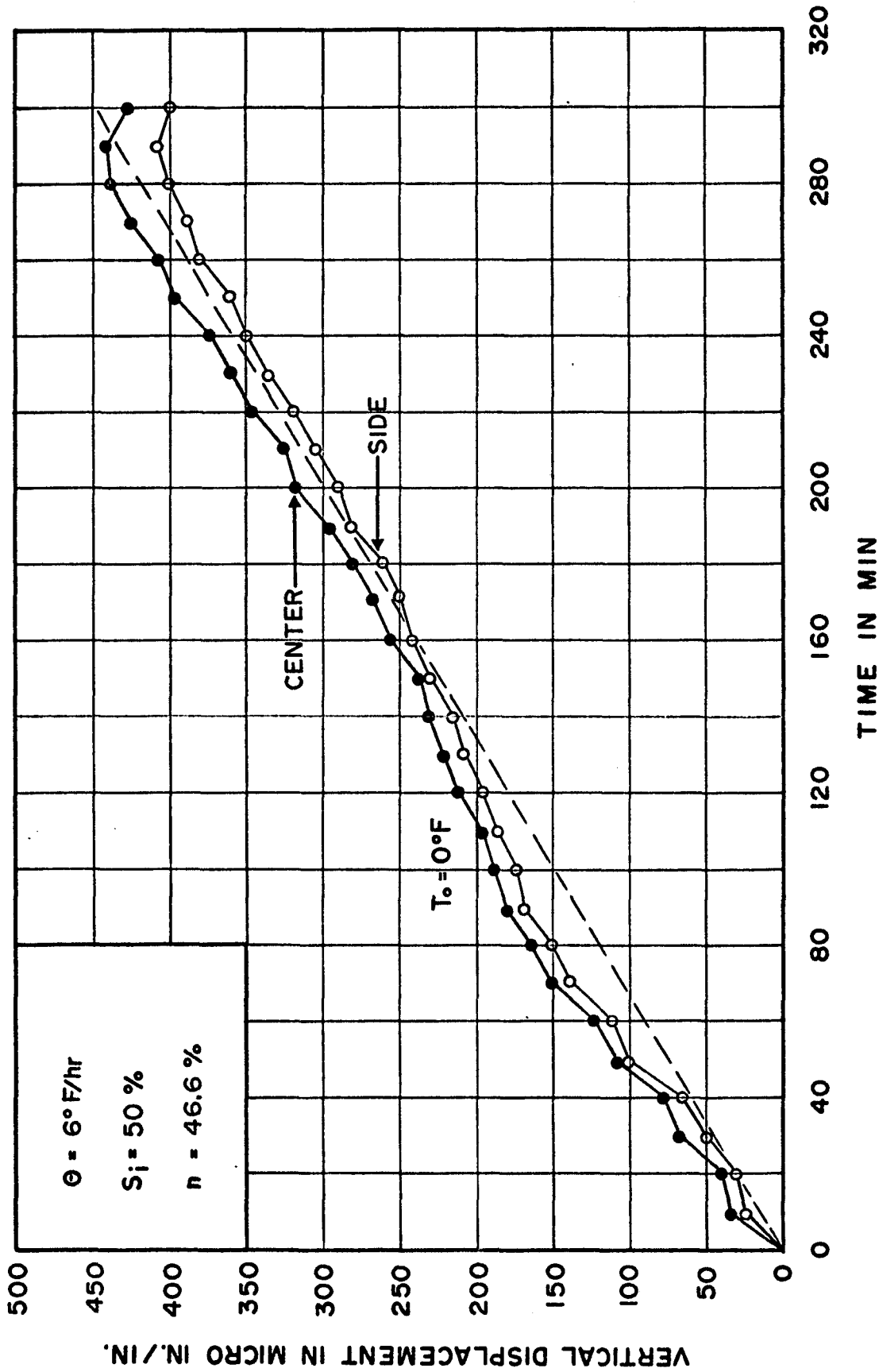
Fig. 69   Vertical Displacement-Time Curves for Sand No. 1 at Initial
Temperature 0°F and Ice Saturation 50%
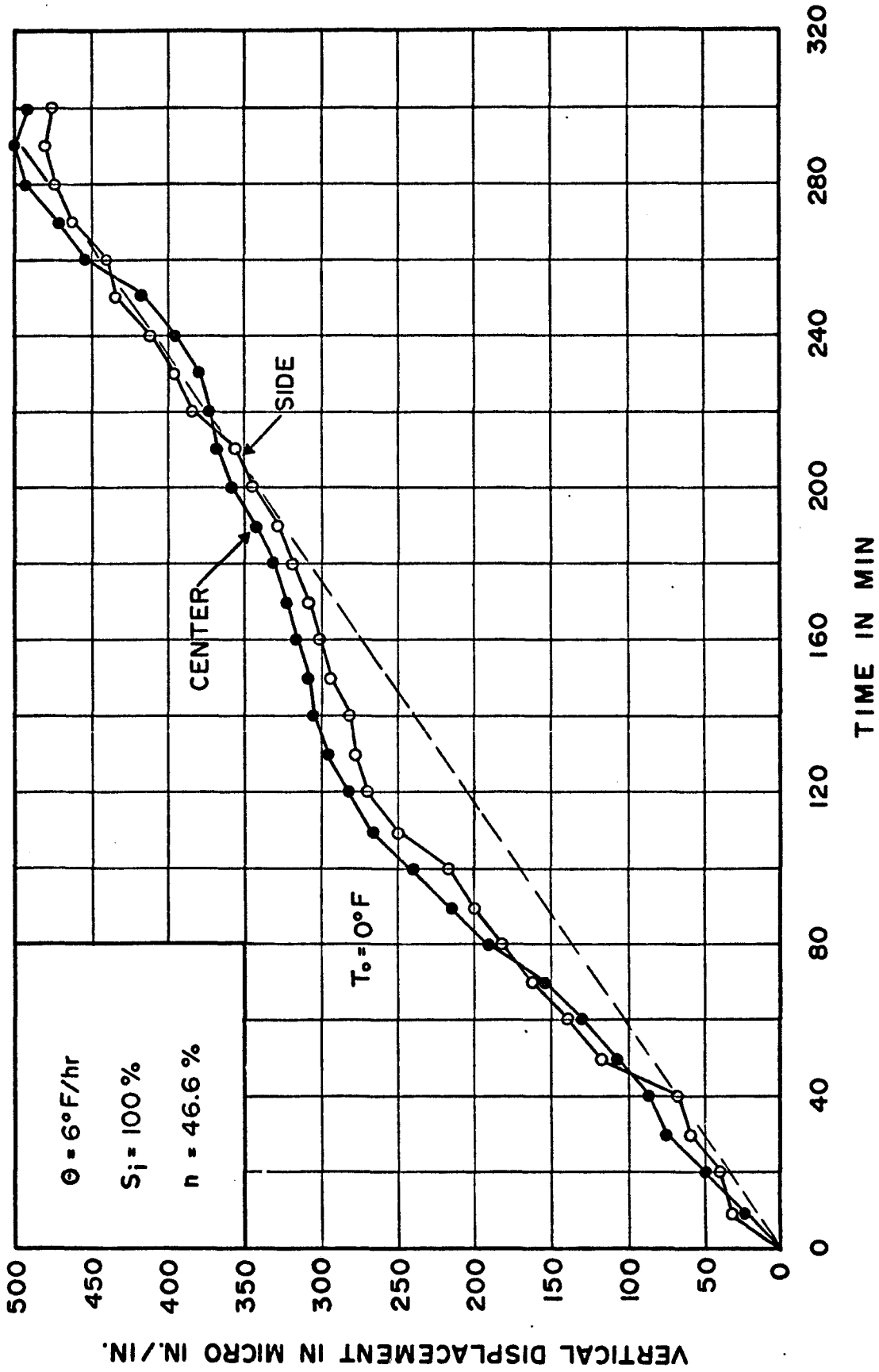
Fig. 70 Vertical Displacement-Time Curves for Sand No. 1 at Initial
Temperature 0° and Ice Saturation 100%

HEAT
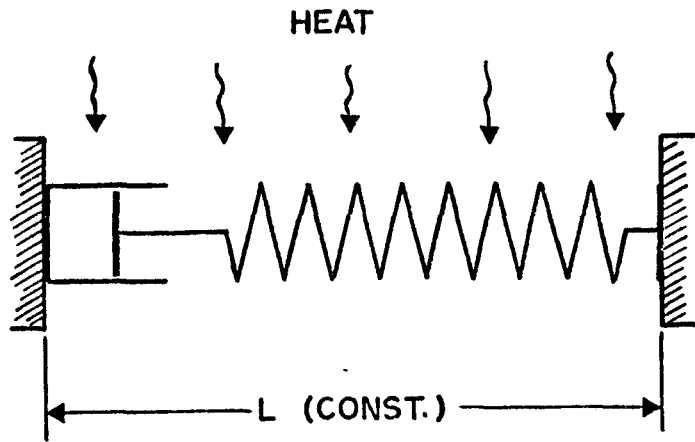
Fig. 71 Viscoelastic Model

$6X = 6Y = 6$
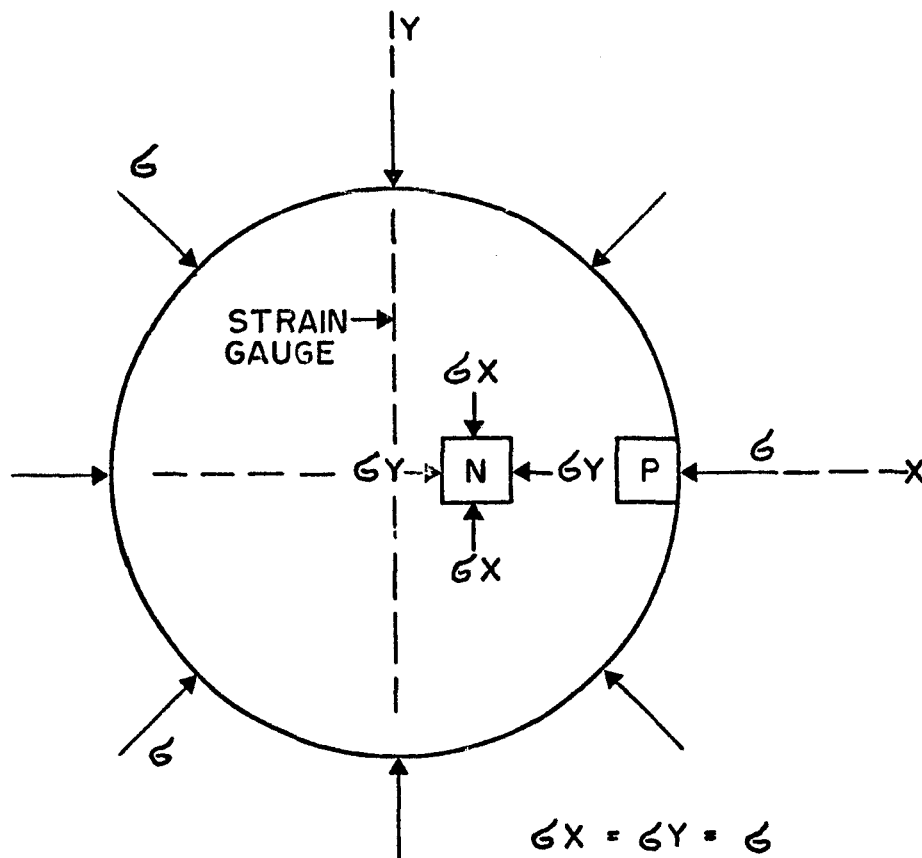
Fig. 72 Compressive Stresses in Sand-Ice
Specimen
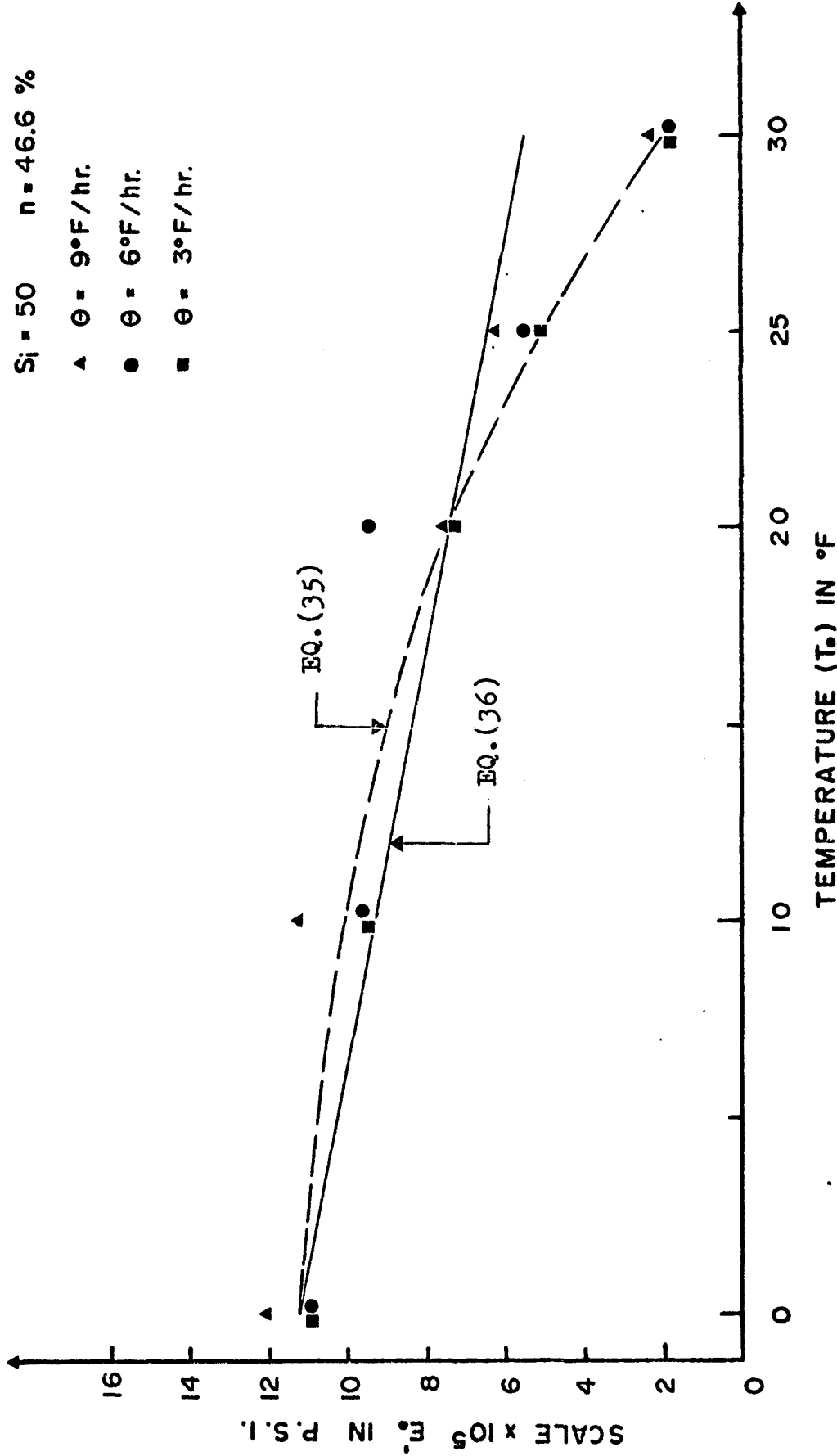
Fig. 73 Initial Modulus of Elasticity vs. Initial Frozen Sand Temperature

Fig. 74 Theoretical Pressure-Time Curve for Specimen "Z"

SAND No. I
$S_i = 50\%$
$\Theta = 6°F/hr.$
$T_o = 0°F$

$\delta_{max} = 36$ psi
$t_m = 60$ min
$A = 1.631$ psi/min

$\delta = 1.631\,t\,\exp(-t/60)$

δ_{max}

δ(psi)
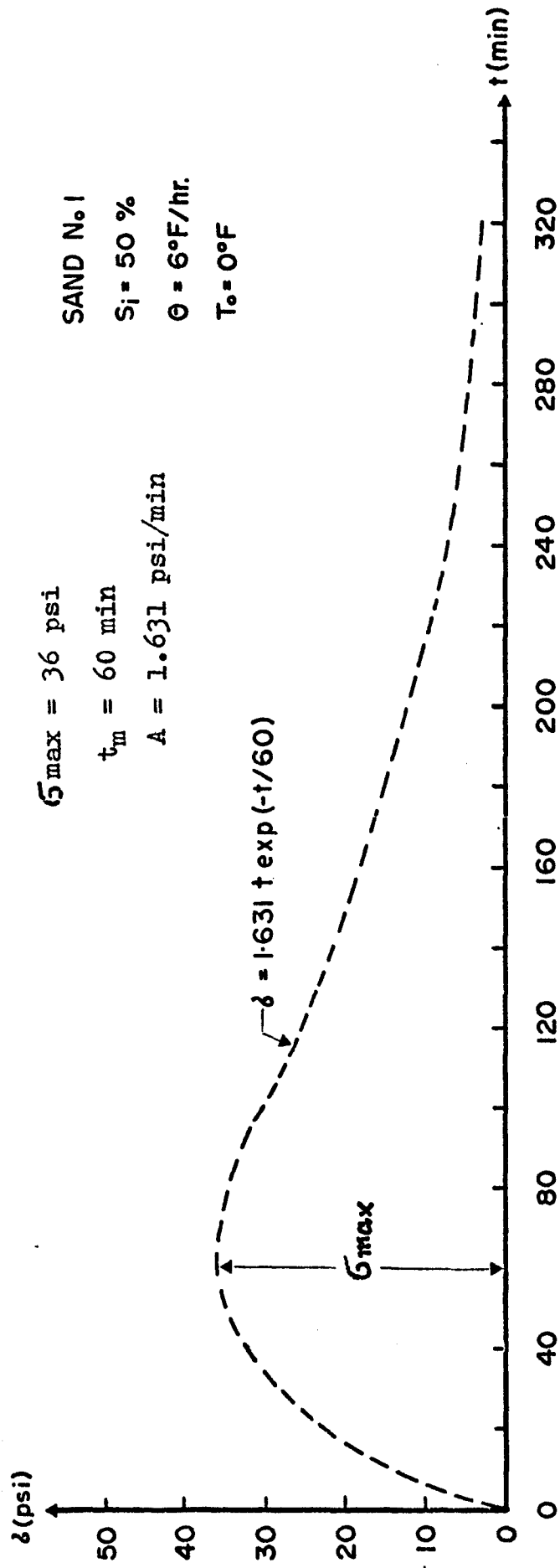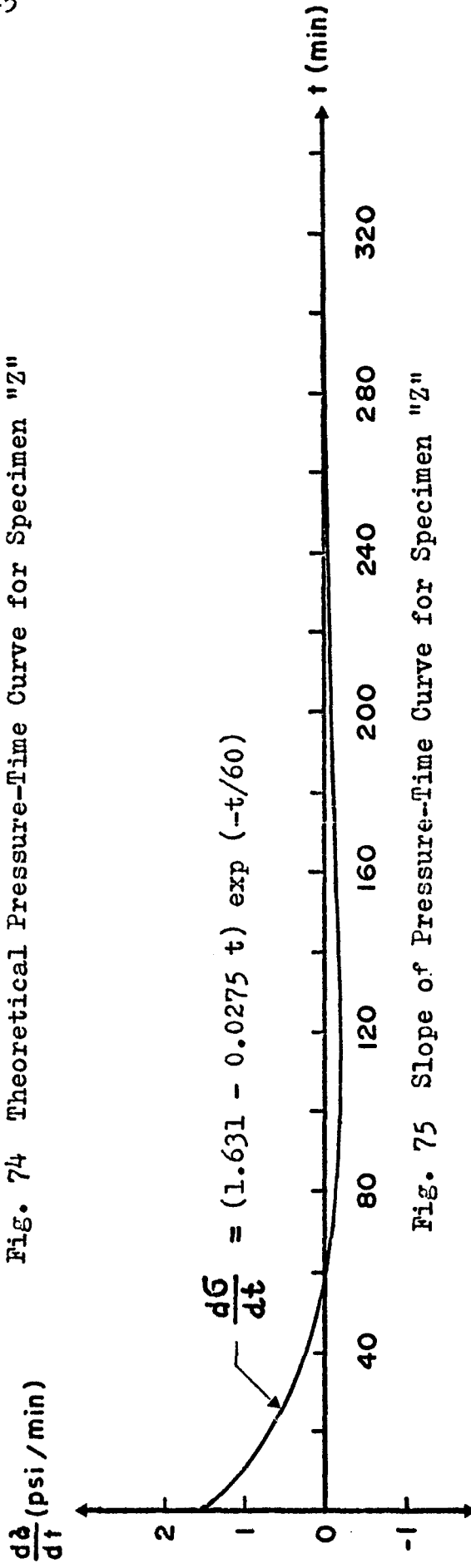
Fig. 75 Slope of Pressure-Time Curve for Specimen "Z"

$\dfrac{d\delta}{dt} = (1.631 - 0.0275\,t)\,\exp(-t/60)$

$\dfrac{d\delta}{dt}$ (psi/min)
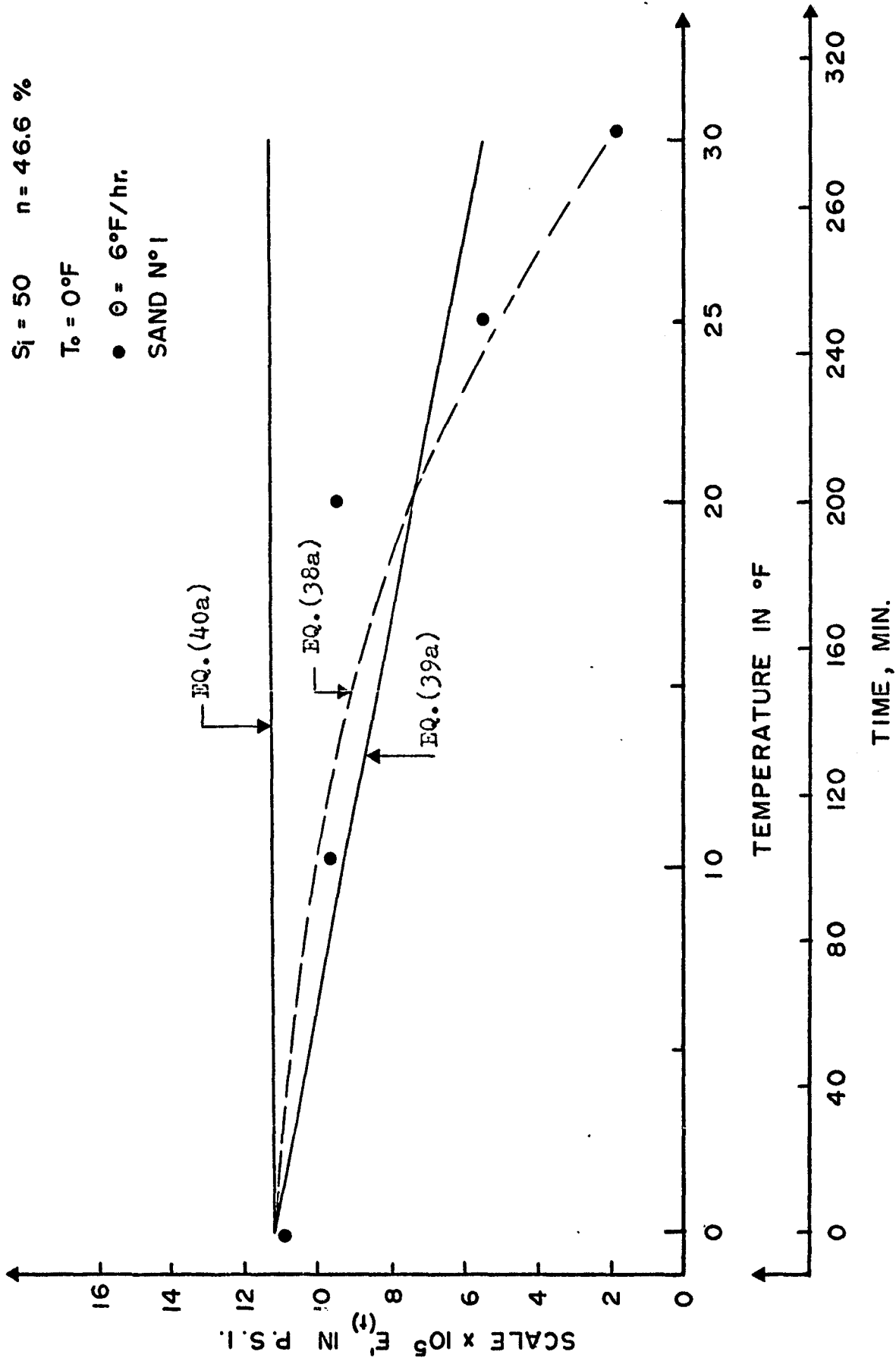
Fig. 76 Modulus of Elasticity vs. Time (or Temperature) for Specimen "Z"
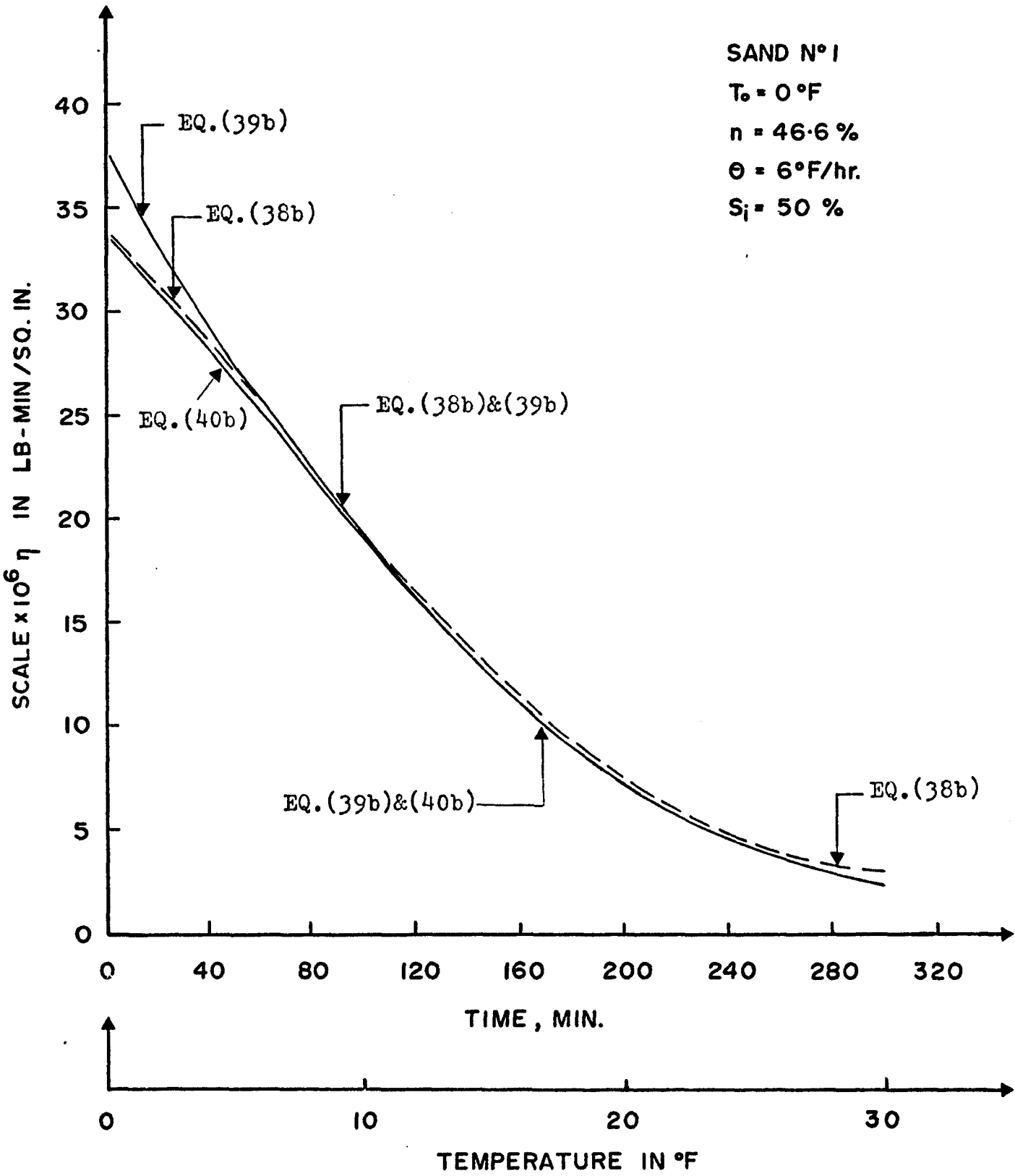
Fig. 77 Coefficient of Viscosity vs. Time (or Temperature)
For Specimen "Z"
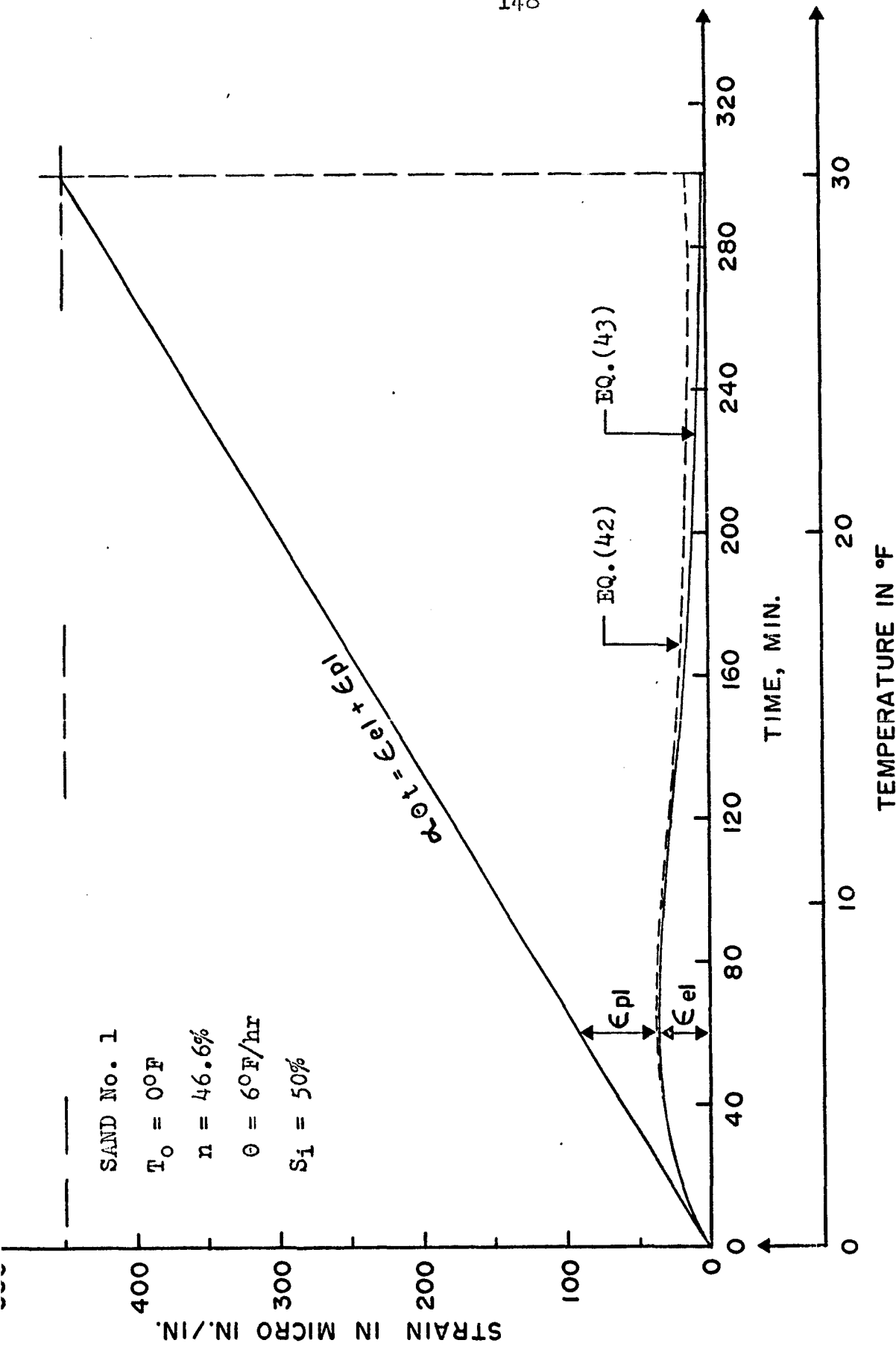
Fig. 78 Elastic and Plastic Strain Components vs. Time (or Temperature) for Specimen "Z"

A P P E N D I X

T A B L E S

TABLE I

THERMAL PROPERTIES

Material	Thermal Conductivity Btu/hr/ft/$^{\circ}$F	Volumetric Heat Btu/c.f./$^{\circ}$F
Air	0.014	0.019
Water	0.35	62.4
Ice	1.30	28
Snow, loose	0.06	
Snow, compact	0.20	
Sandy soil, unfrozen	0.35 to 1.1	
Sandy soil, frozen	0.35 to 1.2	
Silt and clay soil, unfrozen	0.60 to 1.85	
Silt and clay soil, frozen	0.40 to 2.40	
Bituminous Concrete	0.84	28
Portland-Cement Concrete	0.54	30

TABLE II

Experimentally Obtained Values of 6 max and t_m

SAND No. 1 S_i = 33.3%   n = 46.6%

Θ (°F/hr)	T_o (°F)	6 max (psi)	t_m (min)	A (psi/min) From Eq. 18
	0	24	70	0.932
	10	16	50	0.870
3	20	7	30	0.634
	25	3	15	0.544
	30	1	7.5	0.276
	0	30	50	1.631
	10	18	35	1.398
6	20	11	22.5	1.329
	25	3	12.5	0.652
	30	0.5	5	0.272
	0	32	40	2.174
	10	20	30	1.812
9	20	13	20	1.766
	25	4	10	1.087
	30	0.75	5	0.408

TABLE III

Experimentally Obtained Values of 6 max and t_m

SAND No. 1 $\qquad$ $S_i = 50\%$ $\qquad\qquad$ $n = 46.6\%$

θ ($^{\circ}$F/hr)	T_o ($^{\circ}$F)	6 max (psi)	t_m (min)	A (psi/min) From Eq. 18
3	0	30	100	0.815
	10	18.5	70	0.718
	20	8	40	0.543
	25	3.5	25	0.380
	30	0.5	10	0.136
6	0	36	60	1.631
	10	24	45	1.450
	20	13	25	1.413
	25	6	20	0.815
	30	0.5	5	0.279
9	0	45	45	2.718
	10	28	30	2.536
	20	12.5	20	1.699
	25	6.5	12.5	1.411
	30	1	5	0.544

TABLE IV

Experimentally Obtained Values of 6 max and t_m

SAND No. 1 $S_i = 83.3\%$ $n = 46.6\%$

θ (°F/hr)	T_o (°F)	6 max (psi)	t_m (min)	A (psi/min) From Eq. 18
3	0	59	140	1.145
	10	35	90	1.057
	20	15	55	0.741
	25	6	30	0.544
	30	1	10	0.272
6	0	65	85	2.078
	10	45	60	2.038
	20	22	40	1.495
	25	6	25	0.652
	30	0.5	5	0.272
9	0	73	60	3.307
	10	49	45	2.960
	20	25	30	2.265
	25	7	15	1.268
	30	1.5	5	0.815

TABLE V

Experimentally Obtained Values of σ max and t_m

SAND No. 1 $S_i = 100\%$ $n = 46.6\%$

θ ($^{\circ}F/hr$)	T_o ($^{\circ}F$)	σ max (psi)	t_m (min)	A (psi/min) From Eq. 18
3	0	65	170	1.039
	10	42	100	1.140
	20	19	60	0.861
	25	7.5	30	0.679
	30	1.5	10	0.408
6	0	81	105	2.097
	10	54	70	2.097
	20	24	40	1.631
	25	10	20	1.359
	30	1.5	5	0.814
9	0	91	70	3.533
	10	59	50	3.207
	20	28	30	2.537
	25	13	15	2.356
	30	1.75	5	0.952

TABLE VI

Comparison Between Experimentally Obtained and Calculated

Values of 6 max and t_m

SAND No. 1 $S_i = 33.3\%$ $n = 46.6\%$

θ ($^{\circ}$F/hr)	T_o ($^{\circ}$F)	6 max (psi)		t_m (min)	
		Experimental	From Eq.(19)	Experimental	From Eq.(20)
3	0	24	20.83	70	66.3
	10	16	13.89	50	46.3
	20	7	6.94	30	29.8
	25	3	3.47	15	17.5
	30	1	0.2	7.5	4.99
6	0	30	24.77	50	47.1
	10	18	16.51	35	31.3
	20	11	8.25	22.5	19.4
	25	3	4.12	12.5	12.5
	30	0.5	0.4	5	3.9
9	0	32	27.42	40	35.1
	10	20	18.28	30	23.0
	20	13	9.14	20	14.1
	25	4	4.57	10	10.0
	30	0.75	0.6	5	3.4

TABLE VII

Comparison Between Experimentally Obtained and Calculated

Values of $\mathbf{6}$ max and t_m

SAND No. 1 $S_i = 50\%$ $n = 46.6\%$

Θ ($^\circ$F/hr)	T_o ($^\circ$F)	$\mathbf{6}$ max (psi)		t_m (min)	
		Experimental	From Eq.(19)	Experimental	From Eq.(20)
3	0	30	31.68	100	92.0
	10	18.5	21.12	70	63.2
	20	8	10.56	40	40.1
	25	3.5	5.28	25	23.6
	30	0.5	0.3	10	6.7
6	0	36	38.01	60	64.4
	10	24	25.34	45	41.8
	20	13	12.67	25	25.3
	25	6	6.33	20	16.3
	30	0.5	0.6	5	5.0
9	0	45	42.28	45	47.7
	10	28	28.18	30	30.3
	20	12.5	14.09	20	18.2
	25	6.5	7.04	12.5	12.8
	30	1	0.9	5	4.3

TABLE VIII

Comparison Between Experimentally Obtained and Calculated

Values of σ max and t_m

SAND No. 1 $S_i = 83.3\%$ $n = 46.6\%$

θ (^{O}F/hr)	T_o (^{O}F)	σ max (psi)		t_m (min)	
		Experimental	From Eq.(19)	Experimental	From Eq.(20)
3	0	59	54.26	140	138.7
	10	35	36.17	90	93.5
	20	15	18.08	55	58.3
	25	6	9.04	30	30.3
	30	1	0.5	10	9.7
6	0	65	66.22	85	95.5
	10	45	44.15	60	60.2
	20	22	22.07	40	35.5
	25	6	11.03	25	23.0
	30	0.5	1.0	5	7.0
9	0	73	74.41	60	70.0
	10	49	49.60	45	43.1
	20	25	24.80	30	25.0
	25	7	12.40	15	17.6
	30	1.5	1.5	5	5.9

TABLE IX

Comparison Between Experimentally Obtained and Calculated

Values of σ max and t_m

SAND No. 1 $\qquad$ $S_i = 100\%$ $\qquad$ $n = 46.6\%$

θ ($^{\circ}F$/hr)	T_o ($^{\circ}F$)	σ max (psi)		t_m (min)	
		Experi-mental	From Eq.(19)	Experi-mental	From Eq.(20)
3	0	65	66.04	170	160.6
	10	42	44.02	100	107.6
	20	19	22.01	60	66.7
	25	7.5	11.00	30	39.2
	30	1.5	0.6	10	11.1
6	0	81	81.30	105	110.0
	10	54	54.20	70	68.9
	20	24	27.10	40	40.1
	25	10	13.55	20	25.8
	30	1.5	1.2	5	7.9
9	0	91	91.82	70	80.4
	10	59	61.21	50	48.8
	20	28	30.60	30	28.0
	25	13	15.30	15	19.8
	30	1.75	1.8	5	6.6

TABLE X

Experimentally Obtained Values of 6max and t_m

SAND No. 2   n = 36%

S_i (%)	Θ (°F/hr)	T_o (°F)	6 max (psi)	t_m (min)	A (psi/min) From Eq. 18
	3	10	18	60	0.815
	3	25	4	22.5	0.483
50	6	10	19	37.5	1.377
	6	25	5	17.5	0.799
	9	10	25	30	2.265
	9	25	5.5	15	0.997
	3	10	37	80	1.257
	3	25	7.5	25	0.815
100	6	10	45	60	2.038
	6	25	9	20	1.223
	9	10	52.5	45	3.171
	9	25	11	20	1.495

TABLE XI

Experimentally Obtained Values of σ max and t_m

SAND No. 2   n = 40.8%

S_i (%)	θ ($^\circ$F/hr)	T_o ($^\circ$F)	σmax (psi)	t_m (min)	A (psi/min) From Eq. 18
	3	10	21	60	0.951
	3	25	4.5	22.5	0.544
50	6	10	23	40	1.562
	6	25	4	20	0.544
	9	10	27	35	2.097
	9	25	6	10	1.631
	3	10	44	90	1.323
	3	25	13	30	1.178
100	6	10	54	55	2.669
	6	25	12.5	25	1.359
	9	10	56	45	3.383
	9	25	11	15	1.993

TABLE XII

Experimentally Obtained Values of σmax and t_m

SAND No. 1   n = 40.8%

S_i (%)	Θ ($^\circ$F/hr)	T_o ($^\circ$F)	σmax (psi)	t_m (min)	A (psi/min) From Eq. 18
	3	10	20	55	0.988
	3	25	4	20	0.544
50	6	10	23	45	1.389
	6	25	6	15	1.087
	9	10	25	30	2.265
	9	25	5	15	0.906
	3	10	41	80	1.393
	3	25	12	25	1.305
100	6	10	51	60	2.310
	6	25	11	20	1.495
	9	10	55	50	2.990
	9	25	13	20	1.767

TABLE XIII

Experimentally Obtained Values of δmax and t_m

SAND No. 1   n = 43.5%

S_i (%)	θ (°F/hr)	T_o (°F)	δmax (psi)	t_m (min)	A (psi/min) From Eq. 18
	3	10	22	65	0.920
	3	25	5	25	0.544
50	6	10	25	45	2.718
	6	25	5.5	20	0.747
	9	10	27	35	2.097
	9	25	6.5	15	1.178
	3	10	43	95	1.230
	3	25	14	30	1.268
100	6	10	52	65	2.174
	6	25	12	15	2.175
	9	10	57	50	3.099
	9	25	11	20	1.495

TABLE XIV

Duplicate Tests Performed on the Same Sand-Ice Samples

SAND No.	n (%)	T_o (°F)	θ (°F/hr)	S_i (%)	σ max (psi)	R (psi)	$\bar{x}$ (psi)	v (psi)	V (%)
1	46.6	0	6	50	36, 39	3	37.5	1.5	4.00
1	46.6	10	9	100	58, 62	4	60.0	2.0	3.33
1	46.6	20	6	33.3	8, 10	2	9.0	1.0	11.10
2	40.8	10	6	50	22, 23	1	22.5	0.5	2.20
2	40.8	25	9	50	5, 6	1	5.5	0.5	9.10

Legend:

$\bar{x}$ = mean value of σ max.   v = standard deviation

R = range   V = coefficient of variation

TABLE XV

Equivalent Sand-Ice Samples Tested Under the Same Conditions in Sets of Three

SAND No.	n (%)	T_o (°F)	θ (°F/hr)	S_i (%)	σ max (psi)	R (psi)	$\bar{x}$ (psi)	v (psi)	V (%)
1	46.6	0	6	50	32, 36, 39	7	35.67	2.87	8.00
1	46.6	10	9	100	52, 59, 62	10	57.67	4.19	7.26
1	46.6	20	6	33.3	7, 10, 11	4	9.33	1.10	18.20
2	40.8	10	6	50	23, 23, 26	3	24	1.15	4.80
1	40.8	10	3	50	19, 20, 24	5	21	2.16	10.30
2	36.0	25	9	100	9, 11, 11.5	2.5	10.5	1.08	10.30
2	36.0	25	6	100	8.5, 9, 11.0	3.5	9.5	1.08	11.40

Legend:

$\bar{x}$ = mean value of σ max. v = standard deviation

R = range V = coefficient of variation

TABLE XVI

Temperature Effect on Modulus of Elasticity (E_0')

SAND No. 1 $S_i = 50\%$ $n = 46.6\%$

$$\alpha = 15 \times 10^{-6}$$

θ (°F/min)	T_0 (°F)	A psi/min	$E_0' \times 10^{-5}$ psi From Eq. (33)
0.05	0	0.815	10.866
	10	0.718	9.574
	20	0.543	7.240
	25	0.380	5.066
	30	0.136	1.812
0.10	0	1.631	10.874
	10	1.450	9.666
	20	1.413	9.420
	25	0.815	5.434
	30	0.279	1.860
0.15	0	2.718	12.080
	10	2.536	11.270
	20	1.699	7.550
	25	1.411	6.270
	30	0.544	2.418

TABLE XVII

Elastic Modulus $E'(t)$ in psi

SAND No. 1 $T_o = 0^oF$, $S_i = 50\%$, $\theta = 6^oF/hr$, $n = 46.6\%$

t (min)	$E'(t) \times 10^{-5}$ From Eq. (38a)	$E'(t) \times 10^{-5}$ From Eq. (39a)
0	11.3000	11.3000
10	11.2897	11.1000
20	11.2588	10.9000
30	11.2073	10.7000
40	11.1352	10.5000
50	11.0425	10.3000
60	10.9292	10.1000
70	10.7953	9.9000
80	10.6408	9.7000
90	10.4657	9.5000
100	10.2700	9.3000
110	10.0537	9.1000
120	9.8168	8.9000
140	9.2812	8.5000
160	8.6632	8.1000
180	7.9628	7.7000
200	7.1800	7.3000
220	6.3148	6.9000
240	5.3672	6.5000
260	4.3372	6.1000
280	3.2248	5.7000
300	2.0300	5.3000

TABLE XVIII

Coefficient of Viscosity $\eta'_{(t)}$ lb-min/in^2

SAND No. 1 $T_o = 0°F$, $S_i = 50\%$, $\theta = 6°F/hr$, $n = 46.6\%$

t (min)	$\eta'_{(t)}$ From Eq.(38b)	$\eta'_{(t)}$ From Eq.(39b)	$\eta'_{(t)}$ From Eq.(40b)
1	33786203.00	37725500.00	33758652.00
5	33319112.00	36917372.00	33188966.00
10	32711868.00	35910720.00	32468745.00
20	31425531.00	33911688.00	31003681.00
30	30055698.00	31937003.00	29511077.00
40	28617931.00	29993197.00	27998007.00
50	27128284.00	28086892.00	26472266.00
60	25603024.00	26224652.00	24942226.00
70	24058247.00	24412873.00	23416660.00
80	22509539.00	22657622.00	21904525.00
90	20971654.00	20964525.00	20414762.00
100	19458213.00	19338640.00	18956054.00
110	17981462.00	17784343.00	17536597.00
120	16552102.00	16305253.00	16163916.00
130	15179161.00	14904171.00	14844675.00
140	13869947.00	13583033.00	13584540.00
150	12630061.00	12342917.00	12388093.00
160	11463466.00	11184048.00	11258778.00
170	10372592.00	10105848.00	10198895.00
180	9358502.00	9106994.70	9209647.40
190	8421055.80	8185495.60	8291200.80
200	7559110.50	7338781.40	7442790.30
210	6770730.40	6563798.80	6662838.50
220	6053405.90	5857114.10	5949083.80
230	5404291.10	5215001.10	5298710.70
240	4820493.90	4633541.30	4708484.60
250	4299464.90	4108705.50	4174871.40
260	3839656.40	3636428.00	3694148.30
270	3441893.60	3212675.40	3262503.80
280	3112891.20	2833500.80	2876119.90
290	2876749.10	2495085.80	2531237.80
300	2828765.40	2193780.20	2224217.50

TABLE XIX

Comparison Between Elastic and Plastic Strain,

when $E'_{(t)} = 11.3 \times 10^5 - 10.3\ t^2$

SAND No. 1 $T_o = 0°F$ $S_i = 50\%$ $\theta = 6°F/hr$

t (min)	σ (psi)	$\epsilon_{el} \times 10^6$ (in/in)	$\epsilon_{pl} \times 10^6$ (in/in)
0	0.00	0.000	0.000
10	13.81	12.232	2.768
20	23.37	20.757	9.243
30	29.68	26.482	18.518
40	33.50	30.084	29.916
50	35.44	32.094	42.906
60	36.00	32.939	57.061
70	35.55	32.930	72.070
80	34.39	32.318	87.682
90	32.75	31.292	103.708
100	30.81	30.000	120.000
110	28.68	28.526	136.474
120	26.49	26.984	153.016
140	22.14	23.854	186.146
160	18.13	20.927	219.073
180	14.62	18.360	251.640
200	11.64	16.211	283.789
220	9.17	14.521	315.479
240	7.17	13.358	346.642
260	5.57	12.842	377.158
280	4.29	13.303	406.697
300	3.30	16.256	433.744

TABLE XX

Comparison Between Elastic and Plastic Strain,

when $E'(t) = E'_0 = 11.3 \times 10^5$

SAND No. 1 $T_0 = 0°F$ $S_i = 50\%$ $\theta = 6°F/hr$

t (min)	σ (psi)	$\epsilon_{el} \times 10^6$ (in/in)	$\epsilon_{pl} \times 10^6$ (in/in)
0	0.00	0.000	0.000
10	13.81	12.221	2.779
20	23.37	20.681	9.319
30	29.68	26.265	18.735
40	33.50	29.646	30.354
50	35.44	31.363	43.637
60	36.00	31.858	58.142
70	35.55	31.460	73.540
80	34.39	30.434	89.566
90	32.75	28.982	106.018
100	30.81	27.265	122.735
110	28.68	25.381	139.619
120	26.49	23.442	156.558
140	22.14	19.593	190.407
160	18.13	16.044	223.956
180	14.62	12.938	257.062
200	11.64	10.301	289.699
220	9.17	8.115	321.885
240	7.17	6.345	353.655
260	5.57	4.929	385.071
280	4.29	3.796	416.204
300	3.30	2.920	447.080

VITA AUCTORIS

1925   Jan Tadeusz Laba was born in Przemysl, Poland on
            June 28th, 1925.

1943   He completed his secondary education in Przemysl,
            Poland, obtaining his Senior Matriculation in
            June 1943.

1946-51   In September 1946, he enrolled at P.U.C. Univ-
            ersity College, London, England, to study civil
            engineering. He graduated in 1951, obtaining the
            degree of Dipl. Ing.

1951-61   He was working in industry for Dominion Bridge Co.
            Montreal, Quebec. Falconbridge Nickel Mines,
            Sudbury, Ontario. Giffels and Associates, Windsor,
            Ontario, also he was engaged in private practice as
            consulting engineer in Sudbury, Ontario.

1960   In September 1960, he enrolled at Assumption Univ-
            ersity of Windsor to obtain the degree of M.A.Sc.

1961   He joined the teaching staff of Assumption Univ-
            ersity of Windsor, in the Faculty of Applied
            Science.

1963   Received the degree of M.A.Sc. in Civil Engineering,
            from Assumption University of Windsor.